UNIVERSITÀ DEGLI STUDI DELL'INSUBRIA

PhD SCHOOL IN MOLECULAR AND CELLULAR BIOLOGY

XXVII CYCLE

Development of engineered nanoparticles for biomedical and industrial applications.

Coordinator: Professor Magda De Eguileor

Supervisor: Professor Giovanni Bernardini

PhD Student:

Francesca Cappellini

TABLE OF CONTENTS

CHAPTER II – SYNTHESIS OF MAGNETIC NANOPARTICLE SYSTEM FOR CANCER THERAPY: NP@DAAO

CHAPTER III – SYNTHESIS OF MAGNETIC NANOPARTICLE SYSTEM FOR ANTIBACTERICAL THERAPY: NP@TEICOPLANIN

CHAPTER IV – SYNTHESIS OF NP@ACYLASE

CHAPTER V – SYNTHESIS OF NP@LASPO

SUMMARY

In this work four nanoparticle systems were designed: two for medical and two for industrial applications.

The purpose of the first part of my study concerns the manufacture of a NPs-enzyme system for cancer therapy: Fe_3O_4 NPs@APTES-DAAO. This system combines the magnetic properties of iron oxide nanoparticles (Fe_3O_4 NPs) with the ROS generating enzyme D-amino acid oxidase (DAAO), in order to efficiently direct the enzyme into the tumor and kill tumor cells. Under our best experimental condition, we have immobilized 100% of the enzyme in term of activity and quantity. The system showed an activity of 7U/mg of NPs and an apparent K_m for D-Ala similar to that of the free enzyme. In vitro cytotoxicity demonstrates the higher efficacy of the system in respect to free enzyme. *In vivo* experiments did not have highlighted adverse side effects of Fe_3O_4 NPs@APTES-DAAO at a concentration of 20mg/kg. At the tested concentrations our NPs do not pass brain-blood barrier and do not accumulate in the heart.

The second medical system designed consists in magnetic iron oxide nanoparticles conjugated with the antibiotics teicoplanin. Similar to the previous system,

Fe₃O₄ NPs@Teicoplanin takes advantage of the magnetic character of NPs for a specific targeting of the antibiotic. Teicoplanin has been conjugated on Fe_3O_4 NPs@CMCS with efficiency in term of quantity over the 90%. Unfortunately, the reaction was not reproducible and some problems are associated with storage. The main problem is probably due to the wide active site of teicoplanin: interactions with NPs may affect some of the residues involved in substrate recognition, leading to a loss of activity. The optimization of reaction conditions, by protecting the active site, might solve the problem.

The first system for industrial application is composed by Fe_3O_4 NPs and the enzyme cephalosporin C acylase (VAC). Despite the efficiency of VAC conjugation on NPs (90%), the low specific activity of the enzyme does not allow to obtain en efficient system on an adequate support (24mg of NPs for 0.48U if VAC). Moreover bioconversion analysis indicates that Fe_3O_4 NPs@APTES interfere with the assay. For this reason there is the need to find other methods to assess the bioconversion ability of the enzyme (for example by HPLC). In order to make the system more efficient, future efforts will be aimed at finding a VAC mutant with a higher specific activity, in order to increase the specific

Summary

activity of the system.

The last enzyme system for industrial application designed in this study is composed of Fe_3O_4 NPs conjugated to L-aspartate oxidase (LASPO). LASPO was conjugated on Fe_3O_4 magnetic NPs with efficiency in term of unit of 60%. 1U of enzyme was conjugated on 216mg of NPs. The system was efficiently used for the resolution of a racemic mixture of D,L-aspartate: 1U converts 250mM of D,L-aspartate in 240min. Moreover Fe_3O_4 NPs@APTES-LASPO seems to have a stable activity in a wide pH range (8-10), with an optimum around pH 9. Thanks to the high stability of the system it was possible to use Fe_3O_4 NPs@APTES-LASPO for several cycles of bioconversion. This is a great advantage and makes Fe_3O_4 NPs@APTES-LASPO an excellent system for the resolution of racemic solution of D,L-aspartate.

CHAPTER I

INTRODUCTION

I.I. BACKGROUND

I.1 NANOTECHNOLOGY AND NANOPARTICLES

In recent years, nanoparticles (NPs) and other nanomaterials have permeated essentially all areas of our everyday lives. In industrial applications, they have become indispensable components of catalysts [1], sensor [2] and photovoltaic devices [3]. In the biomedical field, they have found widespread use as nanovaccines [4], nanodrugs [5] and diagnostic imaging tools [6].

Nanostructures and nanosystems are of great interest beyond the simple scaling down of larger structures. Among the countless motivations for nano-research, the most important is that nanoscale systems have peculiar properties. When an object is scaled, the volume changes by the said scale cubed, and the surface area changes by that scale squared. In fact, the surface area and volume of a cube and of a sphere respectively can be found with the following equations:

$$S=6l^2 \text{ and } V=l^3 \qquad\qquad S=4\pi r^2 \text{ and } V=(4\pi r^3)/3$$

The growth in volume is always greater than the increase in surface area. This is true for cubes, spheres, or any other object whose size is augmented without changing

its shape. This means that the surface area to volume ratio increases by the scaling factor as the system scales down (a radius diminution by a factor of 1 million corresponds to a growth of the surface area to volume ratio by a factor of 10^6).

There are also effects that occur for reasons other than the strict scaling law effects mentioned. For example, as a spherical particle gets progressively smaller the curvature of the surface increases. This is notable because surface curvature can affect certain types of physical interactions (see paragraph I.4). This effect is not strictly a nanoscale effect but a conformal one, where the surface curvature is the key to the result. A study recently showed that gold particles within a certain size range would disrupt cell membranes and cause cytotoxicity [7, 8].

I.2 MAGNETIC NANOPARTICLES

Nanoscale materials are very fascinating also because their magnetic properties differ substantially from the bulk counterparts, due to the increasing role of the surface spins as the particle size is diminished. Moreover at the nanoscale level, magnetic-like behavior could appear in materials that do not have magnetic behavior in the bulk

[9]. Thus nanomaterials are attracting a great deal of interest due to their potential uses in different magnetic disciplines such magnetic recording [10, 11, 12], magnetic resonance imaging and related technologies [13, 14, 15], analytical chemistry [16].

Among magnetic nanoparticles, of great concern are Superparamagneric Iron Oxide Nanoparticles (SPIONs) whose research has been growing exponentially over the last several years. The field continues to drive in the direction of biomedical applications, by exploiting the immense qualities of IONs [17]. SPIONs belong to the class of inorganic based particles having an iron oxide core, coated by either inorganic materials (silica, gold) or organic materials (phospholipids, fatty acids, polysaccharides, peptides or other surfactants and polymers). In contrast to other nanoparticles, their magnetic properties, based on their inducible magnetization, allow them to be directed to a defined location and/or heated in the presence of an externally applied magnetic field [18].

Among all iron oxides, magnetite Fe_3O_4 possesses the most interesting properties because of the presence of iron cations in two states, Fe^{2+} and Fe^3. Up to date Fe_3O_4 NPs have found applications in several biomedical field

[19], being the only one magnetic NP approved by FDA [20]. These particles are chemically very active and can oxidize when exposed to air. Fe_3O_4 NPs oxidation result in a partial loss of the magnetic character, thus it is necessary to create a coating for stabilizing the particles [21]. In some cases, the coating merely acts as a barrier protecting the NPs against external agents, but in other cases it can drastically affect the electronic properties of the NPs. The modification of the NP surface by means of bonding specific molecules to the surface atoms plays a crucial role in the minimization of the energy and, consequently, in the stabilization of the system. This modification can also act as a support for a further functionalization of NPs with molecules of interest [22].

I.3 FUNCTIONALIZATION OF NANOPARTICLES

Three types of structure can be identified when NPs are coated: core-shell, matrix and shell$_a$-core-shell$_b$ (figure 1).
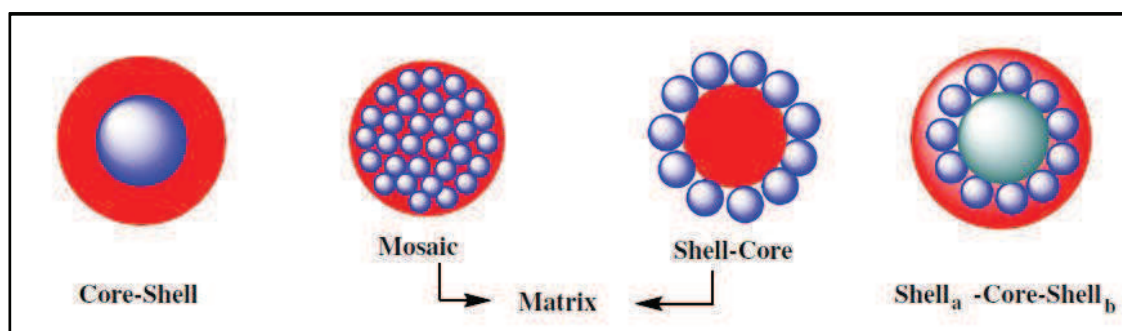

Fig. 1: Different structures for coated NPs [21].

- The first consist of a core of iron oxide NPs coated by any sort of material including organic ones.

- Matrix includes two structures: mosaic and shell-core. In the first one the shell layer, made of organic molecules, is coated to a lot of uniformly IONPs. The second one consists of an organic compound NPs core and IONPs shells connected with the organic core by the interaction of chemical bound.

- In the shell$_a$-core-shell$_b$ structure, a shell layer made of organic molecules is coated to shell-core structurally functionalized IONPs [21].

There are two strategies for introducing functional groups to surfaces and NPs (figure 2).
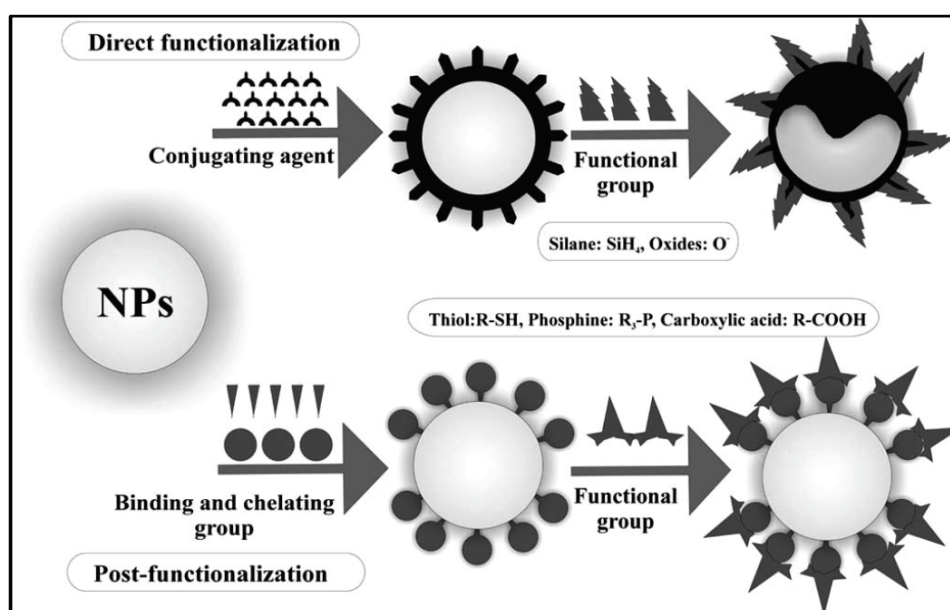

Fig. 2 Two different types of NP functionalizations [23].

The first method is direct functionalization, where the whole functional ligand is a bi-functional organic compound. In this approach, one of the functionally reactive groups is used to attach to the NPs surface (complexing agent) and the second group contains the required active functionality (NP surface modifying group). The second method is post-functionalization, which is generally preferred because of its versatility and because the nature of the functionalizing moieties may not be fully compatible with the NP synthesis conditions. The functionalizing moiety is a bifunctional compound where a binding chelating group is reacted first and the group of coupling site can be converted, in a second step, to the final functional group. Post-functionalization of the particles requires a molecule to be grafted on the surface, producing a structure that can be described as N-C-F (Nanoparticle-Chelating agent-Functional group). For post-functionalization, silane-like compounds have been generally used [23].

Among silane compound of great interest is 3-Aminopropyltriethoxysilane (APTES, figure 3) [24]:
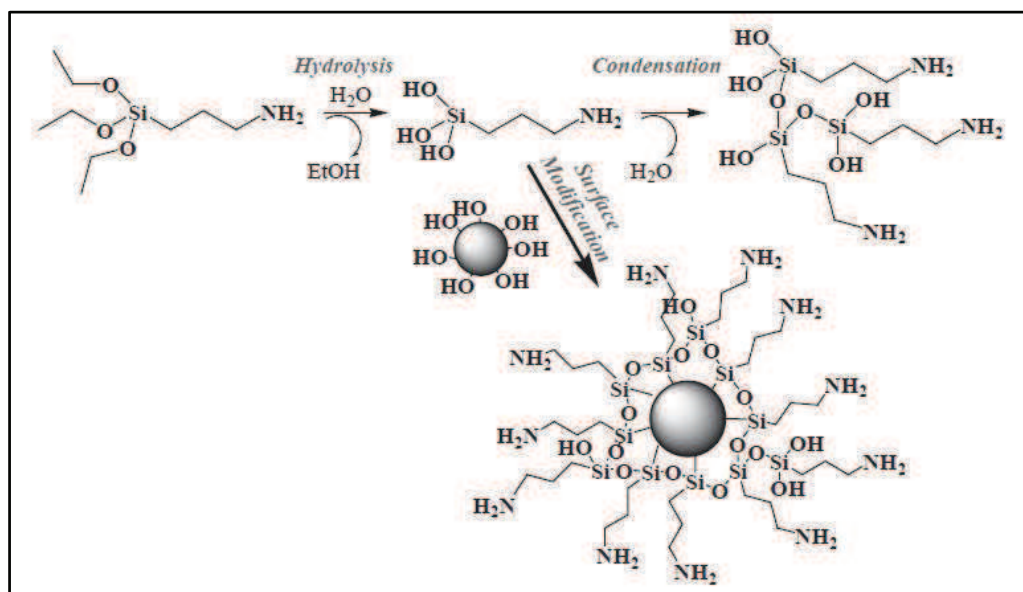
Fig. 3 APTES structure. APTES hydrolysis in water and subsequent condensation to form silane polymer. Silane polymer reacts with NPs.

When APTES is in water, it hydrolyzes and condensates to form a silane polymer. In the hydrolysis reaction, alkoxide groups $-OC_2H_5$ are replaced by hydroxyl groups (OH) to form reactive silanol groups, which condense on the one hand with other silanol groups to produce siloxane bonds (Si–O–Si) and on the other hand with -OH on the NPs surface to produce NP-O-Si bonds. NH_2 groups remain free for further bonds with other molecules [25].

Another very common polymer for functionalization is chitosan and its derivatives. Chitosan is a natural macromolecule consisting of β-1,4-linked 2-amino-2-deoxy-D-glucopyranose and is derived by N-deacetylation of chitin in aqueous alkaline medium.

Since it is a well-known biocompatible, biodegradable and low-toxicity biomaterial, many applications of chitosan have been developed in the biomedical and tissue engineering fields [26]. However chitosan with high degree of acetylation is insoluble in water because of the strong intermolecular hydrogen bonding (H-bond). Nevertheless, some modifications on the –OH and –NH$_2$ position of chitosan can be done to improve its water solubility. Among the numerous water-soluble chitosan derivatives, o-carboxymethylchitosan (OCMCS) is the most promising (figure 4) [27].
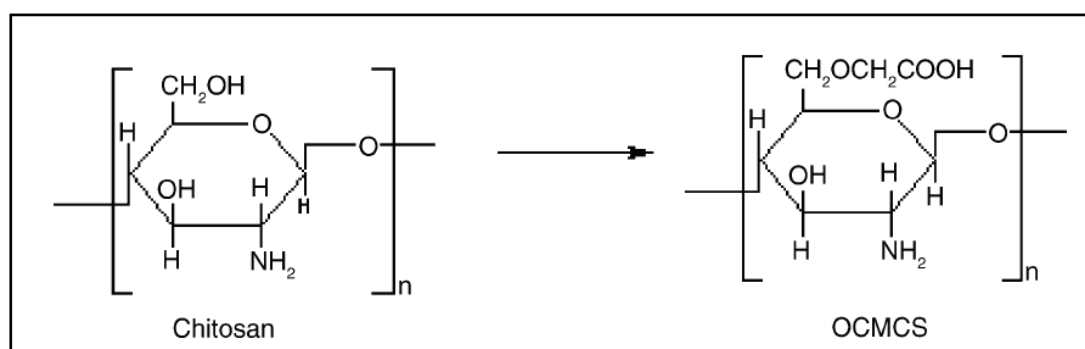
Fig. 4 Chitosan and its derivate o-carboxymethylchitosan monomers [27].

Moreover, also OCMCS can act as a support for further NPs functionalization with molecules of interest, creating a core-shell system for any application [28]. In this study post-functionalization method was used for all NPs produced.

In core-shell particles, the shell thickness can be tuned to provide the binding of biomolecules for the purpose of targeted drug delivery, bio-sensing or whatever application needed, creating a multifunctional particle as shown in figure 5 [29].

Fig. 5 Scheme of multifunctional nanoparticle for molecular imaging, drug delivery and therapy. Optionally functionalized and devised nanoparticles could be achieved for individualized diagnosis and treatments [28].

I.4 NP INTERACTIONS

NPs, either naked or functionalized, may invade the human body via inhalation, ingestion or through the skin.

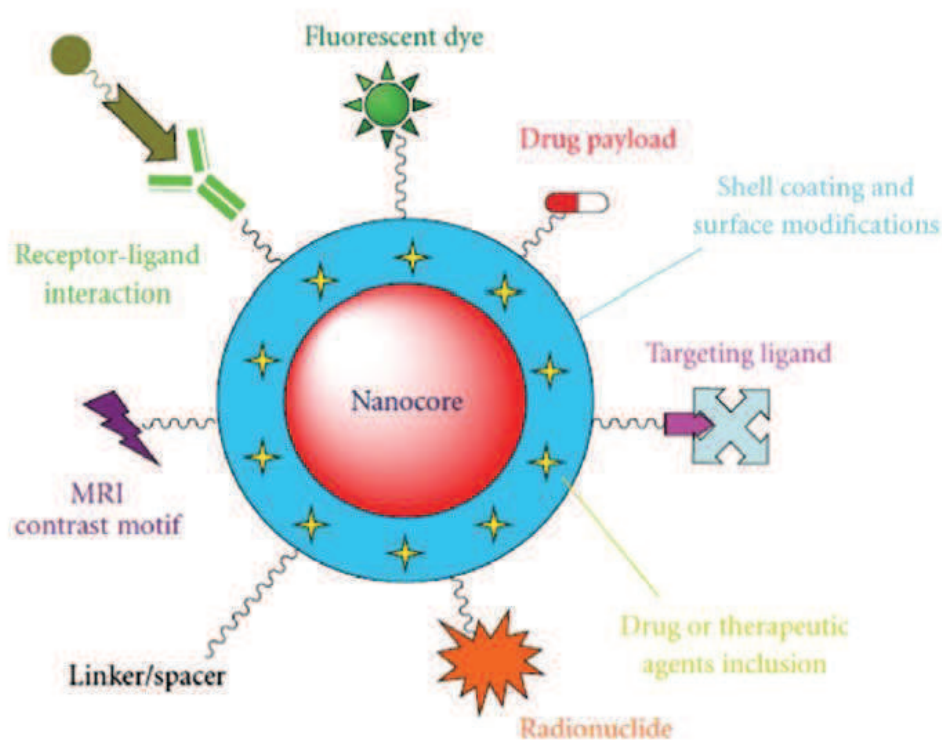Once they have entered a biological milieu, NPs will inevitably come into contact with a huge variety of biomolecules that are dissolved in body fluids (interstitial fluid between cells, lymph or blood). These biomolecules immediately coat NPs and form the so-called 'corona', which determines the biological identity of the NP. The great majority of these molecules are protein. The composition of the corona is dynamic and depends on the relative concentrations of the individual components and on their affinities toward the NP surface (figure 6) [30].
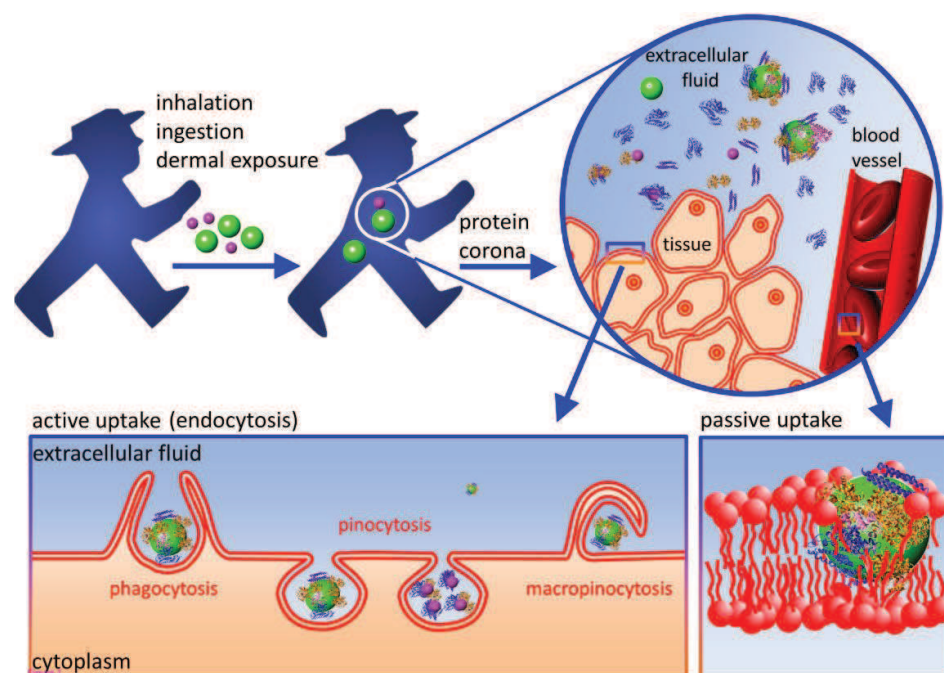

Fig. 6 NPs enter the human body via different way. In extracellular fluids NPs are coated with the protein corona and come into contact with cell membrane, entering cells by active or passive uptake [30].

Corona composition varies also according to NP size and shape. As surface changes from flat to spherical and as the particles become smaller, the composition and organization of associated protein will change dramatically. Indeed, highly curved surfaces can suppress protein adsorption to the point where it no longer occurs. As already said, the protein corona is a dynamic identity, so it is important to highlight that it is not just the composition and organization of this protein layer, but the exchange times of the protein on the nanoparticles that is "read" by cells. Moreover the exchange process is important when particles redistribute from one compartment or organ to another, such as upon uptake into cells from the bloodstream, or upon transport from the cytosol to the nucleus [31].

Once entered the human body, NPs have to surmount the cell membrane. Large macromolecular agglomerates, protein assembles, virus and also NPs are encapsulated in vesicles and selectively transported into and out the cell via endo- or exocytosis. Different types of endocytosis mechanisms are known (figure 6), but regardless of the specific internalization mechanism, the cell-NPs interactions are, on the one hand, modulated by physicochemical properties of the NPs including size,

shape, surface charge and surface chemistry [32] and, on the other hand, by cell-specific parameters such as cell type or cell cycle phase [33].

A size-dependent uptake in different cell lines has been observed for Au [34, 35, 36], mesoporous silica [37], polystyrene [38] and iron oxide NPs [39], with the maximum cellular uptake at a NP core size in the range of 30–50 nm, which suggests that there is an optimal size for active uptake. The size-dependent interaction of NPs with the cell membrane is likely related to the membrane-wrapping process that initiates receptor-mediated endocytosis. Small NPs have less ligand-to-receptor interactions than larger ones; thus, several small NPs need to interact simultaneously with receptors in close proximity to trigger membrane wrapping. In contrast, an individual large NP can act as a cross-linking agent to cluster receptors and induce uptake. Thermodynamically, a 50-60 nm NP is capable of recruiting enough receptors to successfully trigger internalization. The nature of the protein corona, which is controlled by the NP surface ligands, may also affect the membrane response and, thereby, modify the cellular responses toward the NPs [40, 41].

The size, as well the coating, can also influence the subcellular distribution of the internalized NPs. Lovrić et al. demonstrated that positively charged 5.2-nm CdTe QDs were distributed throughout the cytoplasm of N9 cells but did not enter the nucleus, whereas positively charged 2.2-nm QDs were localized predominantly in the nuclear compartment [42].

Once inside a cell or tissue, the surface layer, including the adsorbed biomolecules, and also the NP core material will likely be metabolized. Subsequently, the organism may excrete the remnants of the NPs. These processes are again dependent on the physicochemical properties of NPs including their size [43].

All these interactions with the biological environment can trigger toxicity (figure 7). Smaller NPs appear to be more toxic than larger ones. Small NPs possess a high surface area relative to their total mass, which increases the chance to interact with surrounding biomolecules and, as a consequence, to trigger adverse responses. Surface functionalization also plays important roles. For example, cationic NPs are considered more toxic than neutral or anionic ones, possibly due to their high affinity towards the negatively charged plasma membrane.
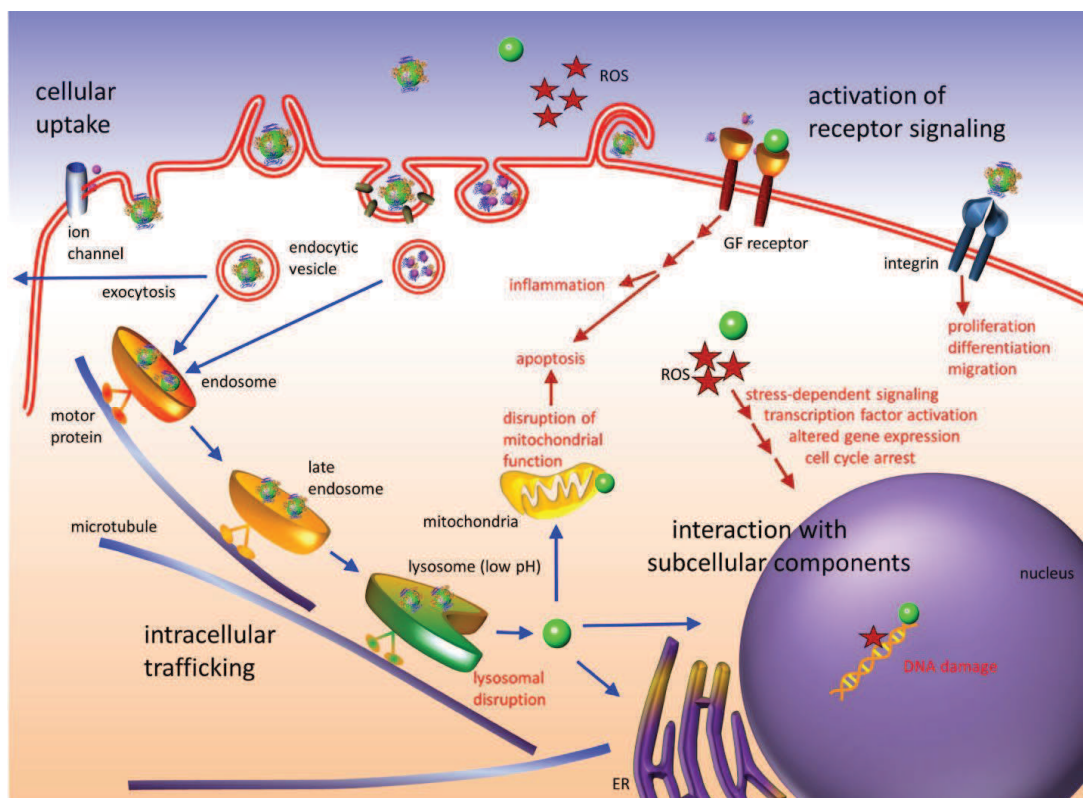
Fig. 7 NPs may interact with membrane bound cellular receptor and, after internalization, with pathways inducing cell responces and maybe citotoxic effect [30].

In conclusion the size, shape, surface functionalization and chemistry of NPs has a strong effect on their interactions with living cells, influencing uptake efficiency, internalization pathway selection, intracellular localization and cytotoxicity [30].

I.5 APPLICATIONS

Although nanotechnology is a relatively new branch of science, it has found a large use in many fields. The potential of engineered sub-micron structures, which are

comparable in size to biological molecules, has been recognized ever since the 1950s. However, the rapid development of applied nanotechnology only began in the 1990s following the discovery of the Nobel Prize-winning technique scanning tunneling microscopy and, several years later, atomic force microscopy [44]. Both these methods, which allow the visualization and handling of small-scale physical matter with exceptional accuracy, triggered an exponential growth in nanoscience. By the year 2000, nanotechnology was universally recognized as a landmark innovation, and named the sixth truly revolutionary technology introduced in the modern world [45]. In response to the widespread practical applications of nanotechnology, many countries have introduced specialized courses in nanoscience as part of high school, undergraduate and graduate curricula, and promoted dedicated international research initiatives [46]. Over the last decade, nanotechnology has been extensively introduced into biological, medical and industrial applications [47]. Estimates suggest that the number of nanotechnology patents, related only to healthcare, has increased from less than 200 in the year 2000 to nearly 10,000 by the year 2010, doubling almost every three

years and thus reflecting the rapid expansion of this pioneering industry [48].

Among the most recent applications could be included those concerning water purification, wastewater treatment [49], environmental remediation [50], food processing and packaging [51], agriculture production and crop protection [52]. The majority of applications in these areas have focused on the nanomaterials for improved efficiency and productivity.

I.5.1 MEDICAL APPLICATIONS

Nanoparticles used in biomedical applications include liposomes, polymeric micelles, inorganic and polymeric nanoparticles, nanorods and quantum dots. All have been tested pre-clinically or clinically for targeted drug/gene delivery or as agents to enhance diagnostic imaging output like in MRI [53]. Other nanoparticles, like water-soluble synthetic polymers (dendrimers), were tested in pre-clinical models for the delivery of drugs, genes and as imaging agents, showing a rich versatility for tailoring their binding properties to several requirements, among them facilitation of cellular uptake of drugs (e.g. cancer drugs) [54, 55].

On-going improvement in the safety of biomedical nanomaterials, along with the accumulation of experimental evidence supporting the benefits of nanomaterial-based agents in terms of selectivity, sensitivity, affinity and detection limits, has led to the expansion of nanobiotechnological tools in a number of applications (such as cardiovascular, neurological gastrointestinal, autoimmune inflammatory, infectious and, reproductive diseases). Nevertheless, traditionally, the main scope of nanobiotechnology lies in the field of cancer diagnostics and treatment, with the aim to select and destroy affected cell populations with ultimate precision [44].

NANOONCOLOGY

The impact of nanobiotechnology on oncology (shown schematically in figure 8) is huge and includes fields ranging from discovery of tumor biomarkers to development of devices for cancer surgery [56]. In particular, drug-delivery is the most explored field, which aims to design carriers that deliver drugs more precisely to tumor cell and maintain them at a therapeutic concentration over a long period. Besides considerable progress in cancer therapy and the many anticancer

drug approved and in phase II clinical trials (http://www.cancer.gov/CLINICALTRIALS), treatment of cancer still has a lot of side effects [57]. For this reason nanoparticles could be an efficient alternative to conventional tumor therapies, serving as systems capable of enhancing efficacy, while simultaneously reducing side effects.
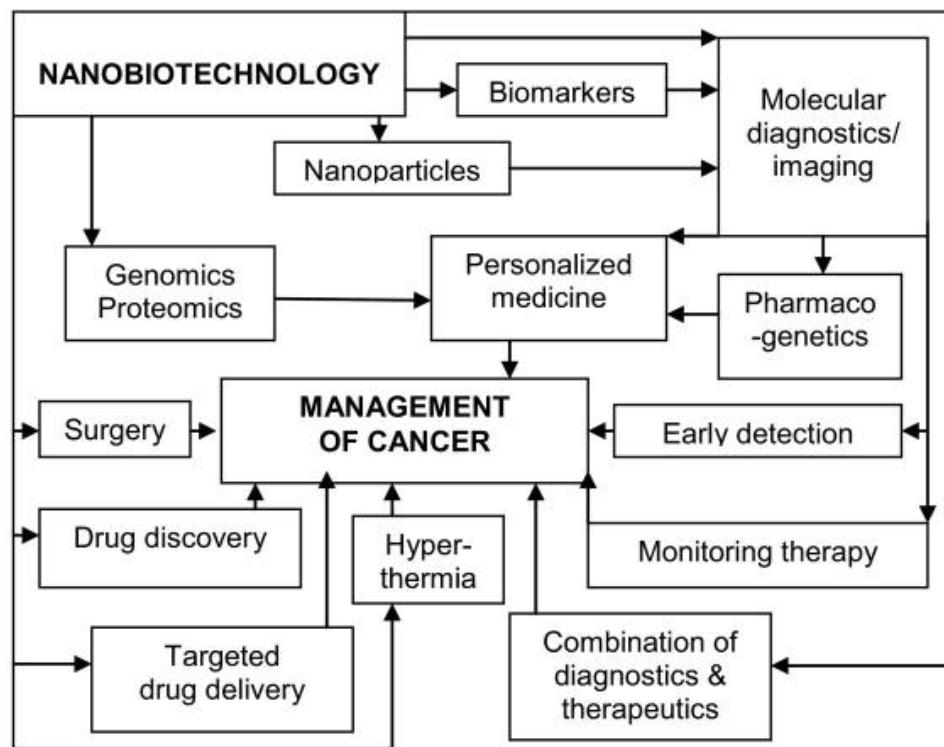

Fig. 8 Role of Nanobiotechnology in the management of cancer [56].

There are two cancer specific physiological strategies: passive targeting by Enhanced Permeability and Retention (EPR) effect or active targeting. The first strategy takes advantage of the peculiar physiology of

tumor in respect of normal tissue. Tumor presents an enhanced permeability of vessels with a little lymphatic drainage, leading to a passive accumulation and retention of NPs with prolonged circulation times (EPR effect).

The second strategy may exploit molecular binding receptor or magnetic guidance. NPs, in fact, on the one hand can be modified with surface markers that enable their specific recognition by target cells, facilitating effective delivery in the tumor tissue. On the other hand, magnetic NPs can be functionalized with anticancer drug and guided along an externally placed magnet into the tumor. Moreover, magnetic NPs produce heat through various energy losses under an external alternating magnetic field, causing cancer destruction by activating cell-death signaling (hyperthermia) [58]. Many works have been published in the literature in this regard [59-63].

I.5.2 INDUSTRIAL APPLICATIONS

Maybe more than in medicine, nanotechnology has expanded in industrial area, where, by now, NPs are used in almost each field. Table 1 gives an overview of

industrial market segment based on nanoparticulate material (table 1).

Automotive industry	Chemical industry	Engineering
• lightweight construction • painting (fillers, base coat, clear coat) • catalysts • tires (fillers) • sensors • Coatings for windscreen and car bodies	• fillers for paint systems • coating systems based on nanocomposites • impregnation of papers • switchable adhesives • magnetic fluids	• wear protection for tools and machines (anti blocking coatings, scratch resistant coatings on plastic parts, etc.) • lubricant-free bearings
Electronic industry	**Construction**	**Cosmetics**
• data memory (MRAM, GMR-HD) • displays (OLED, FED) • laser diodes • glass fibres • optical switches • filters (IR-blocking) • conductive, antistatic coatings	• construction materials • thermal insulation • flame retardants • surface-functionalised building materials for wood, floors, stone, facades, tiles, roof tiles, etc. • facade coatings • groove mortar	• sun protection • lipsticks • skin creams • tooth paste
Textile/fabrics/non-wovens • surface-processed textiles • smart clothes	**Energy** • fuel cells • solar cells • batteries • capacitors	**Sports /outdoor** • ski wax • antifogging of glasses/goggles • antifouling coatings for ships/boats • reinforced tennis rackets and balls
Food and drinks • package materials • storage life sensors • additives • clarification of fruit juices	**Household** • ceramic coatings for irons • odors catalyst • cleaner for glass, ceramic, floor, windows	

Table 1 Overview of material based on nanotechnology in different areas [64].

Nanotechnology has aroused much interest particularly in enzyme biocatalysis, where nanomaterials can provide the upper limits on enzyme-efficiency-determining factors [65].

Enzyme Biocatalysis

Enzymes are versatile biocatalysts and are useful in many areas of research, including organic synthesis, immunoassays, and substrate sensing. The specific chemo-, regio-, and stereoselectivity of enzyme-mediated transformations remarkably demonstrate their superiority compared to chemical catalytic reactions [66]. However, the use of free enzymes shows some significant drawbacks, such as thermal instability, susceptibility to attack by protease, activity inhibition, high sensitivity to several denaturing agent and the impossibility of separating and reusing free catalysts at the end of reaction.

Among the countless procedure for circumventing these constrains and improve enzyme stability, enzyme immobilization is the most worthy. Immobilized enzymes have the advantage of a larger pH range and better thermal stability, in addition to an easy separation from the solution. Immobilized enzymes have the advantage of being easily removed from the bioreactor and replaced when they lose their activity. Other advantages are enhanced enzyme activity, modification of substrate selectivity/enantioselectivity and multienzyme reaction [67, 68]. Moreover many biomolecules, such as

membrane proteins, perform their specific biorecognition or biocatalytic events while immobilized on the surfaces of cells or organelles; hence also these enzymes take advantage of their immobilization.

Several synthetic scaffolds and supports, including gels, macromolecules, planar surfaces, and nanocomposites, have been used to immobilize enzymes. Among them, NPs provide an almost ideal mix of properties (minimal diffusional limitation, maximum surface area and high effective enzyme loading) to optimize the performance of immobilized enzymes, while harnessing the fluorescent, magnetic and interfacial behavior of the resulting nanomaterial [69]. Compared with enzymes immobilized on micrometric supports, a nanobiocatalyst could achieve a much higher enzyme loading capacity and significantly enhanced mass transfer efficiency [70]. Magnetic NPs have received increasing attention due to their distinct properties such as ease of surface modification and magnetic character, which facilitate the recovery using a magnetic field [66]. Among magnetic NPs, Fe_3O_4 NPs have recently emerged as promising supports for immobilization because they are cheap and biocompatible. In particular, Fe_3O_4 nanoparticles coated with a thin layer of silica have

beneficial properties, such as invariant catalytic activity and stability [71].

I.II   NANOPARTICLE   SYSTEMS   FOR   MEDICAL   APPLICATIONS

II.1 ANTITUMOR SYSTEM: Fe₃O₄ NP@DAAO

The purpose of the first part of my study concerns the manufacture of a magnetic NPs system for cancer therapy. The system is proposed as a broad spectrum, low cost and potentially able to cross biological barriers (such as the blood-brain barrier) alternative to conventional tumor therapies. It is composed of magnetic iron oxide NPs conjugated with the ROS generating enzyme D-aminoacid oxidase (DAAO). Fe_3O_4 NP@DAAO wants to combine the advantages of magnetic NPs (low-toxicity, specific target by a magnetic field, ability to cross biological barriers) with those of DAAO (no-toxicity, easy modulation of the activity, hence of ROS generation). The system can be i.v. Injected and addressed by an external magnetic field in the tumor area. Here D-amino acids (naturally present or externally injected) act as substrate for the enzyme, causing H_2O_2 production and tumor cell death by apoptosis (figure 9).

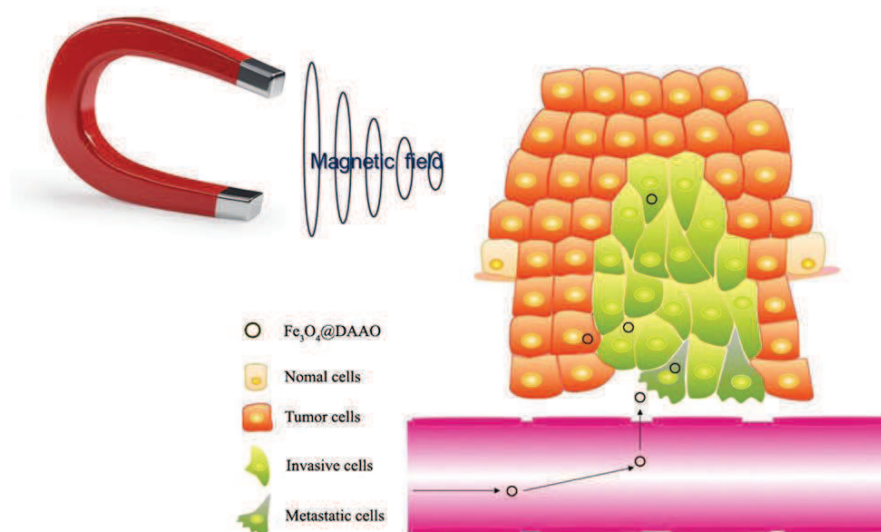**Fig. 9** Schematic representation of Fe_3O_4 NPs@DAAO antitumor system.

II.1.1 DAAO

DAAO is a flavoenzyme and catalyzes the dehydrogenation of D-amino acids to yield a-imino acids and, upon subsequent hydrolysis, a-ketoacids and ammonia. Oxygen, the terminal redox acceptor, reoxidizes the reduced FAD cofactor to give hydrogen peroxide [72].
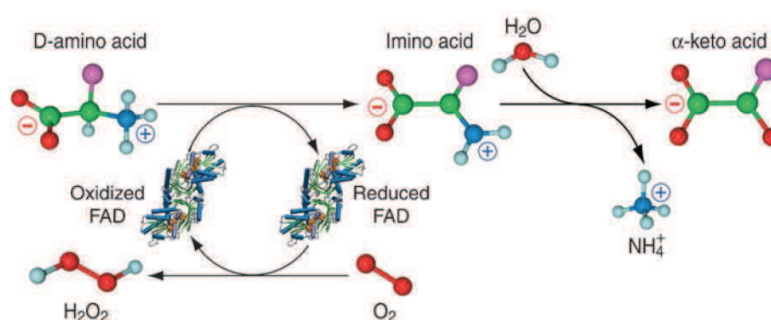

Fig. 10 Scheme of the reaction catalyzed by D-amino acid oxidase [73].

This flavoxidase was discovered in 1935 by Krebs and all the chemical aspects of the enzyme reactivity were described in detail between 1950 and 1990, using the protein purified from pig kidney (pkDAAO) that for many years represented the only DAAO available in fairly good amounts and in a homogeneous form. Starting in the mid-1980s, other DAAO proteins became available, especially from the microorganisms (*Rhodotorula gracilis*, RgDAAO and *Trigonopsis variabilis*, TvDAAO) and, few years ago, even human DAAO (hDAAO) was cloned. Putative DAAO genes have been identified in all kingdoms; the main exception is represented by plants, in which a DAAO was purified only from the alga *Chlorella vulgaris*. DAAO is present in prokaryotes and is almost ubiquitous in eukaryotic organisms, from the simplest such as fungi, through fish to mammals, where it is present mainly in the kidney, liver and brain [73].

DAAO IN PROKARYOTES

In prokaryotes there is a flavoenzima called D-amino acid dehydrogenase (DAAdH), which oxidizes D-amino acids into the corresponding a-ketoacids. DAAdH in *E.coli* is a heterodimer composed of two subunits of 45 and 55 kDa; the smallest contains FAD as a coenzyme. It seems to be a peripheral membrane protein, associated

with the inner membrane of the cell and appears to have a dual role: it permits the bacteria growth (allowing the use of D-amino acids as a source of energy) and it prevents the local concentration of amino acids, which could have an inhibitory effect on bacteria growth [74].

DAAO IN EUKARYOTES

In eukaryotic microorganisms, such as fungi, DAAO is a peroxisomal enzyme. This location allows an efficient removal of the toxic hydrogen peroxide produced during the reaction.

RgDAAO is a very stable homodimer; each subunit binds a FAD non-covalently. The primary structure of RgDAAO comprises from 345 to 368 amino acids, corresponding to a molecular mass of 40076 Da for monomer [73].
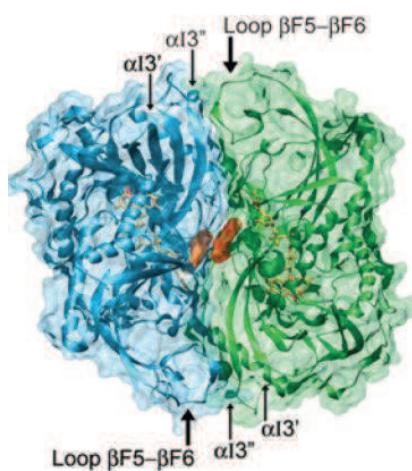

Fig. 11 Monomer-monomer interaction, head-to-tail, in *R. gracilis*. The thick arrows identify the βF5-βF6 loop and the thin arrows identify the α-helices αl3 and αl3 [73].

The secondary structure consists of 11 α-helices and 13 β-sheets. The N-terminus contains the dinucleotide-binding domain characterized by a motif βαβ. The whole cofactor is buried inside the protein. The C-terminus contains a long loop of 21 amino acids (not present in other known DAAO sequences), which is involved in the head-tail dimerization. The active site of RgDAAO is a cavity delimited by the two long β-strands I4 and I8 bent around the isoalloxazine ring of the flavin and the two short β-strands I5 and I6 situated close to the substrate-binding site. The flavin forms the "bottom" of the cavity. All these β-strands have an antiparallel orientation and are connected to each other by H-bonds resulting in a rather rigid arrangement [75].

DAAO BIOLOGICAL ROLE IN EUKARYOTES

The biological role of the D-amino acid oxidase is to metabolize D-amino acids, which are derived from exogenous and endogenous sources. D'Aniello and colleagues in 1993 showed that about 80% of D-amino acids in the diet is metabolized by the organism. The D-amino acids once oxidized in the corresponding α-ketoacids, can be on the one hand converted into L-amino acids and integrated into the proteins, on the other hand used directly for the metabolism. If the D-

amino acids are not metabolized, accumulate in tissues and cause extensive damage [76]. Accumulation of D-amino acids in mammals is one of the characteristics of aging; accumulation of D-aspartate was observed in the white matter of the human brain. Recently it was also found that DAAO has a very important role in maintaining adequate levels of D-serine in different brain tissues. D-serine is an important regulator of the receptors N-methyl-D-aspartate (NMDA) which dysfunction, due to erroneous DAAO gene expression, is one of the possible causes of schizophrenia. Finally, it was found a lower activity of DAAO in tumor cells of kidney and liver compared to the healthy ones and therefore this parameter could be used for early tumor detection in these organs [77].

INDUSTRIAL AND MEDICAL APPLICATIONS OF RGDAAO

The most important industrial application of DAAO is the enzymatic deamination of cephalosporin C to 7-(5-oxoadipoamido) cephalosporanic acid, a key intermediate for the production of semisynthetic cephalosporins. This reaction without the use of DAAO would be very laborious and expensive, so this enzyme allows a faster and cheaper production of semisynthetic cephalosporin antibiotics. Among all DAAOs, RgDAAO is

preferred because of its high turnover rate and FAD binding stability [78].

In the medical field the DAAO can be used for the production of a-ketoacids, these are used as a food additive for patients with chronic uremia. Moreover, the production of hydrogen peroxide by DAAO immobilized on a support can be used for the tumor treatment.

DAAO AND TUMORS

DAAO may be regarded as a promising anticancer therapeutic whether used in protein therapy [79], gene therapy [80] or as a ROS generating enzyme. In this last case DAAO may act as angiogenesis inhibitor in combination with other factor like 3-bromopyruvate and citrate [81], or as an apoptosis enhancer by production of H_2O_2 [82]. In this regard many ROS generating enzyme have attracted interest in the past, like glucose oxidase (GO) or xanthine oxidase (XO). However, regulation of ROS production is critical. Exogenous administration of GO substrate (oxygen and glucose) is problematic because the availability of its substrates cannot be significantly modulated.

Similarly XO production of superoxide cannot be regulated *in vivo*, because it is a promiscuous enzyme

with a wide range of ubiquitous substrates. DAAO, on the contrary, is an optimal candidate for ROS generating therapy, because D-amino acid are poorly present in human organism and the stereoselectivity of *Rhodotorula gracilis* DAAO appears to be absolute. Thus, production of ROS by RgDAAO in tumor cells could be regulated by exogenous administration of D-amino acids [83].

II.2 ANTIBACTERIAL SYSTEM: NP@TEICOPLANIN

This medical system is composed of magnetic iron oxide nanoparticles (Fe_3O_4) conjugated with the antibiotics teicoplanin. Similar to the previous system, NP@Teicoplanin wants to takes advantage of the magnetic character of NP for a specific targeting of the antibiotic.

II.2.1 ANTIBIOTICS CONCERN

Pathogenic bacteria remain a major health concern, because they are responsible of a large number of deaths and hospitalizations each year. Despite the great progress in antimicrobial development, many infectious diseases, especially intracellular infections, remain difficult to treat. One major reason is that many antimicrobials are difficult to transport through cell

membrane and have low activity inside the cells, thereby imposing negligible inhibitory or bactericidal effects on the intracellular bacteria. In addition, antimicrobial toxicity to healthy tissue poses a significant limitation to their use [84]. Moreover bacteria are gaining resistance at an alarming rate, that is why new therapeutic are necessary. A range of potential solutions has been researched and a large group of these studies includes the implementation of nanotechnologies and nanomaterials to create new antibacterial nanomedicines that increased effectiveness and efficiency [84]. The first advantage produced by NPs is the reduction of antibiotic dose. Usually for therapeutic purpose, the amount of antibiotics often given for the treatment is much higher than the dose required for killing the pathogens. It has been reported that ampicillin loaded NPs, used for the treatment of salmonella infection in mouse, reduce the drug by 40 folds compared to free ampicillin [85]. Moreover, in some cases the activity of the antibiotic result enhanced by linkage to or in combination with NPs [86, 87, 88]. This is very important because recently has emerging resistance to the so-called "last-resort drugs" such as vancomycin and teicoplanin, which are typically used to

treat infection by pathogens that resist more commonly used antibiotics. Immobilization of these antibiotics on NP may be a very important innovation able to solve resistance emergency [89].

II.2.2 TEICOPLANIN

Teicoplanin from *Actinoplanes teichomyceticus* is a glycopeptide antibiotic of the vancomycin family. It binds to the D-Ala-D-Ala terminus on the cell wall of gram-positive bacteria by hydrogen bonding, thereby preventing enzyme-mediated crosslinking of peptidoglycan and eventually leading to cell death.
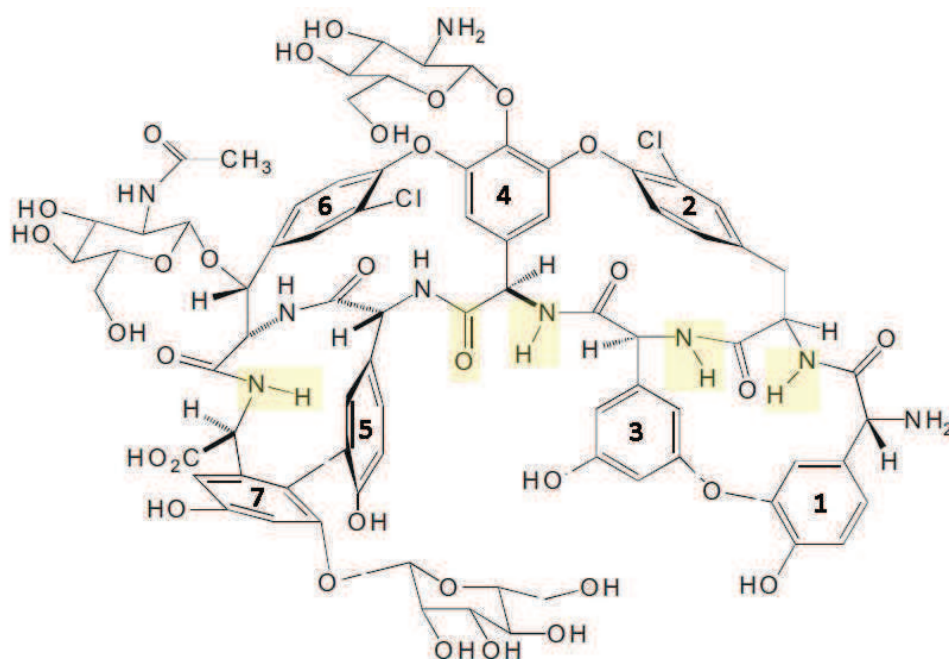
Fig. 12 Structure of teicoplanin from *Actinoplanes teichomyceticus*. Atoms involved in hydrogen bond with substrate are marked in yellow.

Although it is not routinely used in hospitals, teicoplanin is more active than vancomycin against *Staphylococcus* species, including methicillin-resistant strains. Teicoplanin has fewer side effects and exhibits a longer half-life in humans [90]. Teicoplanin binds its cell-wall peptide target with higher affinity than vancomycin and most other glycopeptide antibiotics. Teicoplanin interact with its ligand as a monomer, rather than a back-to-back dimer as vancomycin does; nevertheless teicoplanin is speculated to recognize its ligand in the same manner as vancomycin via five hydrogen bonds (figure 13).
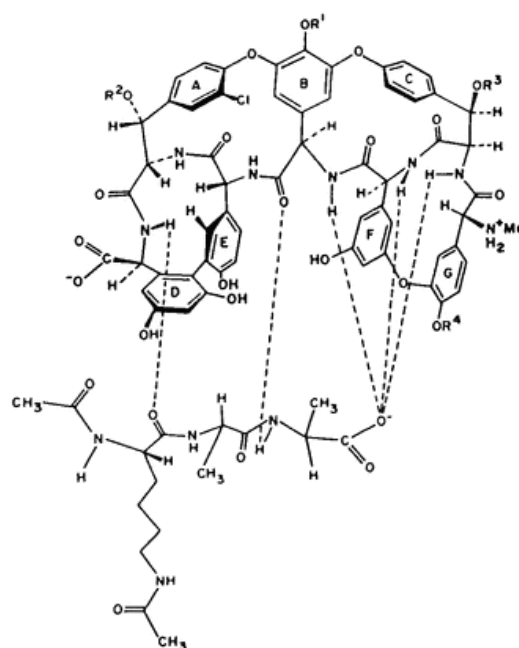
Fig. 13 Diagrammatical representation of the interactions between a peptide ending in –D-Ala-D-Ala and the aglycone of a glycopeptide.

Teicoplanin adopts a curved conformation, with the N- and C-terminus of the antibiotic closing around the target peptide to form a concave binding pocket. The mannose attached to amino acid 7 at the C-terminal end of the antibiotic interacts with a hydroxyl group on the side chain of amino acid 1 at the N-terminal end of the molecule, forming a hydrogen bond; the side chains of amino acids 1 and 7, together with the mannose, form the floor of the ligand-binding pocket. The peptide backbone, together with the side chains of residues 2, 4 and 6, form the rear of the binding pocket. The top of the binding pocket is formed by the glucosamine sugar attached to the side chain of residue 4, which projects outward over the concave binding pocket. The fatty-acyl chain attached to the glucosamine lies on the back (convex) face of the antibiotic. This positioning of the acyl chain sterically prevents teicoplanin from forming the types of back-to-back dimers that are observed with many other glycopeptide antibiotics, such as vancomycin. An additional sugar moiety, an N-acetyl glucosamine attached to amino acid 6, contributes steric bulk that may also contribute to blocking back-to-back dimer formation [91].

I.III NANOPARTICLE SYSTEMS FOR INDUSTRIAL APPLICATIONS

In industrial enzymatic application processes, immobilization of enzymes can offer several advantages, including the ability to be used repeatedly, improvement of enzyme stability and broadening the optimum pH range of enzyme [92].

III.1 NP@ACYLASE

Semisynthetic cephalosporins are the most widely used antibiotics and are primarily synthesized from 7-aminocephalosporanic acid (7-ACA), which is usually obtained by chemical deacylation of the natural antibiotic cephalosporin C (CephC). The chemical route includes, however, several expensive steps and requires treatment of toxic wastes. A two-step enzymatic route can also be used that, in two separate reactors, uses DAAO and glutaryl-7-amino cephalosporanic acid acylase (gl-7ACA) activity (figure 14). Although this route solves the environmental safety problems, it is also expensive and not entirely satisfactory for industrial production. Therefore, enzymatic conversion of CephC to 7-ACA is of great interest to cephalosporin antibiotics

manufacturers (an annual worldwide market of 400 million US dollars has been estimated) [93].
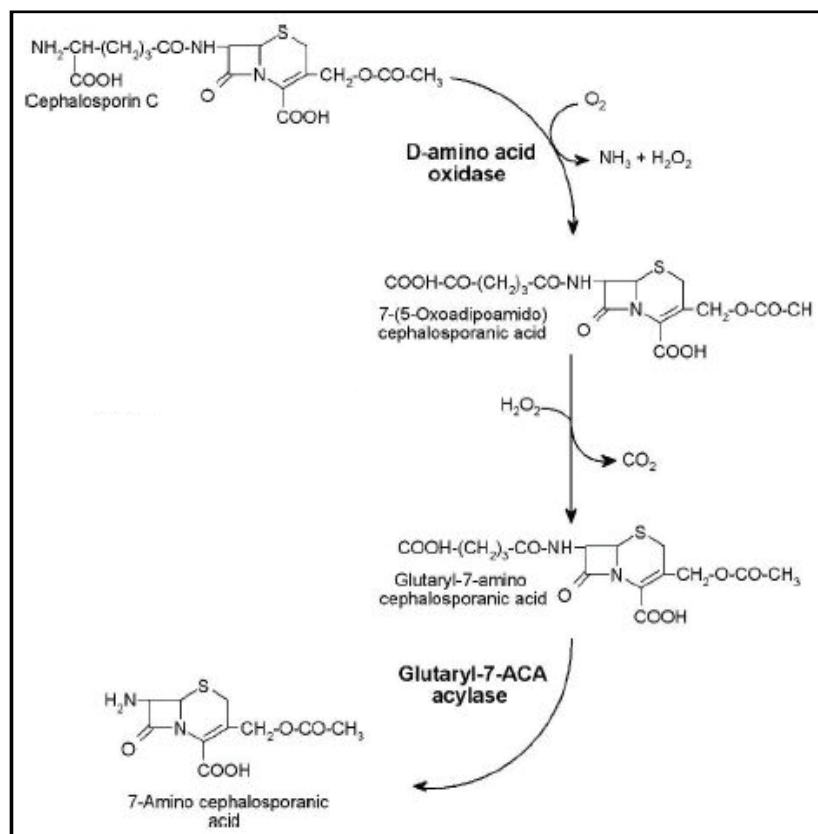
Fig. 14 Bioconversion of CephC into 7-ACA [93].

Several groups have attempted to implement a "one-step" conversion of CephC by using DAAO and gl-7ACA in a single reactor, but the process still comprises two enzymatic conversions and has some drawback. The main problem is that DAAO produces hydrogen peroxide as a by-product; H_2O_2 affects DAAO as well as gl-7ACA stability. To solve this problem is necessary also the addition of catalase in the reaction.

The alternative enzymatic approach is a one-step process in which CephC is directly converted to 7-ACA by a true CephC acylase. This approach is very attractive at the industrial level because of the prospects of simplifying the process and reducing costs (figure 15).
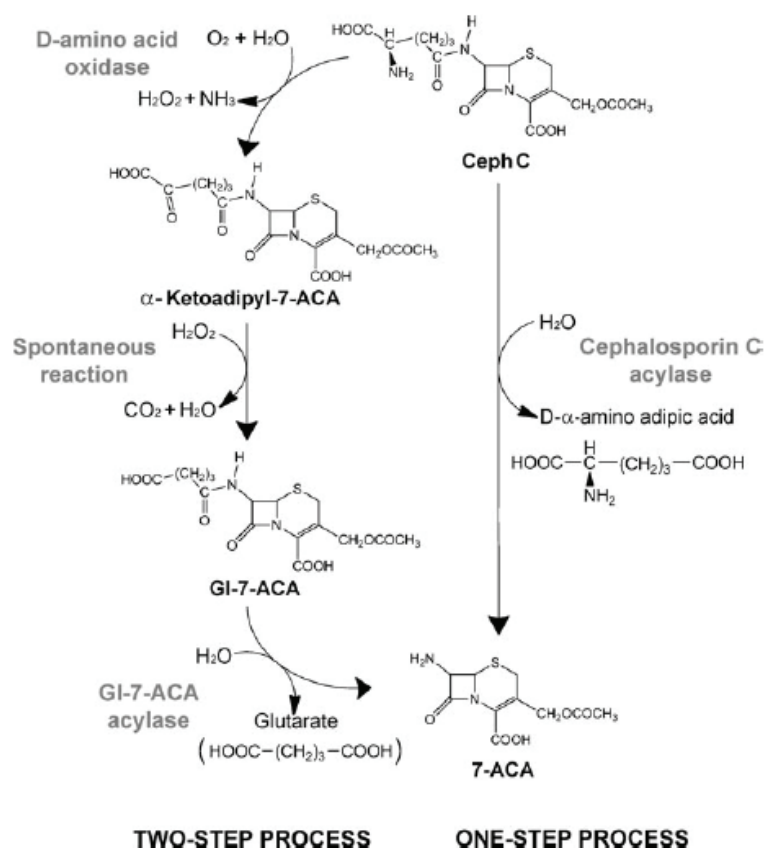
Fig. 15: Bioconversion of CephC. *Left*: two-step conversion by DAAO and gl-7ACA acylase. *Right*: one step conversion by CephC acylase [94].

However the great hindrance is that this enzyme takes 7ACA as primary substrate and its activity is too low for CephC.

III.1.1 VAC Acylase

Gl-7ACA acylase are members of the N-terminal hydrolases class of hydrolytic enzymes. According to their substrate specificity and sequence conservation, known glutaryl acylases have been divided into five classes. While all gl-7ACA are active on 7-ACA, only member of class I and II show an appreciable activity on CephC. Gl-7ACA acylases form *Pseudomonas diminuta* N176 showed the highest activity on both 7-ACA and CephC [94]. Numerous effort have been made for improve N176 acylase activity on CephC. Recently Pollegioni *et al.* designed, on the basis of the primary sequence of N176 acylase, a synthetic gene named VAC, which has been used as the starting scaffold to develop a CephC acylase. They introduced genetic variability into the VAC cDNA using random mutagenesis and saturation mutagenesis, finding 3 mutants showing an increase in kinetic efficiency on CephC compared to wild-type VAC (see table 2). Among these mutants H296S-H309S has the lowest K_m and a decrease of 22-fold in the kinetic efficiency on 7-ACA compared to wild-type. Moreover, like other mutants, H296S-H309S do not shows any substrate inhibition and is less sensitive to inhibition by

product [93]. For these reasons in this study the mutant H296S-H309S was used.

	CephC			gl-7ACA		
	V_{max} (U/mg)	K_m (mM)	V_{max}/K_m	V_{max} (U/mg)	K_m (mM)	V_{max}/K_m
Wild type	0.7	11	0.06	24.2	1.6	15.1
Combination of multiple mutations						
A215Y-H309S	3.9	17.2	0.23	41.7	0.9	44.4
H296S-H309S	3.0	12.2	0.24	4.8	6.9	0.7
A215Y-H296S-H309S	3.8	17.8	0.21	2.7	2.5	1.1

Tab. 2 Kinetic properties of purified wild type and mutants of VAC on CephC and 7ACA as substrate. Highlighted mutant used in this study [93].

With the aim to further improve the one-step conversion of CephC to 7-ACA H296S-H309S VAC acylase was immobilized to Fe_3O_4 magnetic NPs. This conjugation could allow a simplest reuse and a greater stability of the enzyme, leading to a reduction of costs.

III.2 NP@LASPO

The last enzyme system for industrial application designed in this study is composed of Fe_3O_4@APTES NPs conjugated to L-aspartate oxidase (LASPO).

III.2.1 LASPO

LASPO is a prokaryotic enzyme that catalyzes the first step of de novo nicotinamide adenine dinucleotide (NAD^+) biosynthesis: the product iminosuccinate *in vivo* is condensed with dihydroxyacetone phosphate resulting

in the production of quinolinate and, eventually, NAD+. *In vitro* LASPO can use both O_2 and fumarate in cofactor re-oxidation, which enables it to perform catalysis under both aerobic and anaerobic condition. In fact, under aerobic condition, free LASPO oxidizes L-aspartate to iminosuccinate, which is then nonenzymatically hydrolyzed to oxaloacetate (figure 16).
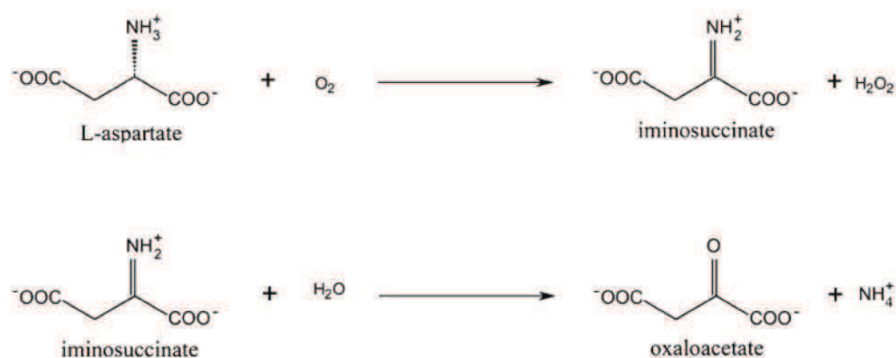
Fig. 16 oxidation of L-aspartate to iminosuccinate by LASPO and subsequent nonenzymatically hydrolyzation to oxaloacetate [96].

Among LASPO from different prokaryotes, those from thermophilic microorganisms, such as *Sulfolobus tokodaii* (StLASPO), are of potential interest. StLASPO is monomeric (52 kDa) in solution, show the classical properties of FAD-containing oxidases and possesses a high thermal stability: the enzyme is fully stable at 80°C. StLASPO shows distinctive features that makes it an attractive tool for biotech applications: high thermal

stability and high temperature optimum, stable activity in a wide range of pH (7.0-10.0), weak inhibition by the product oxaloacetate and by D-aspartate and thigh binding of the FAD cofactor. Recombinant StLASPO was efficiently used for the resolution of a racemic mixture of D, L-aspartate: low amount of StLASPO (9U) allowed to reach quantitative conversion and >99.5% e.e.. Indeed and because of the high stability, this enzyme can be used for additional cycles of bioconversion. Conjugation on a support like NPs could further improve StLASPO qualities [95, 96, 97].

CHAPTER II

SYNTHESIS OF MAGNETIC NANOPARTICLE SYSTEMS FOR CANCER THERAPY: NP@DAAO

II.I: MATERIALS AND METHODS

IN VITRO STUDIES

ENZYMES

In this work three variants of DAAO were used: the wild type RgDAAO (named DAAO) and two mutants, R285ADAAO (named R285A) and 1903DAAO (named 1903). In the first mutant the arginine (R) 285 has been substituted with an alanine (A), generating a non-active DAAO [98]. 1903 mutant contains 5 amino acid substitutions: Serine in 19 has been substituted with glycine (S19G), serine in 120 with proline (S120P), lysine in 321 with methionine (K321M), alanine in 345 with valine (A345V) and glutamine in 144 with arginine (Q144R). These substitutions do not affect the contents of secondary and tertiary structure of the protein, but enhance the activity of the enzyme at low oxygen concentrations [99].

Fe$_3$O$_4$ NPs@APTES
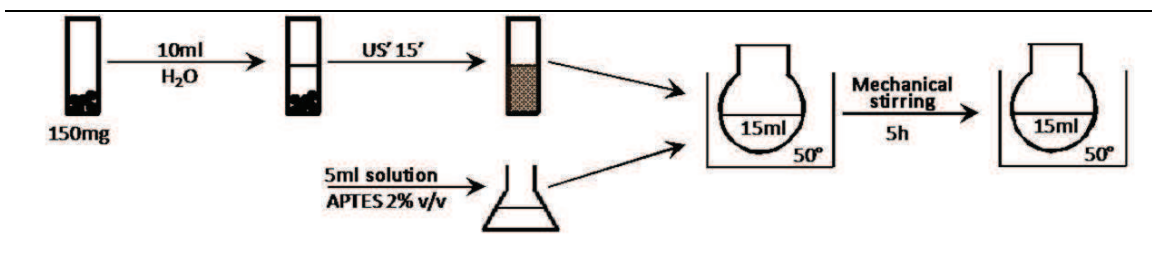
Fig. 17 Functionalization of Fe$_3$O$_4$ NPs with APTES.

150mg of Fe$_3$O$_4$ NPs (Sigma, n.cat: 637106) were ultrasonicated in 10ml of H$_2$O MilliQ for 15min. A solution of 5ml APTES (2% v/v, Sigma n.cat. A3648) in H$_2$O MilliQ was then added and the reaction was maintained under mechanical stirring for 5h at 50°C, according to del Campo *et al.* [24]. Fe$_3$O$_4$ NPs@APTES were then separated from unbound APTES by a commercial parallelepiped neodymium magnet (Webcraft GmbH, Uster, Switzerland; Ni-Cu-Ni plated; magnetization: N45; size: 30x30x15 mm), washed several times with water and anhydrificated with ethanol overnight. NPs were suspended again in water, ultrasonicated for 30' and leaved at room temperature for 1h. Longer suspended nanoparticles were isolated and dried at 50°C overnight.

Fe$_3$O$_4$ NPs@APTES-DAAO: First method
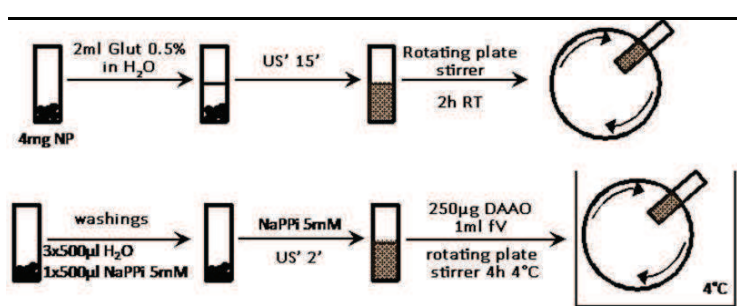
Fig. 18 Conjugation of DAAO on Fe$_3$O$_4$ NPs@APTES, method one.

A suspension of 4mg of Fe$_3$O$_4$ NPs@APTES in 2ml glutaraldehyde (0.5% v/v, Sigma n.cat. G6257) in water

obtained by ultrasonication for 15min (Sonica® 5300MH; Soltec, Milano, Italy) was allowed to react for 2h using a rotating plate tube stirrer at room temperature. The produced adduct was separated from the supernatant with a neodymium magnet, washed three times with 500µl of MilliQ, then with 500µl of 5mM sodium pyrophosphate buffer (NaPPi, Sigma, n.cat. P8135) at pH 8.5. Functionalized Fe_3O_4 NPs were suspended in 5mM NaPPi pH 8.5 and the mixture sonicated for 1min. Finally, 250µg of pure RgDAAO was added (1ml of final volume of 5mM NaPPi pH 8.5 buffer) and the reaction was carried out for 4h at 4°C using a rotating plate tube stirrer. Subsequently, Fe_3O_4 NPs@APTES–DAAO were collected by a magnet and washed twice with 1ml of 5mM NaPPi pH 8.5. The supernatant was stored for further analysis.

Fe_3O_4 NPs@APTES-DAAO: SECOND METHOD
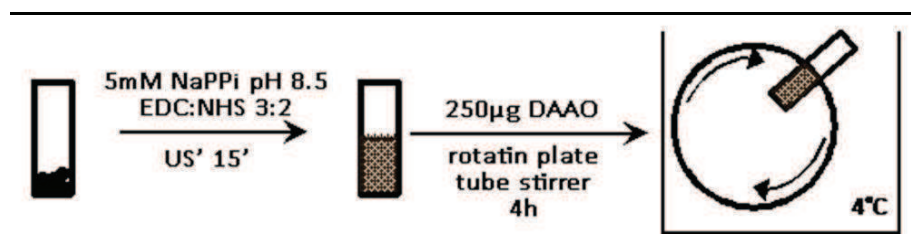
Fig. 19 Conjugation of DAAO on Fe_3O_4 NPs@APTES, method two.

4mg of Fe_3O_4 NPs@APTES were suspended by sonication for 15min with 1-Ethyl-3-(3-dimethylaminopropyl)carbodiimide (EDC, Sigma n.cat: 03450) and N-Hydroxysuccinimide (NHS, Sigma, n.cat: 130672) in 3:2 ratio in buffer 5mM NaPPi pH 8.5. 250µg of DAAO were added and the reaction was carried out for 4h at 4°C using a rotating plate tube stirrer. Subsequently, Fe_3O_4 NPs@APTES-DAAO were collected by a magnet and washed twice with 1ml of 5mM NaPPi pH 8.5. The supernatant was stored for further analysis.

The same procedure has been used to prepare the Fe_3O_4 NPs@APTES system conjugated with the other two DAAO variants used in this work (R285A and 1903).

SPECTRA ANALYSIS

The amount of protein bound to Fe_3O_4 NPs@APTES was determined as the difference between the starting amount of RgDAAO and the protein recovered in the supernatant at the end of reaction. Quantification was performed using the extinction coefficient at 455nm ($12.6mM^{-1}cm^{-1}$) using an UV-Vis V-560 spectrophotometer (JASCO, MD, USA). Characterization of the NP coated samples was performed using the solid phase Fourier transform infrared spectroscopy: spectra were collected

on Nicolet Avatar 360 spectrometer (JASCO). Samples were mixed with infrared grade KBr in a proportion of 2:100 (w/w).

Dynamic Light Scattering (DLS) analysis

Fe_3O_4 NPs, Fe_3O_4 NPs@APTES and Fe_3O_4 NPs@APTES-DAAO were analyzed at concentrations of 250µg/ml, 25µg/ml and 2.5µg/ml in water. Samples dilutions (25µg/ml and 2.5µg/ml) were done in order to analyze the effect of concentration on NP aggregation. Each measurement was preceded by an equilibration time of 90 seconds. Analyzes were performed with Zetasizer Nano ZS90 (Malvern, UK) instrument. Measures were reported as scattering intensity in function to diameter.

Fe_3O_4 NPs@APTES-DAAO characterization

Fe_3O_4 NPs@APTES-DAAO prepared with the two methods were characterized by IR analysis in different conditions. Samples (disks of 2 cm^2 area, ~10 mg cm^{-2}) were placed in a quartz cell equipped with KBr windows. A movable quartz sample holder allows to adjust the pellet in the infrared beam for spectra recording and to displace it into a furnace at the top of the cell for thermal treatment. The cell was connected to a vacuum line for evacuation (Presidual = ~10^{-6} Torr) and for the

introduction of gases into the infrared cell. Spectra were recorded at room temperature. The addition of well known doses of gas in the cell was possible via a pressure gauge for the control of the gas pressure. A Nicolet Nexus spectrometer equipped with a Mercury Cadmium Telluride (MCT) cryodetector and an extended KBr beam splitter was used for the acquisition of spectra in the 600-5500 cm^{-1} range. IR spectra are absorption spectra and the notation used is a.u. for absorption units. The resolution of the spectra was $4cm^{-1}$, and 256 scans were accumulated for each spectrum.

Three kinds of experiments have been performed: first the samples have been dispersed in the KBr, then on the surface of a silica pellet; finally on a silicon disk. In details:

- A wafer containing 98 mg of KBr has been pressed at 4 tons/cm^2, together with ~2 mg of the targeted sample;

- A wafer of 20 mg silica has been casted mixing in its center ~6-7 mg of sample, then pressed to 2 tons per squared cm;

- ~2 mg of powder have been dispersed on the surface of a silicon disk (2 cm^2) by the help of a spot of ethanol.

DAAO ACTIVITY ASSAY

The activity of Fe_3O_4 NPs@APTES–DAAO (and of variant systems) was determined by measuring the absorbance increase accompanying the H_2O_2-induced oxidation of *O*-dianisidine. One DAAO unit corresponds to the amount of enzyme that converts 1µmol of substrate per min at 25°C and at 0.253mM oxygen concentration. The standard assay mixture contained 890µl of 100mM D-Ala in 100mM NaPPi pH 8.5 buffer, 100µl 3.2mg/ml *O*-dianisidine in water, 10µl of 0.4mg/ml horseradish peroxidase in 100mM NaPPi pH 8.5 buffer, and 10µl of 0.4mg/ml Fe_3O_4NPs@APTES–DAAO in the same buffer. The reaction was initiated by the addition of the enzyme and the absorbance increase was monitored at 440nm for 1min using an UV-Vis V-560 Spectrophotometer. The initial velocity at different substrate concentrations (0.1–100mM) were recorded and used to calculate the apparent kinetic parameters using the KaleidaGraph 4.0 software (Synergy Software, PA, USA).

HPLC MEASUREMENTS

D- and L-serine cellular concentrations were determined according to Sacchi *et al.* [100]. In detail, a fixed amount (5×10^5 cells) of SKOV-3 or U87 cells were homogenized in

1ml of cold 5% trichloroacetic acid and then centrifuged at 16,000×g for 45min at 4°C. Trichloroacetic acid was stripped six times from the supernatant using diethylether before lyophilization and storage at -20°C. Lyophilized cell samples were dissolved in 90µl of 0.1M sodium borate buffer, pH 10.4. For amino acid derivatization, 3µl of U87 or 15µl of SKOV-3 samples were treated with 24µg of *N*-acetyl-cysteine and 7.5µg of *o*-phthaldialdehyde in 0.1M sodium borate buffer, pH 10.4.

HPLC separations were performed on a Symmetry® Column C8 (Waters, Milano, Italy; 5 µm) kept at 30°C using a JASCO HPLC system. Flow rate was set at 1ml/min; L- and D-serine were eluted with an isocratic method using 0.1M sodium acetate and 1% tetrahydrofuran at pH 6.2. Derivatized amino acids were detected using a fluorescence detector: excitation at 344nm and emission at 443nm. D- and L-serine quantification was performed by a calibration curve set up using increasing concentrations of standard d-serine (0.25–10pmol) and l-serine (10–200pmol).

CELL CULTURE TEST

SKOV-3 and HCT116 cell lines were maintained as adherent cells in RPMI1640 medium, while U87 cell lines

were maintained in DMEM medium, at 37°C in a humidified 5% CO_2 atmosphere. RPMI1640 medium was supplemented with 10% fetal bovine serum, 1% L-glutamine and 1% penicillin/streptomycin solution, whereas DMEM medium was supplemented with 10% fetal bovine serum, 1% L-glutamine, 1% penicillin/streptomycin and 1% sodium pyruvate. Cells were passaged as needed using 0.25% trypsin–EDTA.

CELL VIABILITY

Cell viability was determined with three different assays: as ATP content by using CellTiter-Glo Luminescent Cell Viability Assay, as activity of mitochondrial dehydrogenases using Cell proliferation Kit (XTT based) and as effective viability measuring membrane integrity with Neutral Red Staining.

For all assays 200μl of cell suspension (containing $2×10^4$, $1×10^4$, $5×10^3$ or $25×10^2$ cells, depending of the exposure time) were seeded into 96-well assay plates and cultivated for 24h at 37°C in 5% CO_2 to equilibrate and become attached prior the treatment. Cells were then exposed to increasing amounts of naked Fe_3O_4 NPs for 0.5, 1, 2, 24, 48 and 72 h. In another series of experiments, $1×10^4$ cells were exposed to increasing amounts of free

DAAO or Fe₃O₄ NPs@APTES–DAAO for 24h. Following the treatment, plates were treated in different ways depending on the kit used, always according to manufacturer's instruction.

CELLTITER-GLO LUMINESCENT CELL VIABILITY ASSAY

Plates were equilibrated for 30min at room temperature and 100µl of CellTiter-Glo Reagent were then added to each well. Plates were shaken for 2min and left at room temperature for 10min prior to the recording of luminescent signals using the Infinite F200 plate reader (Tecan Group, Männedorf, Switzerland). For all cell lines, experiments were performed in triplicate. Cell viability, expressed as ATP content, was normalized against control values. The same procedure has been used for free mutant DAAOs and Fe₃O₄ NPs@APTES–mutantDAAO.

CELL PROLIFERATION KIT (XTT BASED)

50µl of Reaction solution were added to each well and plates were incubated for 4h at 37°C. Then plates were shaken for 2min and Abs at 450nm (specific signal) and 630nm (non-specific signal) were measured using the Infinite F200 plate reader (Tecan Group, Männedorf, Switzerland). Final Abs was obtained by subtraction of non-specific to specific signal. For all cell lines,

experiments were performed in triplicate. Cell viability was normalized against control values.

NEUTRAL RED STAINING

Medium with NPs was removed, cells were washed with PBS (Sigma), 100µl of Neutral Red Medium (Sigma, 40µg/ml in cell medium) were added in each well and cells were leaved for 2h at 37°C. Neutral Red Medium was then removed, wells were washed with 100µl of PBS and 150µl of Neutral Red Solution (50% ethanol, 49% H_2O, 1% acetic acid) were added. Plates were shaken for 10min and Abs at 540nm was measured using the Infinite F200 plate reader (Tecan Group, Männedorf, Switzerland). Abs is directly proportional to viability. For all cell lines, experiments were performed in triplicate. Cell viability was normalized against control values.

MEASUREMENT OF O_2 CONCENTRATION IN THE CELL MEDIUM

The effect of U87 metabolism on the concentration of O_2 in the cell medium was assessed by measuring the oxygen consumption with a Hansatech oxygen electrode. Experimental conditions are reported in table 3:

96well plate	1	2	3	4	5	6	7	8	9	10	11	12
A	Medium DMEM											
B	U87 incubation for 24h											
C	U87 treated for 24h with 10mU 1903 + D-Ala 20mM											
D	U87 treated for 24h with 10mU DAAOwt + D-Ala 20mM											
E	U87 incubation for 48h in DMEM medium											
F	U87 incubation for 48h in DMEM medium with medium changing every 24h.											
G	U87 treated for 24h with 200mU 1903 + D-Ala 20mM											
H	U87 treated for 24h with 200mU DAAOwt + D-Ala 20mM											

Tab 3 Plate scheme used for O_2 depletion measures.

CELLULAR UPTAKE

Cellular uptake and localization was determined on SKOV-3, U87 and HCT116 cells exposed to Fe_3O_4@APTES–DAAO for 24h and analyzed by transmission electron microscopy (TEM) and optical microscopy (OM). For TEM studies, exposed cells were harvested, fixed in 2% glutaraldehyde in 0.1M sodium cacodylate buffer (pH 7.2) for 10min on ice and for 30min at room temperature, washed in the same buffer, and postfixed in dark for 1h with 1% osmium tetroxide in 0.1M sodium cacodylate buffer (pH 7.2) at room temperature. After standard steps of serial ethanol dehydration, samples were embedded in an Epon-Araldite 812 1:1 mixture (Sigma).

Thin sections (70nm) were obtained with a ReichertUltracut S ultratome (Leica, Wetzlar, Germany), stained by standard methods with uranyl acetate and lead citrate, and observed with a JEOL 1010 electron microscope (JEOL, Tokyo, Japan) operated at 90kV.

For OM $5x10^3$ cells were seeded on a coverslip and cultivated for 24h at 37°C in 5% CO_2 to equilibrate and become attached prior the treatment. Cells were then exposed to 40µg/ml Fe_3O_4 NPs naked and 40µg/ml Fe_3O_4 NPs@APTES-DAAO for 24h at 37°C in a humidified 5% CO_2 atmosphere. Cells were then washed twice with 1ml of PBS complete, fixed with cold ethanol for 5min and colored with 1ml of Prussian's Blue (2% hydrochloric acid mixed with 2% potassium ratio 1:1). After two washings with H_2O, cells were colored with 1ml of 0.5% Neutral Red solution for 3min, washed 3 times with H_2O and mounted on a slide.

STATISTICS

Kinetic data and cell viability values were expressed as mean ± standard deviation. Statistical tests were performed using KaleidaGraph 4.0 software (Synergy Software).

IN VIVO STUDIES

Two in vivo studies have been performed. In both experiments CD1 (CD1 (ICR), Charles River Labs Italia S.p.A. Calco, Lecco) male mice were intravenously treated with a single dose of Fe_3O_4 NPs@APTES-DAAO and sacrificed 24h after treatment. All mice were 5 weeks old on the day of dosing and were able to acclimate for 7 days before treatment. In the first experiment mice were injected with 100mg/kg of NPs in NaCl 0.9%, while in the second with 20mg/kg of NPs in NaPPi buffer pH 7.4.

CLINICAL AND BEHAVIOURAL OBSERVATION

Animals were weighted before treatment and before the sacrifice and clinically monitored after the treatment.

The behavioral observation (Irwin test) was performed only at the beginning of the study when the substance was administered for the first time. The test was performed according to the method described by Irwin [101] at time 5, 15, 30, 60 min after treatment.

CLINICAL CHEMISTRY AND HEMATOLOGY

Before necropsy, blood was drawn by intracardiac puncture, collected in heparinized tubes and analyzed for:

- Biochemical parameters: albumin (ALB), total protein (PT), creatinine (CRE), urea, triglyceride (TG), transaminase (ALT/GPT).

- Complete blood count, platelet count, white blood cell (WBC), red blood cell (RBC), hemoglobin (Hb), hematocrit (Ht), mean corpuscular volume (MCV), mean corpuscular hemoglobin (MCH), mean corpuscular hemoglobin concentration (MCHC).

SACRIFICE, SAMPLING, AND PATHOLOGICAL EXAMINATION PROCEDURES

Mice were euthanized at 24h post treatment according to standard procedures and in compliance with local regulations.

Complete necropsy of mice was performed. Liver, spleen and kidney were weighed and the relative organ weight (wet organ/total body weight) was calculated.

Liver, kidney, spleen, lung, heart, brain were sampled, fixed in 10% NBF, and paraffin embedded according to standard MAPLab procedures. 4µm sections from each

tissue were routinely stained with Hematoxylin-Eosin (HE) and evaluated under a light microscope.

4µm sections from each tissue were routinely immunostained with anti-Iba-1 antibody (identification of histiocytes) and evaluated under a confocal microscope.

STATISTICAL ANALYSIS

Statistical significance was assessed by analysis of two-tailed Student's t-test to compare the experimental conditions with the negative control (p<0,05).

II.II: RESULTS AND DISCUSSION

SAMPLE CHARACTERIZATION

Fourier transform infrared spectra of Fe_3O_4 NPs and Fe_3O_4 NPs@APTES are shown in figure 20.
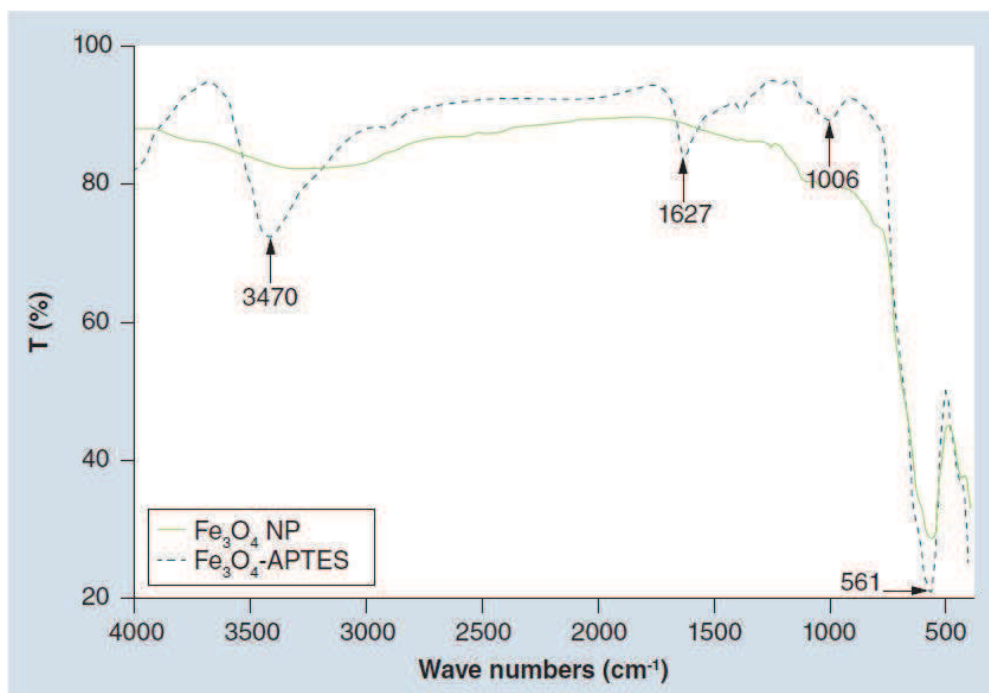
Fig. 20 Fourier Transform infrared spectra of Fe_3O_4 NPs and Fe_3O_4 NPs@APTES.

The peak within 550–570 cm^{-1} is characteristic of Fe-O vibrations related to the magnetite core. The presence of silane on the surface of NPs is confirmed by the presence of characteristic peaks; the peak at 1006cm^{-1} is indicative of the Si-O bond; the peaks at 3470 and 1627cm^{-1} are indicative of the N-H stretching and bending vibrations overlapped with those of vibration

bands of hydrogen-bonded silanols (SiOH groups). Fe_3O_4 NPs@APTES expose the –NH_2 groups, allowing NPs to remain dispersed in the medium.

DLS ANALYSIS

In all samples NPs aggregates of 300nm or more are evident. The size of the aggregates varies with the dilution: at increased dilution the diameter decreases. The polydispersity index (pdI) increases from Fe_3O_4 NPs to Fe_3O_4 NPs@APTES-DAAO. It seems that the enzyme conjugation process induces aggregation. To confirm this it can be noted that the population of Fe_3O_4 NPs@APTES-DAAO is stable around a dimensions of 1µm (figure 21c).
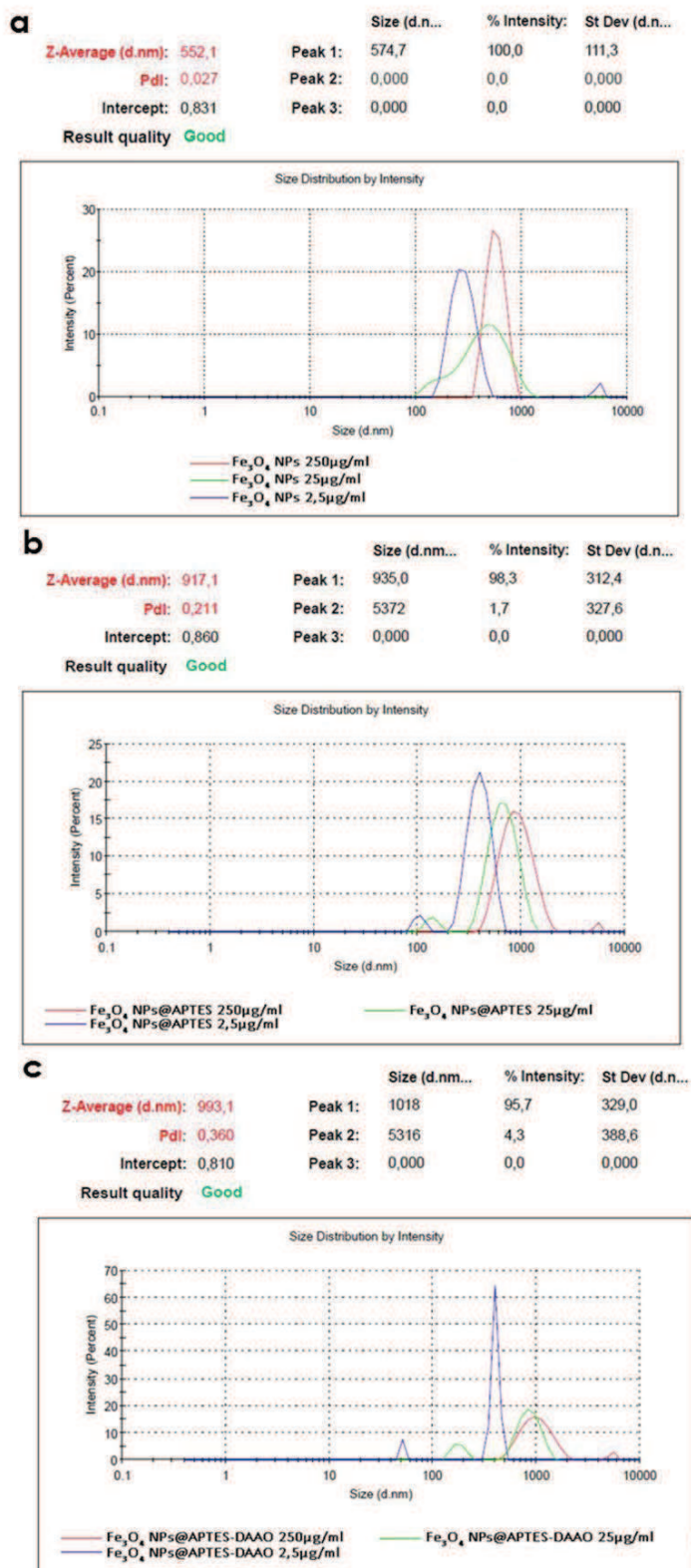
Fig. 21 DLS analysis on Fe₃O₄ NPs (a), Fe₃O₄ NPs@APTES (b) and Fe₃O₄ NPs@APTES-DAAO (c) at different concentrations.

DAAO BINDING EFFICIENCY AND Fe₃O₄ NPS@APTES-DAAO

KINETIC PROPERTIES

RgDAAO was conjugated to Fe₃O₄ NPs@APTES by two different methods described in II.I Materials and Methods section and summarized in figure 22.
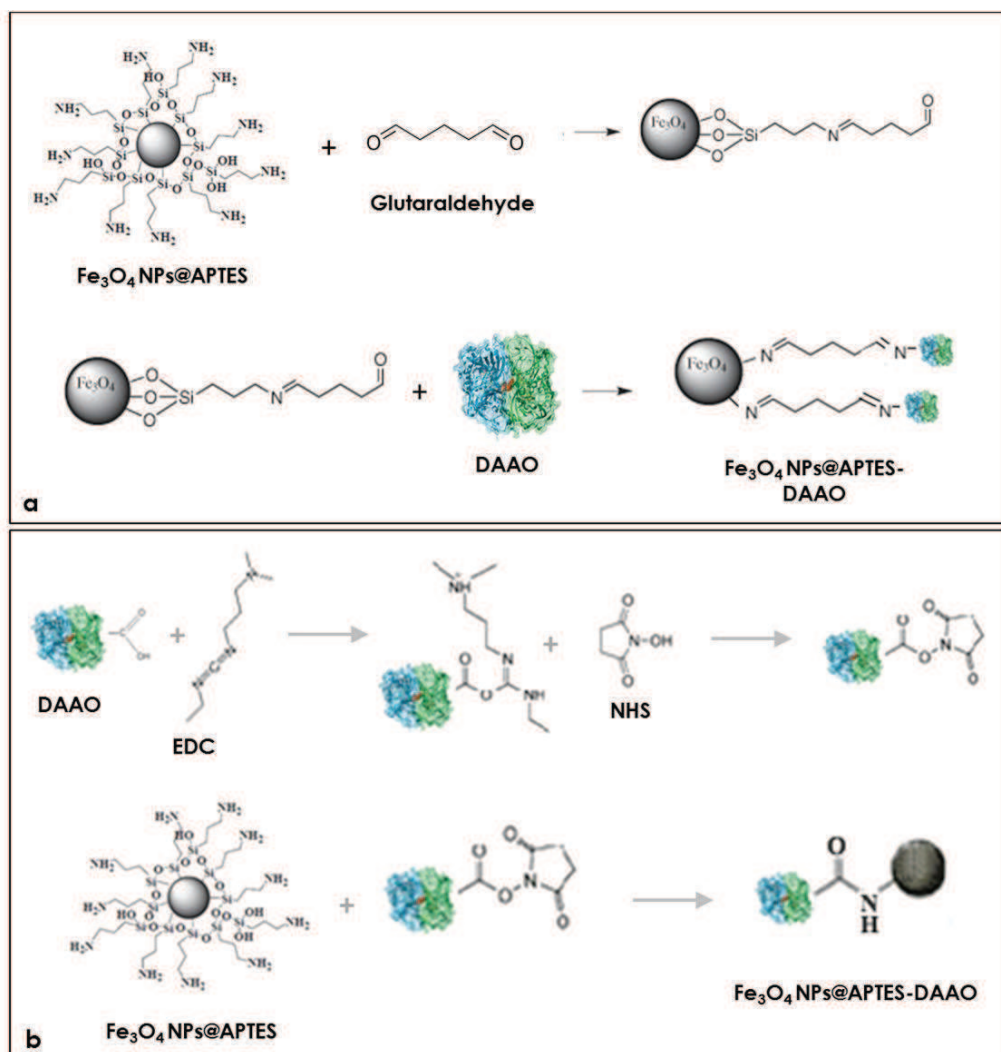
Fig. 22 Schematic representation of the two DAAO conjugation methods on Fe₃O₄ NPs@APTES. a) Conjugation via glutaraldehyde b) Conjugation via EDC and NHS.

	Fe$_3$O$_4$ NPs@APTES-DAAO via glutaraldehyde	Fe$_3$O$_4$ NPs@APTES-DAAO via EDC/NHS
stability 4°C	several month	several month
U/mg NPs bound	4,5	7
µg enzyme bound (%)	70	100
U enzyme bound (%)	70-80	90-100
Km (mM)	1	1

Tab 4 comparison of binding efficiency between the two methods of DAAO conjugation on Fe$_3$O$_4$ NPs@APTES.

The second method is much more efficient as highlighted in table 4. In fact, the amount of enzyme bound to NPs with the first methods is approximately 70%, with an enzymatic activity of 4.5U/mg NPs. The second method reaches the 100% of binding efficiency with an enzymatic activity of 7U/mg NPs. This method is a good optimization of the process of conjugation, reaching the ultimate goal in terms of quantity and activity of enzyme bound. Furthermore this method allows a reduction of 2h of the working times. As what concern system stability, no differences have been highlighted between the two methods: DAAO activity remains stable for 2 weeks at 4°C and a 20% decrease was observed after 2 months. Both coating procedure did not affect the kinetic properties of DAAO, in fact the apparent Km of immobilized enzyme for D-Ala was

identical to that of the free enzyme (0.9 vs 1 mM), as shown in figure 23. Altogether, this conjugation procedure does not seem to alter the flavoenzyme conformation and its binding with the flavin adenine dinucleotide cofactor, which is absolutely required for its catalytic activity.
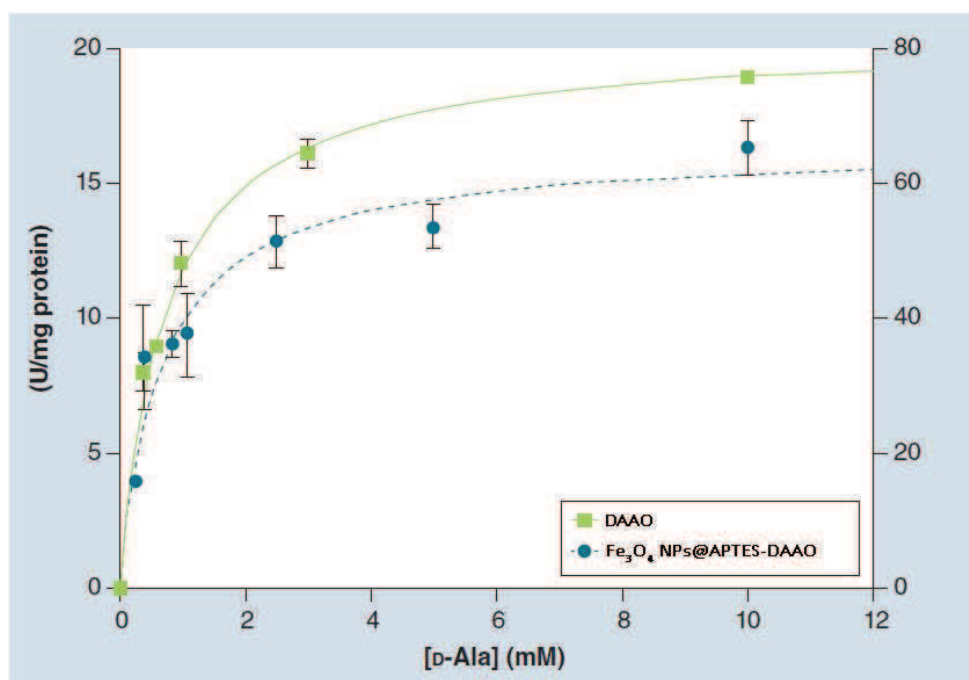

Fig. 23 Michaelis–Menten plot of the activity measured for Fe_3O_4 NPs@APTES-DAAO and free DAAO at increasing D-Ala concentrations.

FE₃O₄ NPS@APTES-DAAO CHARACTERIZATION

The spectra of Fe_3O_4 NPs@APTES-DAAO prepared with the two methods, dispersed in the KBr, are reported in figure 24.
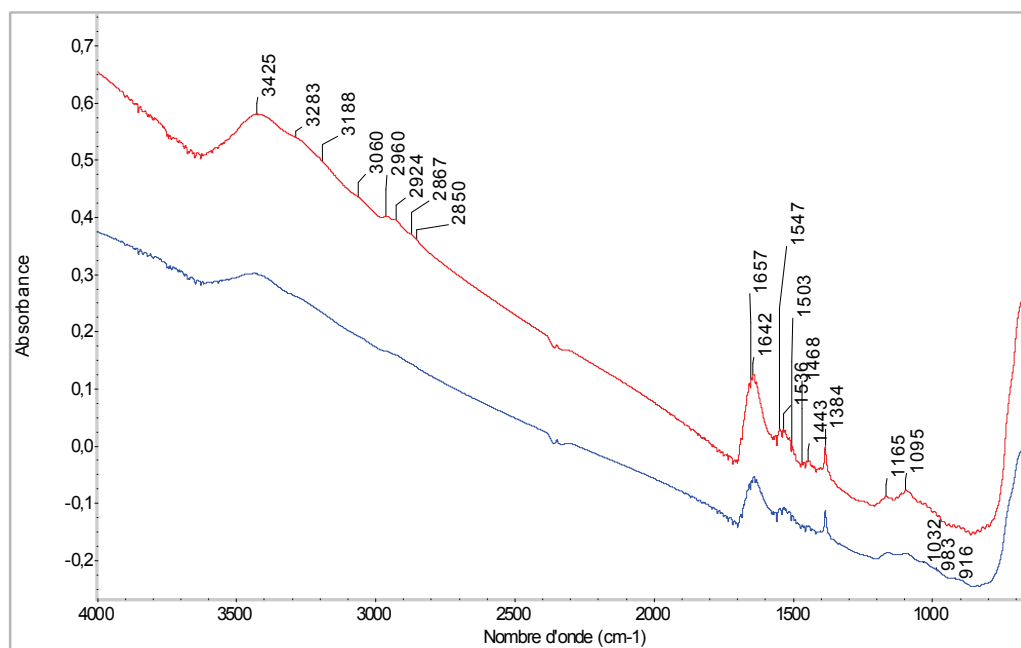
Fig. 24 IR spectra of Fe_3O_4 NPs@APTES-DAAO prepared *via* glutaraldehyde (red) and *via* EDC/NHS (blue). Samples were dispersed in KBr (2% w/w).

The two spectra are similar. At the highest wavenumbers we can observe the stretching of the OH groups of water adsorbed on KBr, likely (3425cm^{-1}). In the region 3300-3000cm^{-1} the ν(NH) vibration are observed; they correspond to the NH$_2$ moieties present in the organic ligand. The intensity being relatively low, their concentration is minor. The corresponding bending mode is at 1650-1640cm^{-1} and 1546cm^{-1}, partially overlapped with the δ(HOH) of water at ~1630cm^{-1}. Below 800cm^{-1}, only structural (saturated) bands are visible, containing bending, twisting and rocking modes,

together with the stretches of M-O bonds. The other bands (in the 1600-1000cm^{-1} region) are due to C-C and C-O bonds, while those in the 3000-2800cm^{-1} interval to C-H stretches, difficult to be discriminated at this step. Interestingly, no bands at ~1745cm^{-1}, typical of the C=O bonds of the aldehydes can be distinguished.

Fig. 25 spectral subtraction of spectra of figure 24: spectrum of Fe$_3$O$_4$ NPs@APTES-DAAO prepared with the first method minus that of NPs prepared with the second method.
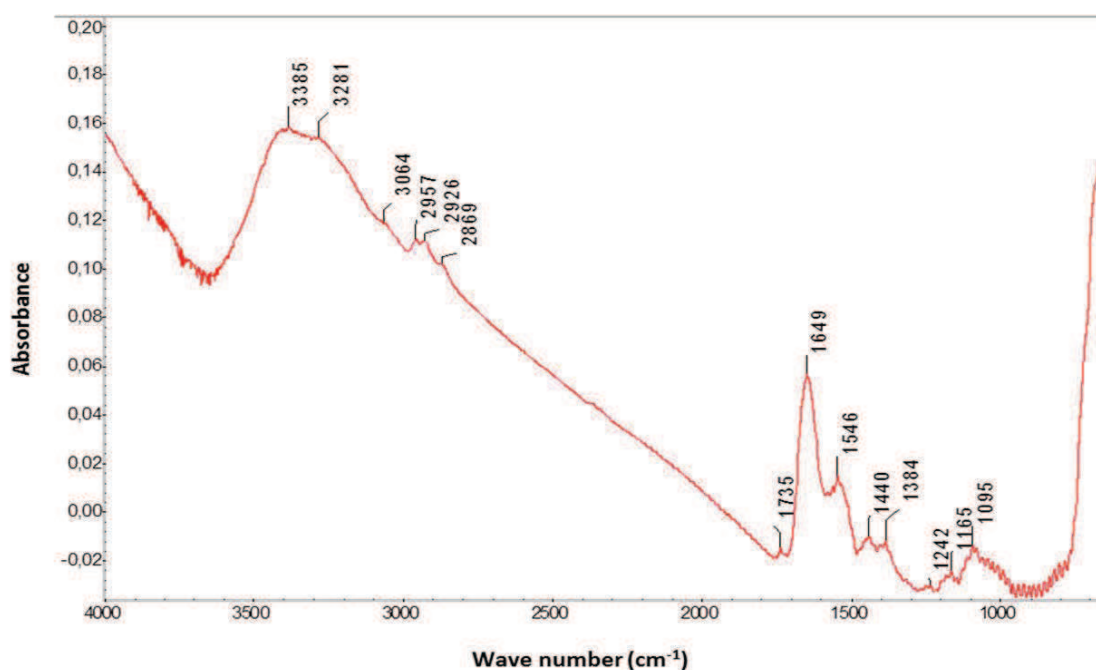
Performing a spectral subtraction we can better scrutinize the differences in the two compounds: the vibrations associated to the NH$_2$ species almost disappear in the compound prepared *via* EDC/NHS, as indicated by the bands in positive in the difference

spectrum (3400-3000cm^{-1} region, plus 1649 and 1546 cm^{-1} peaks) and by the absence of the corresponding bands in the blue spectrum in Fig. 24. A very weak feature appears at 1735cm^{-1}, accounting for aldehyde typical vibration, confirming that traces of these free vibrations can be seen on the glutaraldehyde sample. Therefore we can conclude that all the ligands are functionalized in the EDC/NHS sample, whereas only a small portion of them present free coordination ends in the glutaraldehyde compound. By the way, also silanol signals (as indicated by the material structural formula) are totally absent (band expected at 3746cm^{-1}), probably been taken in a hydrogen bonding configuration.

When dispersing the samples on silica (figure 26), the observed bands essentially deal with OH groups on silica (3746cm^{-1}) and adsorbed water (~3450 and 1630 cm^{-1}). The features at 1972 and 1867 cm^{-1} are overtones and combination bands of silica framework (massif below 1300cm^{-1}) (spectrum blue, Fig. 26). After CO or NO adsorptions, no remarkable differences can be distinguished especially on the glutaraldehyde sample (spectra at the bottom of the figure, cyan, magenta

and green). In the case of the EDC/NHS sample, a weak component appears at 1508cm^{-1} (spectrum red, red arrow), which cannot be related directly with the probe molecules. Eventually, it could be ascribed to CO interactions with some accessible ligand in the organic part, inducing a shift in a C-C or C-O vibration.
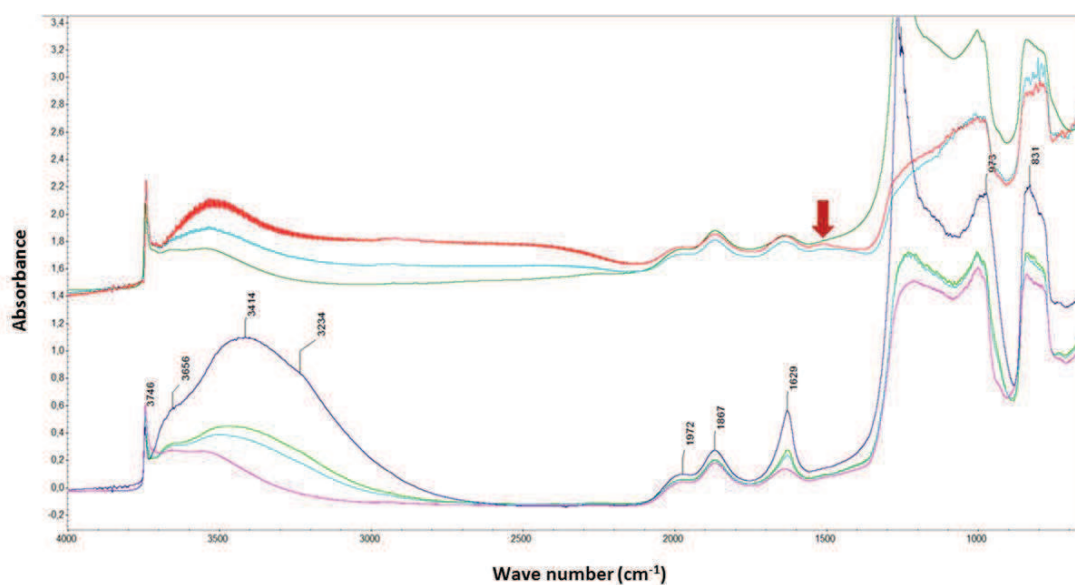
Fig. 26 Spectra of samples dispersed in silica. In the bottom part in blue subtraction spectrum of glutaraldehyde and EDC/NHS samples, in cyan, magenta and green spectra of glutaraldehyde samples after NO and CO adsorption. In the upper part EDC/NHS samples spectra after CO adsorption. Arrow indicates peak at 1508cm^{-1}.

Subtraction spectra (figure 27) confirm that no effect of probe molecule adsorption can be detected, so witnessing for an absence of coordinative unsaturated

sites on the cationic iron species. Practically, we can conclude that all the iron nanoparticles are totally surrounded by the organic compounds.
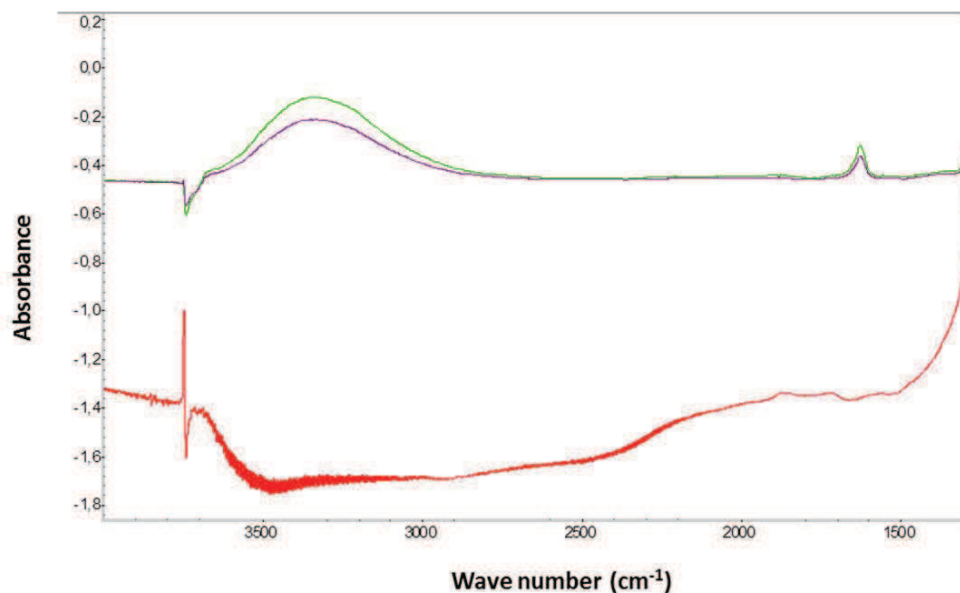
Fig. 27 spectra above: NO adsorption (10 and 18 Torr at the equibrium) on the glutaraldehyde sample; spectrum below: difference before and after the adsorption of CO on the EDCNHS sample.

Finally, we tried to characterize the samples after deposition on a silicon wafer. The corresponding spectra are reported in figure 28. Besides the interference fringes due to the specular surfaces of the Si disks, we can observe only bands due to the organic ligands, already mentioned above. Comparing the spectra during the adsorption of CO and after evacuation (B & A for glutaraldehyde, respectively, and C & D for EDC/NHS),

we cannot observe any difference, if we exclude the changes in the baseline, irrelevant for the present study. Even, this latter approach for the sample analysis seems less appropriate, providing spectra of relatively low quality.
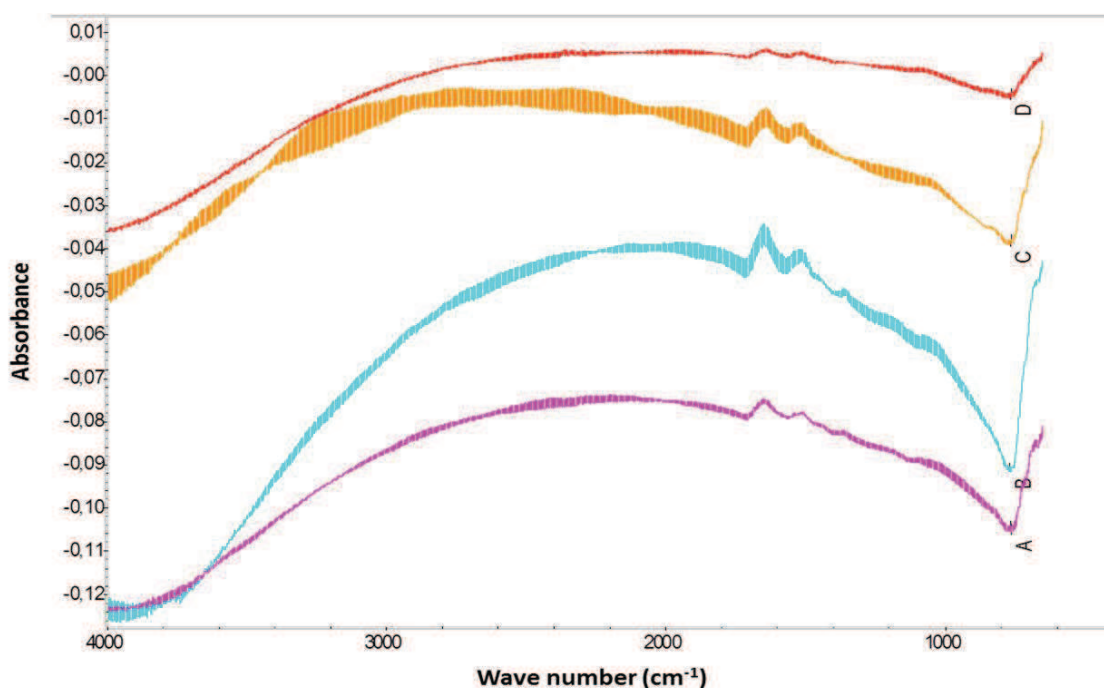
Fig. 28 samples spectra collected on a silicon wafer. A and B are glutaraldehyde samples while C and D EDC/NHS samples.

In conclusion, we can say that the EDC/NHS sample higher activity in respect with glutaraldehyde sample is due to a higher efficiency of bound. In fact, apparently all available NH_2 sites are saturated with DAAO, while glutaraldehyde sample shows some free NH_2 and aldehyde sites. Moreover all conjugation sites of Fe_3O_4

NPs are saturated, indicating that APTES functionalization is absolute.

CYTOTOXICITY

In this study three tumor cell lines have been used. We chose ovarian carcinomas (SKOV-3), colon-rectum adenocarcinomas (HCT116) and glioblastoma (U87) cell lines, because representing cancers particularly frequent and/or lethal. Colon-rectum adenocarcinomas are the third most frequent and lethal cancer. Ovarian cancer is the tenth for the frequency but is lethal in the 63% of cases. Brain tumors are less frequent, compared to the other two cancers, but about 61% of cases results in death and glioblastoma is the most common malignant primary brain tumor among adults [102].

Preliminary analyses were done on SKOV-3 to asses toxicity of Fe_3O_4 NPs and Fe_3O_4 NPs@APTES.

Data are expressed as a percentage reduction of the ATP content and indicate a cell suffering rather than death. All experiments were conducted in 100µl, then all the amount of NPs used must be considered in that volume.

Fe_3O_4 NPs seem not to have significant cytotoxic effects within 4µg and a higher toxicity is caused by acute

treatment 30, 60, 120 min (figure 29a). Fe_3O_4 NPs@APTES show a slightly higher toxicity compared to Fe_3O_4 NPs, especially at the higher doses, 16 and 32 μg (figure 29b). This is probably due to the presence of $-NH_2$ groups belonging to APTES molecule.
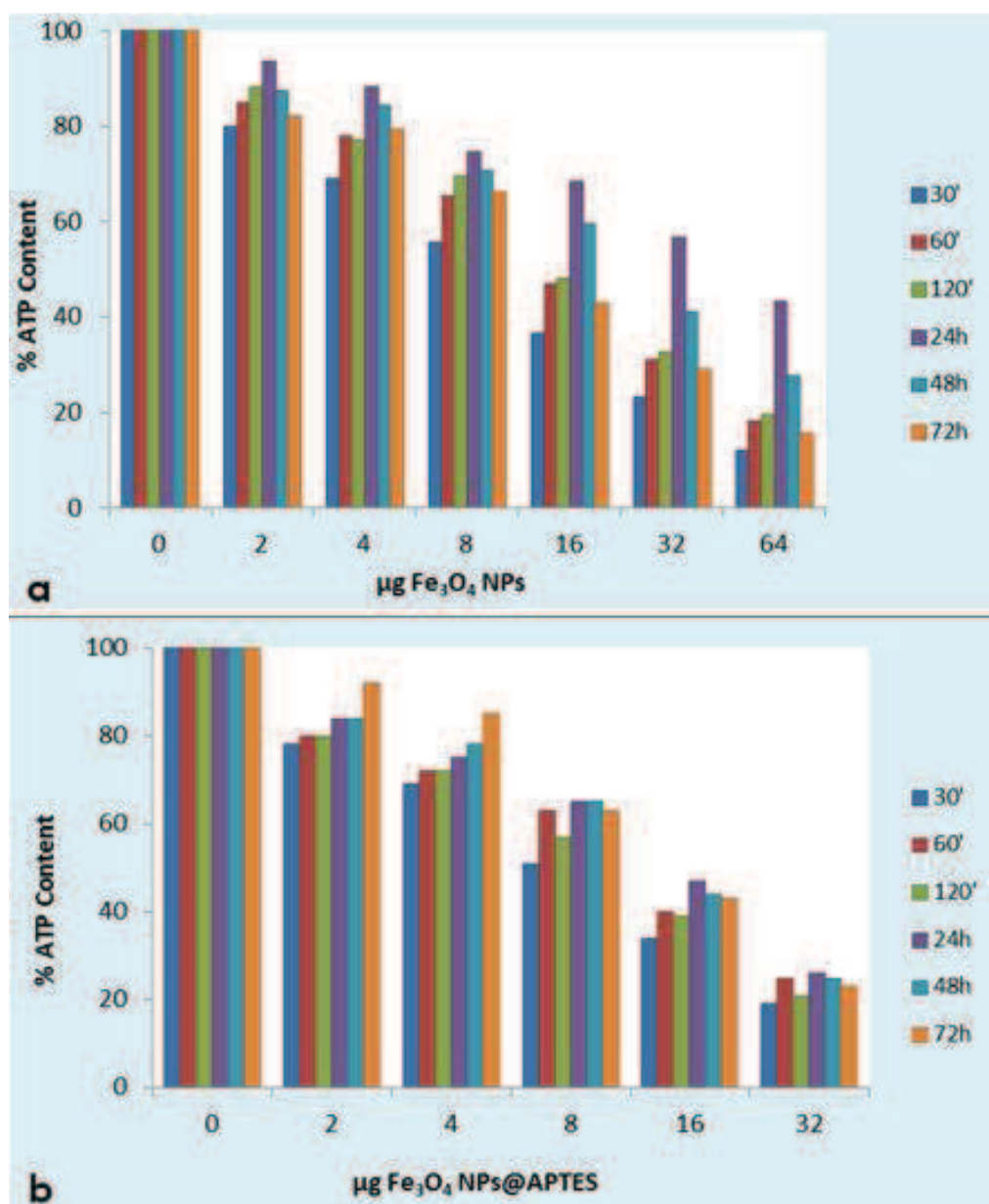
Fig. 29 Cytotoxicity assay on SKOV-3 of Fe_3O_4 NPs (a) and Fe_3O_4 NPs@APTES (b).

Being that SKOV-3 exposed to 16μg of Fe_3O_4 NPs for 24h show a viability of 70%, we decided to expose cells for 24h to the system prepared with the first method (see MATERIALS AND METHODS, Fe_3O_4 NPs@APTES-DAAO, FIRST METHOD), in a way that the amount of Fe_3O_4 NPs within the system is not more than 16μg. The toxicity of the system was tested with and without D-Ala. This amino acid was chosen because it represents the reference substrate for DAAO [73]. It should be emphasized that D-Ala itself had no effect on cell viability at the used concentrations (figure 30).
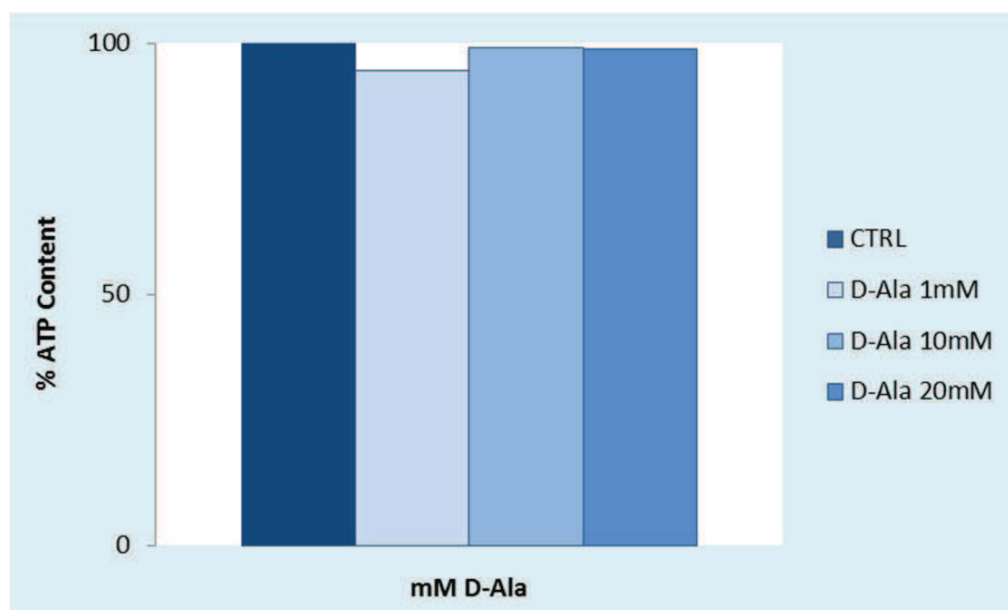
Fig. 30 % ATP content depletion in SKOV-3 exposed for 24h to D-Ala 1, 10 and 20 mM.

The efficacy of the system was then tested in comparison with the toxicity induced by the free

enzyme. The range of concentrations goes from 3.5 to 56 mU, corresponding to maximum 12.5µg of Fe_3O_4 NPs (figure 31).
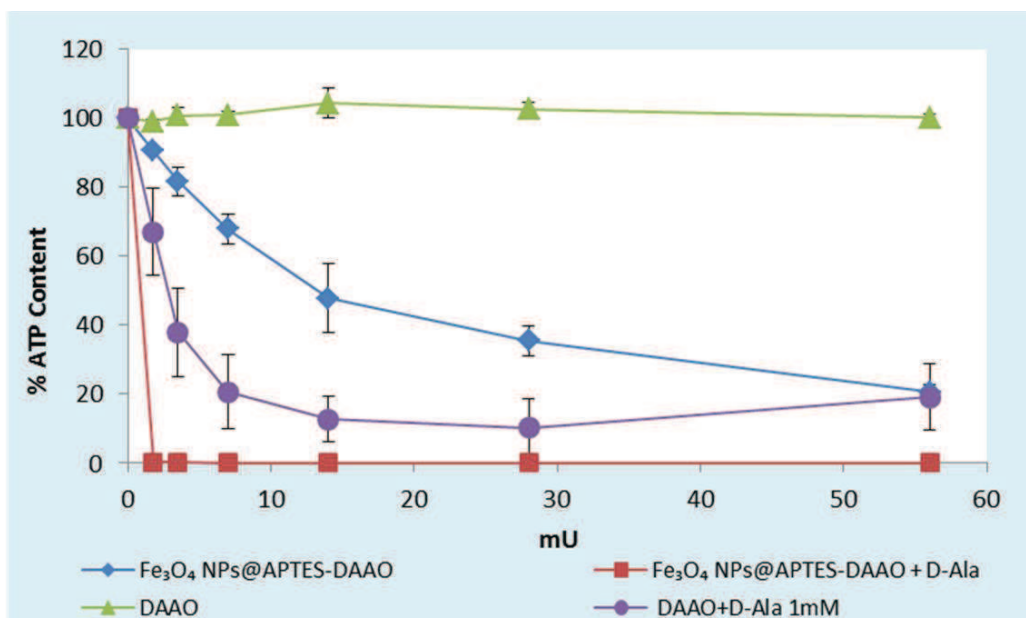
Fig. 31 Cytotoxicity assay on SKOV-3 of Fe_3O_4 NPs@APTES-DAAO and free DAAO with and without the substrate D-Ala 1mM.

In absence of D-Ala, free DAAO did not affect viability. When D-Ala was added, a clear effect was seen. As far as it concerns Fe_3O_4 NPs@APTES-DAAO, it exerts a certain degree of toxicity also in absence of D-Ala. Noteworthy the cytotoxicity is drastically increased by D-Ala addiction, depleting completely the ATP content already at the lower tested concentration of 3.5mM. The conjugation of DAAO to NPs seems to enhance the efficacy of the enzyme on tumor cells. In light of these

preliminary results, we decided to reduce the range of units used (from 3.5 to 14 mU) and we have tested the system prepared with the second method (see MATERIALS AND METHODS, Fe_3O_4 NPs@APTES-DAAO, SECOND METHOD) on SKOV-3 (figure 32).
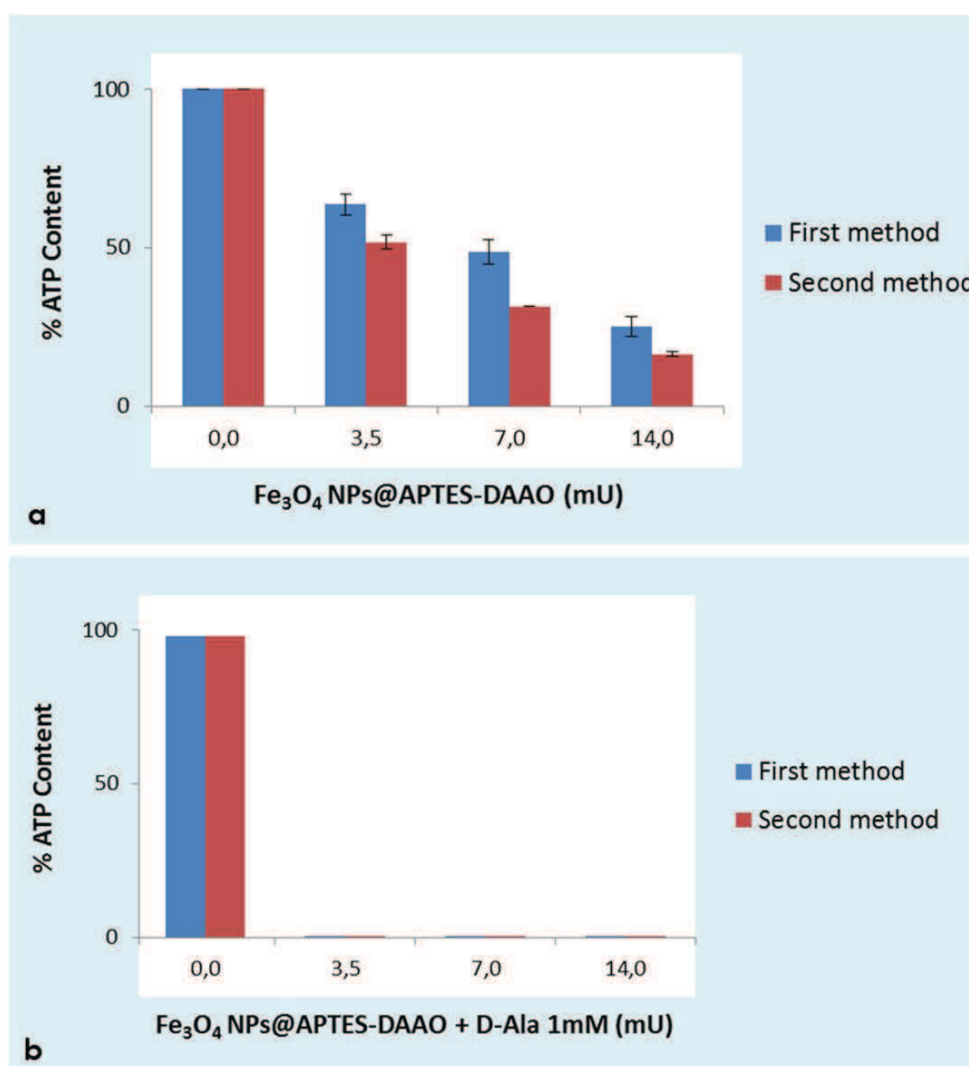
Fig. 32 Comparison of cytotoxicity of Fe_3O_4 NPs@APTES-DAAO prepared with the two methods, with and without D-Ala 1mM, on SKOV-3. 24h treatment.

No significant differences are evident between the two systems. Worthy to note is that the second system allows using a lower amount of Fe_3O_4 NPs, because of the high efficiency in the enzyme conjugation. Considered this and the reduced production times, the second method has been used for the production of all Fe_3O_4 NPs@APTES-DAAO for the next experiments.

In light of all these preliminary results, the system with or without D-Ala 1mM was tested on all cell lines (SKOV-3, U87 and HCT116), in comparison with the free enzyme in the same conditions (figure 33).

Figure 33 confirms the non-toxicity of the DAAO without its substrate and the higher toxicity of the system with D-Ala in respect to free enzyme in the same conditions. U87 cells are less sensitive to the treatment and are insensitive to the free enzyme with D-Ala. This increases the importance of our system in the treatment of brain tumor.

Fig. 33 % ATP content depletion in SKOV-3 (a), U87 (b) and HCT116 (c) cell lines after 24h exposure to Fe₃O₄ NPs@APTES-DAAO and DAAO with and without D-Ala 1mM.

The toxicity of Fe_3O_4 NPs@APTES-DAAO without D-Ala may have two reasons. On the one hand there may be some non-saturated $-NH_2$ group that enhance the toxicity of Fe_3O_4 NPs. On the other hand there may be D-amino acid in culture medium or within the cells, which may act as endogenous substrate for the enzyme. In order to check this last hypothesis, we have measured the content of D-serine in SKOV-3 and U87. D-Ser is one of the major substrate of DAAO and represents the most abundant natural D-amino acid in different brain cells [103]. HPLC analysis showed that the cellular D-Ser content was approximately 1% of the total (L- and D-) serine levels in both cell lines (table 5).

Cell line	pmol D-Ser/10^4 cell	pmol L-Ser/10^4 cell	D-Ser/(D+L)-Ser (%)
U87	0.86	64.2	1.3
SKOV-3	0.15	11.2	1.4

Tab 5 U87 and SKOV-3 content of D- and L-serine measured by HPLC analysis.

Accordingly, if oxidized by DAAO, the natural content of D-Ser should result in the same H_2O_2 production and, thus, should similarly affect the viability of cell lines during treatment. The presence of D-serine within the cells as well as in the culture medium could certainly activate DAAO, affecting cell viability in the same way in all cell

lines. As a matter of fact cytotoxicity induced by the system without D-Ala in all cell lines is the same.

To confirm that the toxicity was mainly due to the enzyme activity, cells were also exposed to the non-active mutant R285A, in the same conditions previously used. Results (figure 34) confirmed that free R285A in presence or not of D-Ala does not affect ATP content, while Fe_3O_4 NPs@APTES–R285A accounts, at most, for 40% of ATP reduction. Moreover Fe_3O_4 NPs@APTES–R285A toxicity is comparable to that induced by Fe_3O_4 NPs@APTES. This once again confirms that the toxicity induced by Fe_3O_4 NPs@APTES-DAAO is caused both by the presence of not saturated -NH_2 groups and by the presence of endogenous substrate.

Fe_3O_4 NPs@APTES-DAAO toxicity on the three cell lines was furthermore investigated with two toxicity assays: XTT and Neutral Red (NR). These two essays give a direct estimate of viability and they base respectively on the activity of mitochondrial enzymes and on the ability of viable cells to incorporate the dye in the lysosomes.

Results in figures 35 and 36 confirm the higher toxicity of the system with its substrate in respect to the free enzyme in the same conditions. Moreover both XTT and NR assays

indicate that Fe$_3$O$_4$ NPs@APTES-DAAO without D-Ala induce cellular suffering rather than death: viability is still at 100% even at the higher tested concentration for all cell lines.
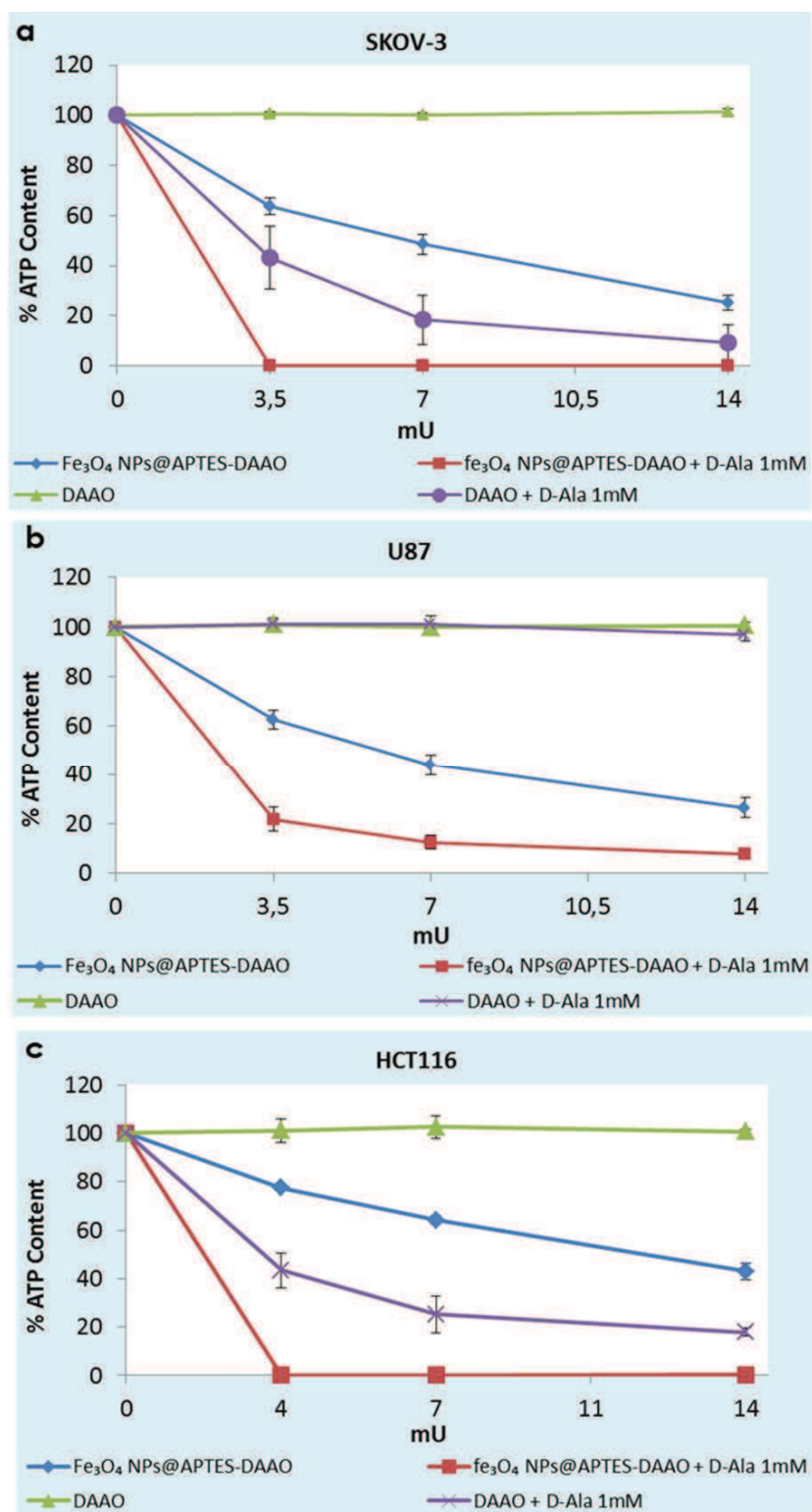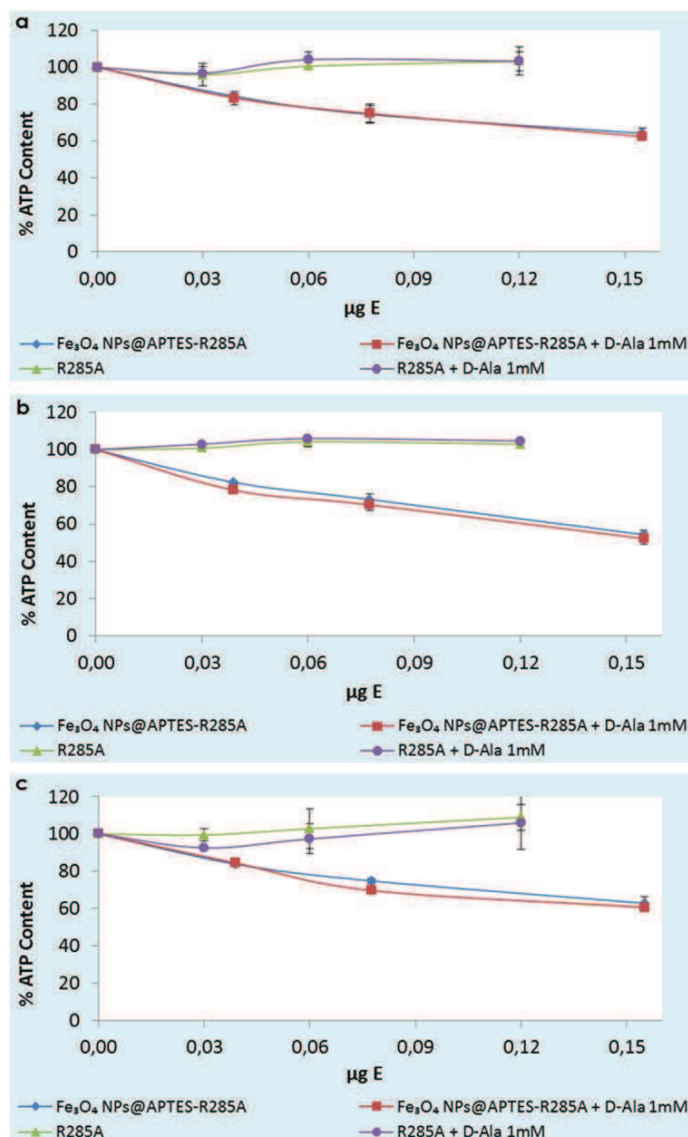

Fig. 34 ATP content depletion in SKOV-3 (a), U87 (b) and HCT116 (c) cell lines after 24h exposure to Fe$_3$O$_4$ NPs@APTES-R285A and R285A with and without D-Ala 1mM.
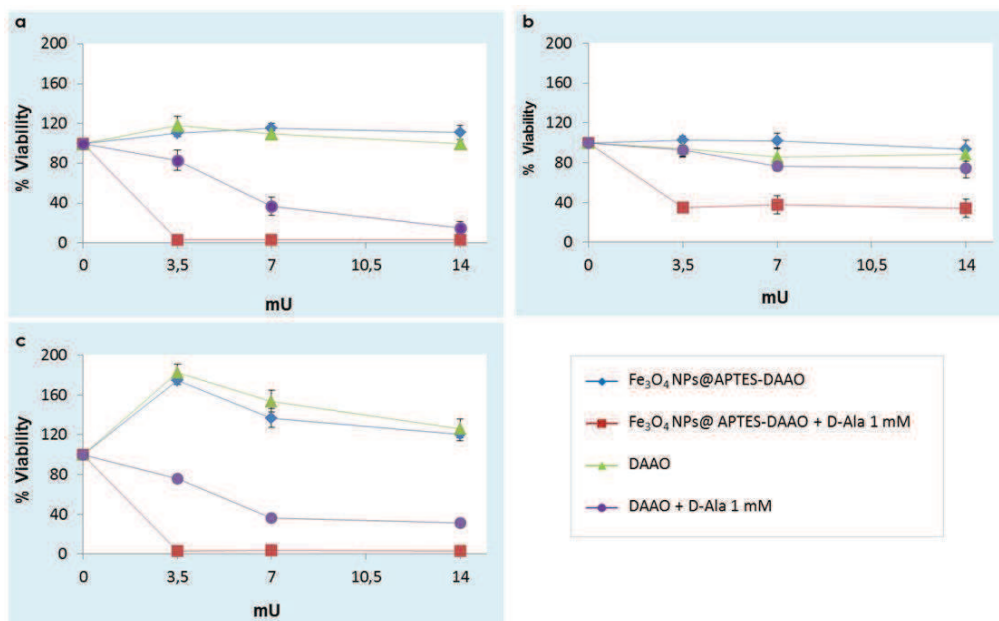
Fig. 35 XTT assay on SKOV-3 (a), U87 (b) and HCT116 (c) cell lines after 24h exposure to Fe_3O_4 NPs@APTES-DAAO and DAAO with and without D-Ala 1mM.
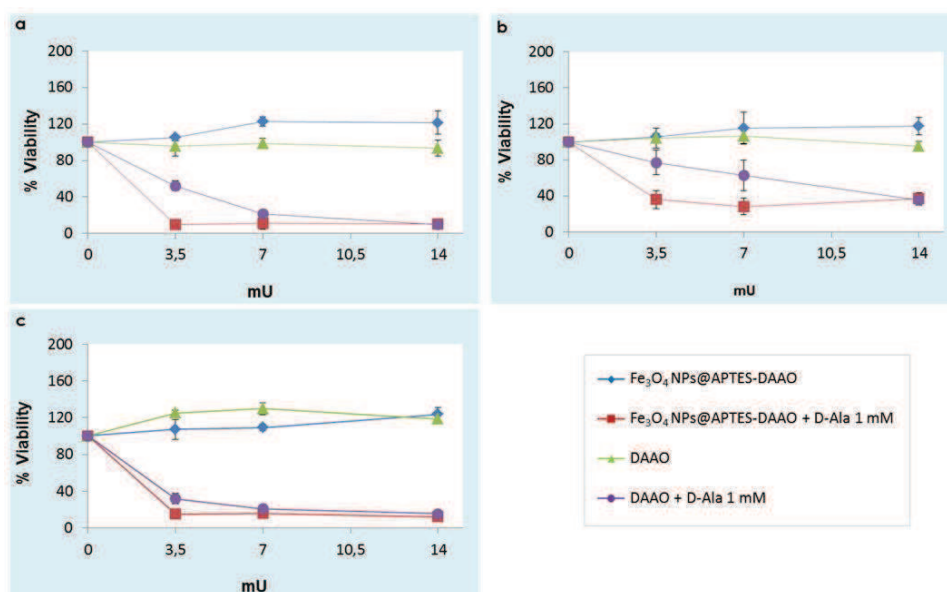
Fig. 36 Neutral Red assay on SKOV-3 (a), U87 (b) and HCT116 (c) cell lines after 24h exposure to Fe_3O_4 NPs@APTES-DAAO and DAAO with and without D-Ala 1mM.

Comparing the three cytotoxicity assays, ATP CellTiter-Glo luminescent cell viability assay is the better one, even though it does not provide a direct measure of cell viability. It is very fast and convenient, both in its preparation and its use; It is stable (the results can be read up to 5h after treatment) and reproducible. This is why it was used for all further cytotoxicity assays.

Looking at all cytotoxicity assays, one can say that U87 cell line is generally less sensitive to the treatment. One of the possible reasons is that the metabolism of these cells depletes oxygen concentration in the medium, reducing DAAO activity. To check this hypothesis the 1903 mutant, more active at low oxygen concentration, was conjugated on NPs and tested on U87 (figure 37). Moreover the oxygen consumption was measured in different experiment condition. The mutant 1903DAAO does not seem to be more active on U87 (Fig. 37a), indicating standard level of oxygen concentration in medium. Further confirmations of this are results deriving from oximeter analysis: oxygen concentration in the medium even after 48 hours of incubation is almost unchanged in respect with the initial concentration. These results indicate that the lesser effectiveness of the

enzyme on U87 is not attributable to a lowering of oxygen. Other mechanisms are then responsible for the decrease in DAAO efficiency on U87. However, these mechanisms must be sought in the extracellular environment characteristics, which change depending on the cell type.

b		
Medium DMEM		232
U87 incubation for 24h		210
U87 incubation for 48h in DMEM medium with medium changing every 24h.		201
U87 incubation for 48h in DMEM medium		188
	DAAO	1903
U87 treated for 24h with 10mU enzyme + D-Ala 20mM	200	185
U87 treated for 24h with 200mU enzyme + D-Ala 20mM	211	197
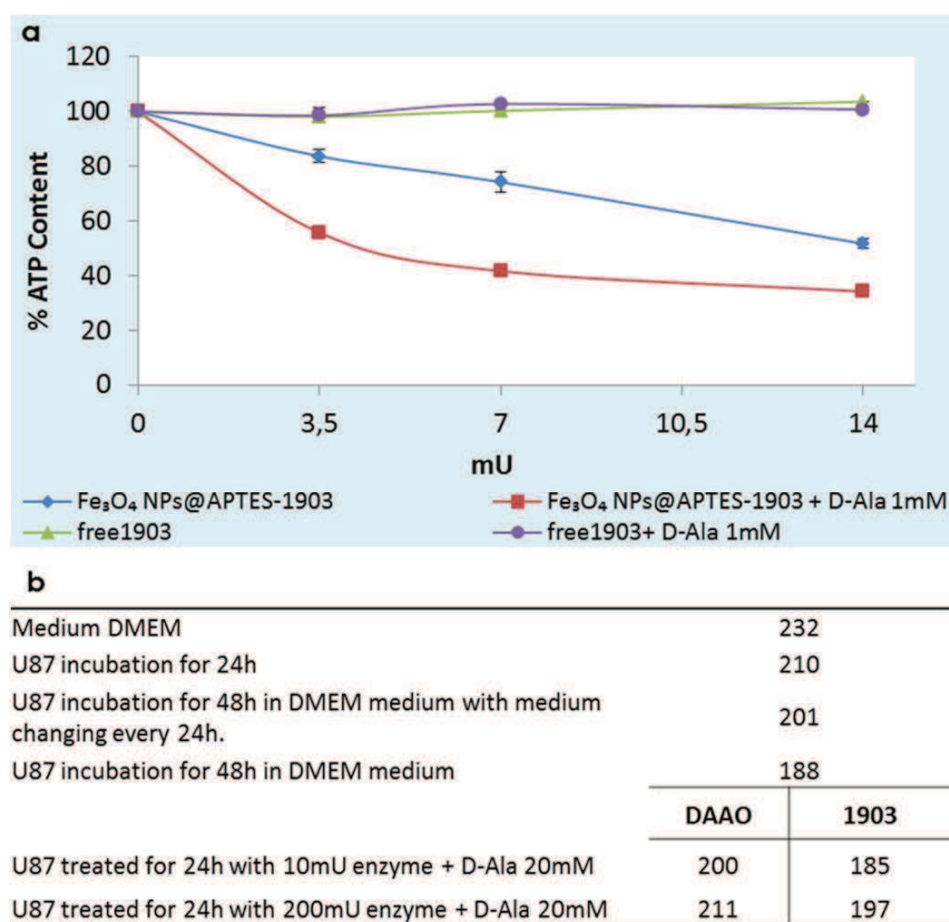
Fig. 37 ATP content depletion in U87 cell line after 24h exposure to Fe_3O_4 NPs@APTES-1903 and 1903 with and without D-Ala 1mM (a). Oxygen concentration (nmol/ml) measured with a Hansatech oxygen electrode (b).

UPTAKE

Internalization of Fe$_3$O$_4$ NPs@APTES-DAAO was analyzed by TEM and OM.
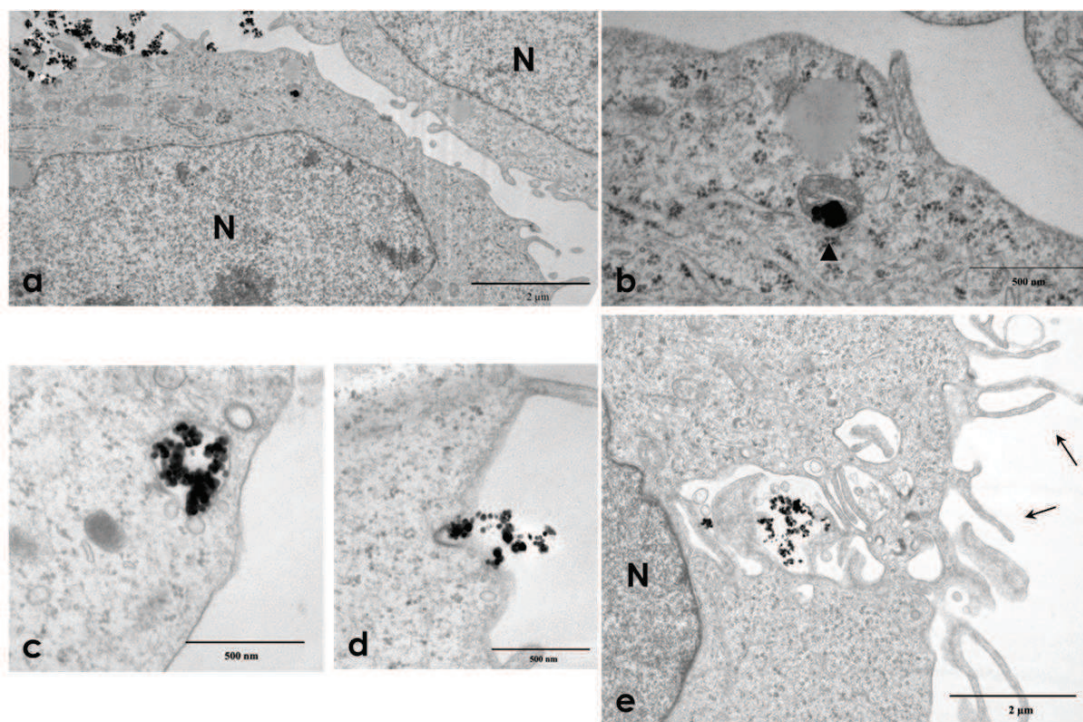
Fig. 38 TEM pictures of SKOV-3 (a, b), HCT116 (c, d) and U87 (e) cells exposed to Fe$_3$O$_4$ NPs@APTES-DAAO for 24h.

Figure 38 shows that Fe$_3$O$_4$ NPs@APTES-DAAO are internalized via endocytosis, in fact pseudopodes (the characteristic structure of this pathway) are evident. Once entered the cells, the majority of NPs remain in the cytoplasm (Fig. 39) inside the endocytic vesicles (Fig. 38c, e). Nevertheless vesicles may undergo mechanical damage, freeing NPs, which could reach different cell districts such as mitochondria (Fig. 38b). However NPs

does not enter nucleus, as it is evident by OM images (Fig. 39). Moreover NPs does not seem to affect mitosis machinery, since nuclei in mitosis are evident (Fig. 39).

Fig. 39 Optical microscope pictures of SKOV-3, HCT116 and U87 cells exposed to Fe_3O_4 NPs and Fe_3O_4 NPs@APTES-DAAO for 24h.

IN VIVO ANALYSIS

Mice treated with Fe_3O_4 NPs@APTES-DAAO for 24 showed no relevant behavioral alterations (tab. 6). Also serum biochemistry and hematology analysis did not show alterations.

Time: +15 min

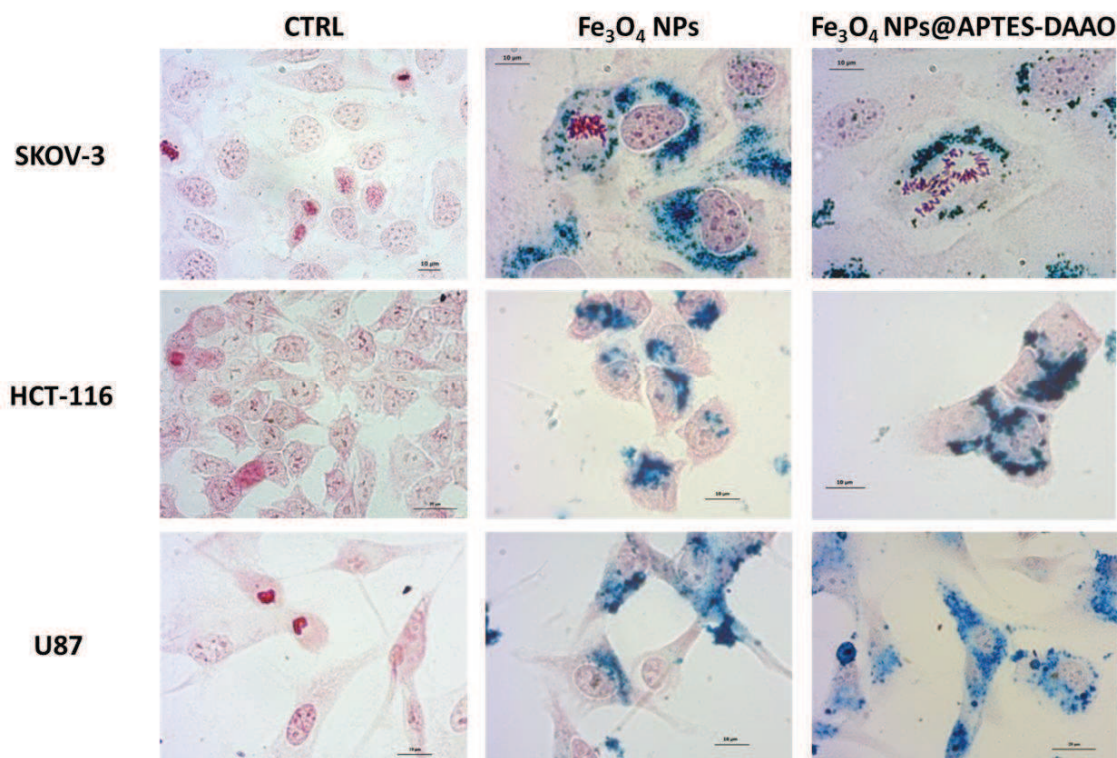| Undisturbed animal	Ref value	CTR		Fe3O4-DAAO 100mg/kg		
		C3	C4	C1	C2	C5
1) Body position	4	4	4	4	4	4
2) Mobility	0	0	0	0	0	0
3) Eye prominence	-	-	-	-	-	-
4) Respiration	4	4	4	4	4	4
5) Tremors	0	0	0	0	0	0
6) Convulsions	-	-	-	-	-	-
7) Grooming	4	0	0	0	0	0
8) Stereotypies	0	0	0	0	0	0
9) Piloerection	0	0	0	0	0	0
Disturbed animal						
1) Touch response	4	4	4	2	4	4
2) Positional passivity	0	0	0	0	0	0
3) Catatonia	0	0	0	0	0	0
4) Grip strenght	4	4	4	4	4	4
5) Abdomen tone	4	4	4	4	4	4
6) Corneal reflex	4	4	4	4	4	4
7) Pinna reflex	4	4	4	4	4	4
8) Tail pinch response	4	4	4	4	4	0
9) Righting reflex	0	0	0	0	0	0
Neurovegetative profile						
1) Skin color	4	4	4	4	4	4
2) Stools	-	-	-	-	-	-
3) Urines	-	-	-	-	-	-
4) Lacrimation	0	0	0	0	0	0
5) Salivation	0	0	0	0	0	0
6) Rhinorrhea	0	0	0	0	0	0
7) Temperature	/	/	/	/	/	/

Time: + 5 min

Undisturbed animal	Ref value	CTR		Fe3O4-DAAO 100mg/kg		
		C3	C4	C1	C2	C5
1) Body position	4	4	4	4	4	4
2) Mobility	4	0	0	4	0	4
3) Eye prominence	-	-	-	-	-	-
4) Respiration	4	4	4	4	4	4
5) Tremors	0	0	0	0	0	0
6) Convulsions	-	-	-	-	-	-
7) Grooming	4	0	0	0	0	0
8) Stereotypies	0	0	0	0	0	0
9) Piloerection	0	0	0	0	0	0
Disturbed animal						
1) Touch response	4	4	4	4	4	4
2) Positional passivity	0	0	0	0	0	0
3) Catatonia	0	0	0	0	0	2
4) Grip strenght	4	4	4	4	4	4
5) Abdomen tone	4	4	4	4	4	4
6) Corneal reflex	4	4	4	4	4	4
7) Pinna reflex	4	4	4	4	4	4
8) Tail pinch response	4	4	4	4	4	4
9) Righting reflex	0	0	0	0	0	0
Neurovegetative profile						
1) Skin color	4	4	4	4	4	4
2) Stools	-	-	-	-	-	-
3) Urines	-	-	-	-	-	-
4) Lacrimation	0	0	0	0	0	0
5) Salivation	0	0	0	0	0	0
6) Rhinorrhea	0	0	0	0	0	0
7) Temperature	/	/	/	/	/	/

Time: +30 min

Undisturbed animal	Ref value	CTR		Fe3O4-DAAO 100mg/kg		
		C3	C4	C1	C2	C5
1) Body position	4	6	4	4	4	4
2) Mobility	4	0	0	0	0	0
3) Eye prominence	-	-	-	-	-	-
4) Respiration	4	4	4	4	4	4
5) Tremors	0	-	0	0	0	-
6) Convulsions	-	-	-	-	-	-
7) Grooming	4	0	0	4	0	0
8) Stereotypies	0	0	0	0	0	0
9) Piloerection	0	0	0	0	0	0
Disturbed animal		JUMP				
1) Touch response	4	8	4	2	4	4
2) Positional passivity	0	0	0	0	0	0
3) Catatonia	0	0	0	0	0	0
4) Grip strenght	4	4	4	4	2	4
5) Abdomen tone	4	4	4	4	4	4
6) Corneal reflex	4	4	4	4	4	4
7) Pinna reflex	4	4	4	4	4	4
8) Tail pinch response	4	4	4	4	4	4
9) Righting reflex	0	0	0	0	0	0
Neurovegetative profile						
1) Skin color	4	4	4	4	4	4
2) Stools						
3) Urines	-	+	-	-	-	-
4) Lacrimation	0	0	0	0	0	0
5) Salivation	0	0	0	0	0	0
6) Rhinorrhea	0	0	0	0	0	0
7) Temperature	/	/	/	/	/	/

Time: +60 min

Undisturbed animal	Ref value	CTR		Fe3O4-DAAO 100mg/kg		
		C3	C4	C1	C2	C5
1) Body position	4	6	4	4	4	4
2) Mobility	4	0	0	0	0	0
3) Eye prominence	-	-	-	-	-	-
4) Respiration	4	4	4	4	4	4
5) Tremors	0	0	0	0	0	0
6) Convulsions	-	-	-	-	-	-
7) Grooming	4	0	0	0	0	0
8) Stereotypies	0	0	0	0	0	0
9) Piloerection	0	0	0	0	0	0
Disturbed animal		JUMP				
1) Touch response	4	8	4	2	2	4
2) Positional passivity	0	0	0	0	0	0
3) Catatonia	0	0	0	0	0	0
4) Grip strenght	4	4	4	4	4	4
5) Abdomen tone	4	4	4	4	4	4
6) Corneal reflex	4	4	4	4	4	4
7) Pinna reflex	4	4	4	4	4	4
8) Tail pinch response	4	4	4	4	4	4
9) Righting reflex	0	0	0	0	0	0
Neurovegetative profile						
1) Skin color	4	4	4	4	4	4
2) Stools		11	12	6	4	2
3) Urines	-	-	-	-	-	-
4) Lacrimation	0	0	0	0	0	0
5) Salivation	0	0	0	0	0	0
6) Rhinorrhea	0	0	0	0	0	0
7) Temperature	/	/	/	/	/	/

Tab 6 Irwin test on mice treated with 100mg/kg Fe_3O_4 NPs@APTES-DAAO for 24h.

Body weight of mice and relative organ weight of liver, spleen and kidneys, expressed as percentages of weight gain, of both experiments, are reported respectively in tables 7 and 8.

Exp 1	Weight gain (%) T 24h	Exp 2	Weight gain (%) T 24h
Ctrl	-1,6 ± 1,9	Ctrl	-2,9 ± 0,4
Fe_3O_4 NPs@APTES-DAAO	-3,5 ± 2,2	Fe_3O_4 NPs@APTES-DAAO	-3,5 ± 2,8
t-test	0,408	t-test	0,784

Tab 7 Percentage of body weight gain in mice treated with 100mg/kg (on the left, Exp 1) and 20mg/kg (on the right, Exp 2).

Exp 1	Liver	Spleen	Kidneys
Ctrl	6,55 ± 1,2	0,48 ± 0,1	1,91 ± 0,0
Fe_3O_4 NPs@APTES-DAAO	7,8 ± 0,3	0,57 ± 0,1	1,63 ± 0,1
T-test	0,431	0,318	0,026*
Exp 2	Liver	Spleen	Kidneys
Ctrl	6,66 ± 0,1	0,5 ± 0,1	1,75 ± 0,1
Fe_3O_4 NPs@APTES-DAAO	6,90 ± 0,2	0,54 ± 0,1	1,59 ± 0,2
T-test	0,151	0,589	0,327

Tab 8 Percentage of relative organ weights gain in mice treated with 100mg/kg (on the left, Exp 1) and 20mg/kg (on the right, Exp 2).

No significant differences in body weight gain and relative organ weight were observed between control and Fe_3O_4 NPs@APTES-DAAO treated groups. The kidney relative organ weight of the first experiment was significantly lower in treated group than in control group

(p<0.05), but this was attributable to the exceptionally high relative weight of kidneys in control mice (as compared to control mice of other experiments performed in similar conditions) and not to a reduced relative weight of kidneys in treated group. This finding can thus be considered not relevant.

As regards pathological examination of the first experiment, a gross examination shows in the liver of 3/3 treated mice a diffuse mild black-brown discoloration compared to control mice. Histopathological examination reported in 3/3 treated mice abundant intracytoplasmic iron pigment in the liver, spleen and lung and only occasionally in the kidney, lymph nodes and intravascular leukocytes. According to histological and immunofluorescence analysis, in the liver the Iron pigment was found mainly in the cytoplasm of Kupffer cells (immunostained with Iba-1), but occasionally also within spindle-shaped cells, likely consistent with hepatic sinusoidal endothelial cells (figure 40).

In 3/3 treated mice the following relevant histopathological lesions were found:

Lung: interstitial neutrophilic and histiocytic pneumonia, multifocal, mild, chronic with intralesional variably sized

aggregates of iron pigment. Occasionally these aggregates were large, approx. 50-100 μm in diameter (figure 41).

Spleen: white pulp, follicular reactive hyperplasia mild to moderate; red pulp, extramedullary hematopoiesis with predominance of myelopoietic precursors and megakaryocytes and likely a decrease of erythroid precursors.

In the light of all these findings we can say that the slight brown-black discoloration of the liver observed grossly in all treated mice was related to the presence of abundant iron pigment found in the cytoplasm of Kupffer cells.

Histologically, intracytoplasmic brown granular material consistent with visible aggregates of iron-containing nanoparticles was observed mainly in the phagocytic cells of liver, spleen, and lung. These cells take Fe_3O_4 NPs@APTES-DAAO directly from the blood stream and store them in their cytoplasm.

In the lung of all treated mice, the aggregates were occasionally very large (up to 100μm), mostly associated with interstitial inflammation or occluding alveolar septa capillaries (Fig. 41). The presence of

large aggregates of iron pigment in the lung may be secondary to IV administration of aggregated nanoparticles, as suggested by the results of DLS analysis (see DLS ANALYSIS), with subsequent embolization to the lung.

In the spleen, reactive follicular hyperplasia was observed. This finding may be interpreted as an antigenic response, likely directed against the enzymatic portion of the nanoparticle

In general no overt adverse effects have been observed at 24 hours after IV administration of 100mg/kg Fe_3O_4 NPs@APTES-DAAO, however the presence of aggregates of iron-containing nanoparticles in the capillaries of the lung, occasionally associated with focal histiocytic and neutrophilic inflammation should be caused by the high dose of NPs injected.

Pathological gross examination of mice treated with 20mg/kg, in fact, shows no relevant changes in respect with control mice. Histological examination shows in 3/3 treated mice small to moderate amount of intracytoplasmic iron pigment in the liver and spleen. In

1/3 treated mice, rare small aggregates were found in the lung interstitium (figure 42).
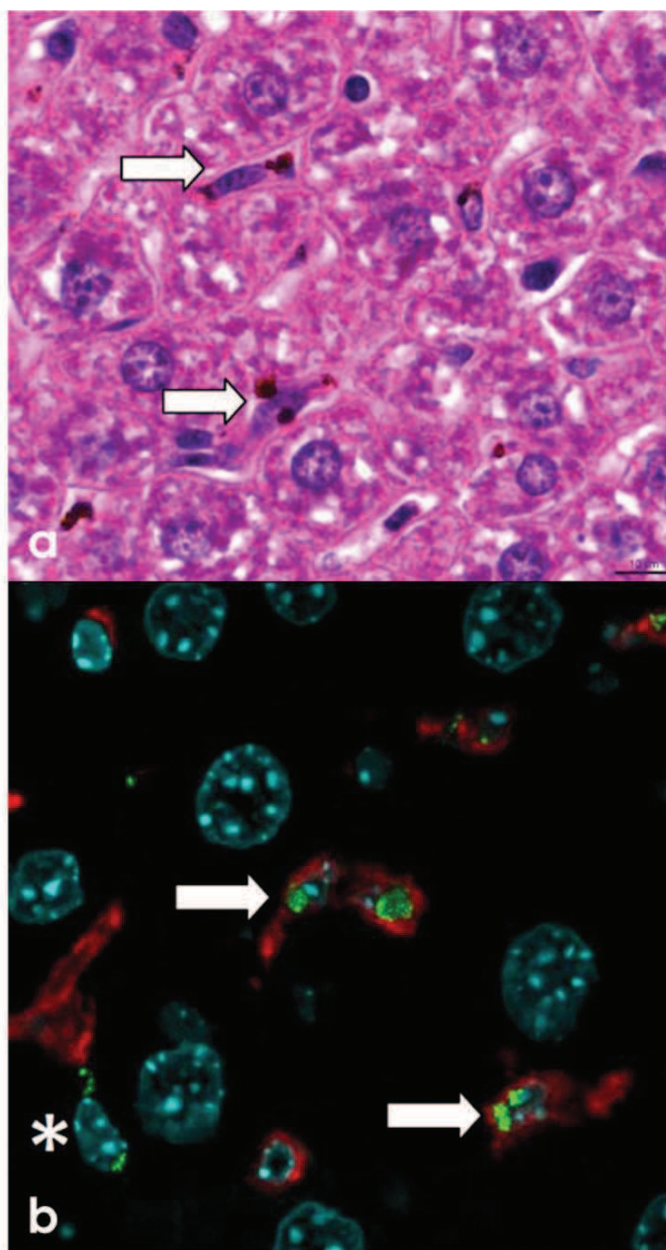
Fig. 40 a) histological examination of mouse liver. Arrows indicate iron NPs aggregates. b) NPs (green) in cytoplasm of Kupffer cells (red, arrows) and in spindled cells (*). Nuclei stained in DAPI (cyan).
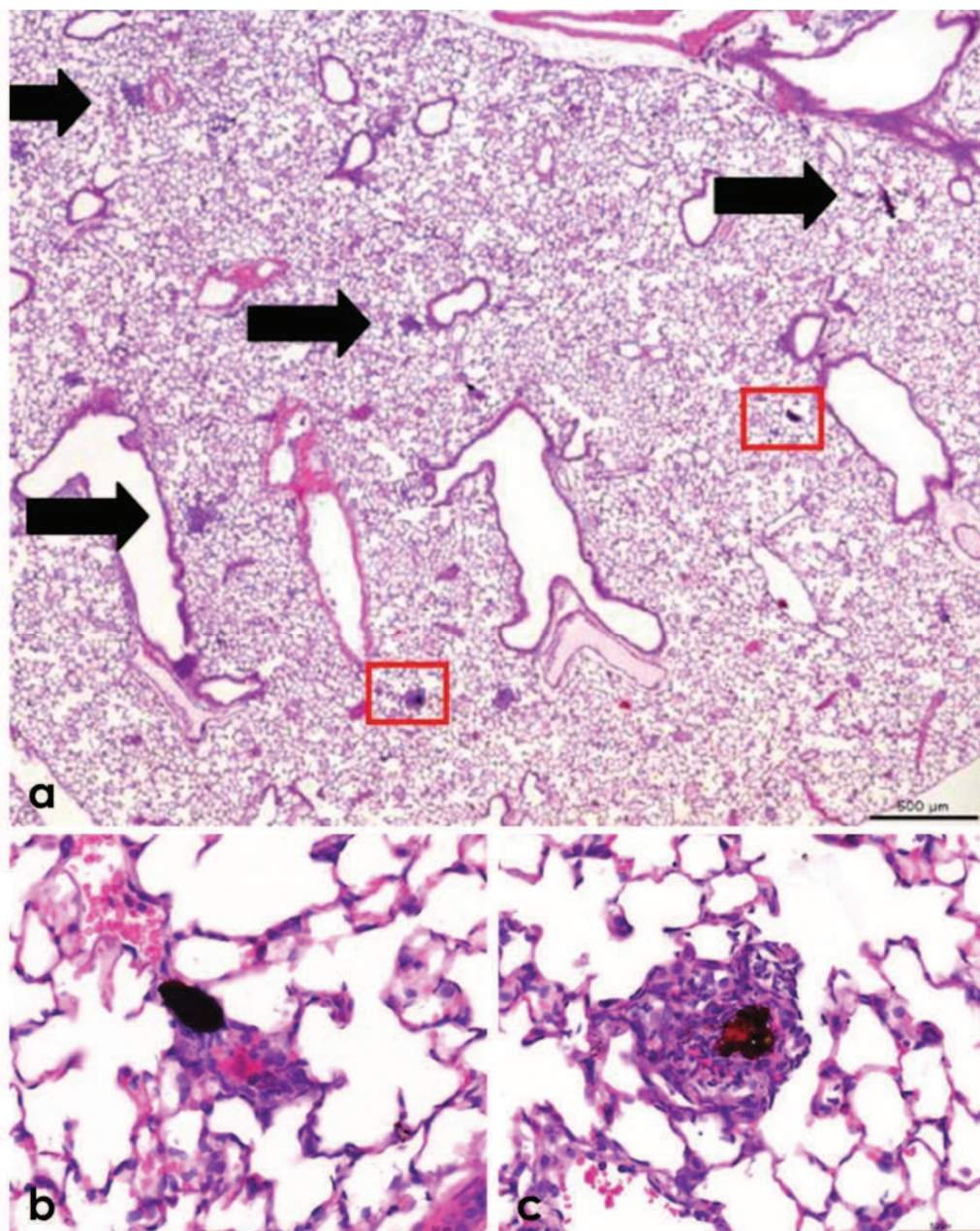
Fig. 41 Histological examination of mouse lung. a) Multiple foci of alveolar septa infiltration (arrows). b) Alveolar septa infiltrated by macrophages and neutrophils surrounding a NPs aggregate. c) Dense and homogenous aggregate of NPs likely occluding an alveolar septum capillary.
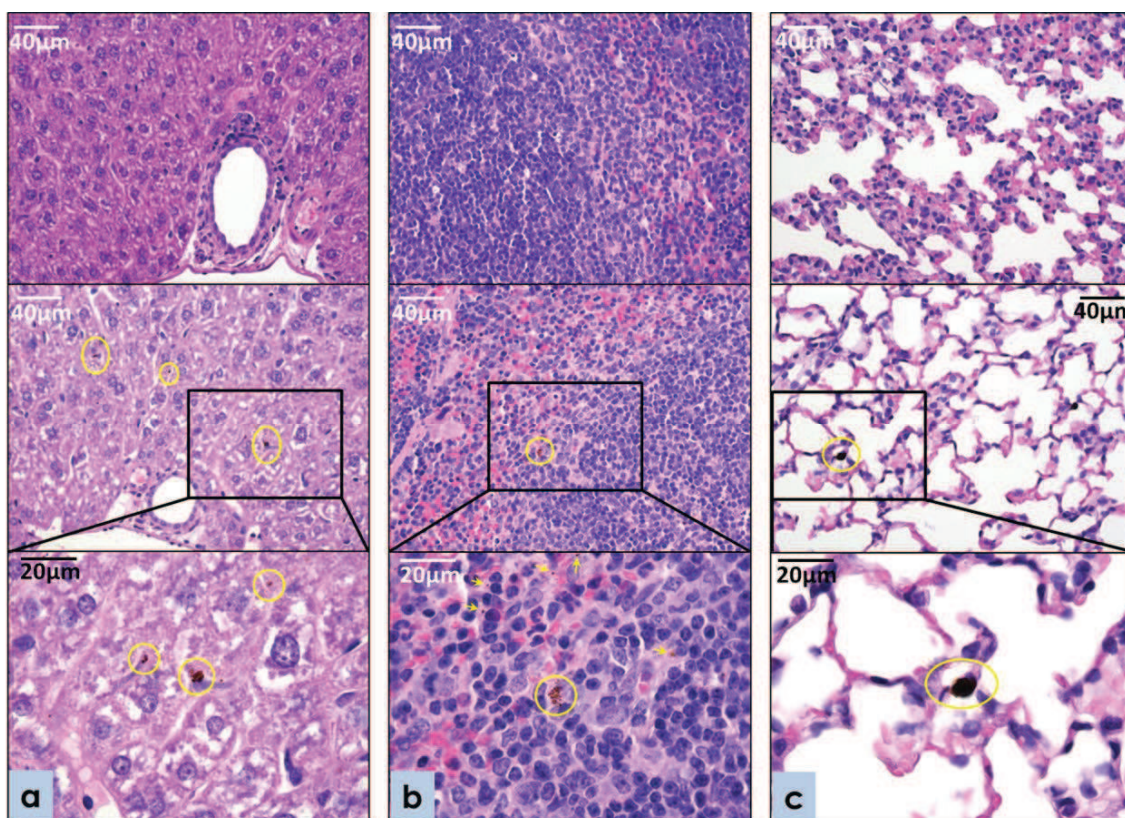
Fig. 42 histological images of liver (a), spleen (b) and lung (c). Brown granular materials, consistent with aggregates of NPs, are evident (yellow circles and arrows).

No adverse effects have been observed at 24h after IV administration of 20mg/kg Fe_3O_4 NPs@APTES-DAAO.

In none of the experiments NPs were found in heart and brain. Testis was examined only for animals treated with 20mg/ml but no positivity was found. This suggests that without an external magnetic field, NPs cannot pass blood-barriers.

A summary of Fe_3O_4 NPs@APTES-DAAO biodistribution is reported in table 9.

Case #	EXP	Liver	Spleen	Lung		Kidneys	Heart	Brain
				macrophages	Intravascular aggregates			
A1	CTR	-	-	-	-	-	-	-
A2	EXP 2	++	+	+	-	+	-	-
A5		++	+	+	-	+	-	-
C1	EXP 1	+++	++	+	+	+	-	-
C5		+++	++	+	+	+	-	-

Legend:
- = negative
+ = rare positive spots
++ = some positive spots
+++ = numerous positive spots

Tab 9 Semi-quantitative results of first and second experiment (Exp 1 and Exp 2) of Fe_3O_4 NPs@APTES-DAAO accumulation in liver, spleen, lung, kidneys, heart and brain.

II.III: CONCLUSIONS

We have designed and produced a NPs-enzyme system for cancer therapy: Fe_3O_4 NPs@APTES-DAAO. Under our best experimental condition, we have immobilized 100% of the enzyme in term of activity and quantity. The system showed an activity of 7U/mg of NPs and an apparent K_m for D-Ala similar to that of the free enzyme. These results are difficult to compare with data in literature [104, 105, 106] due to the disparate experimental conditions used. However, Hsieh *et al.* reported an immobilization efficiency of 85% and a lower conjugated activity than our system [106]. Divakaran *et al.* reported a Fe_2O_3 NPs system conjugate to DAAO from pig (pkDAAO). However, maghemite has lower magnetic properties than magnetite and pkDAAO has a lower activity than RgDAAO, resulting altogether in a system less efficient than Fe_3O_4 NPs@APTES-DAAO [104].

In vitro cytotoxicity demonstrates the higher efficacy of the system in respect to free enzyme. This is probably due to the fact that NPs have the tendency to sediment, bringing and accumulating the enzyme near the cells. In this way there is a localized production of ROS with an enhanced toxicity. Moreover, as seen with optical and

transmission microscope, Fe_3O_4 NPs@APTES-DAAO enter the cells producing an oxidative damage inside the cells. Also free DAAO can enter cells, but the enzyme tends to remain in suspension, the final effect is then a lower concentration of DAAO in the environment near the cells, and then inside them.

In vivo experiments did not have highlighted adverse side effects of Fe_3O_4 NPs@APTES-DAAO at a concentration of 20mg/kg. At the tested concentrations our NPs do not pass brain-blood barrier and do not accumulate in the heart.

Future aim will be to analyze the biodistribution of NPs under application of an external magnetic field. Mice will be injected with the system and subjected to a localized magnetic field. The ability of NPs to accumulate in the area affected by the magnetic field will be investigated. Moreover, the ability of NPs to cross blood-barriers under the magnetic field will be analyzed. Finally system's ability to destroy tumor cells in vivo will be tested.

CHAPTER III

Synthesis Of Magnetic Nanoparticle System For Antibacterial Therapy: NP@Teicoplanin

III.I: MATERIALS AND METHODS

Fe₃O₄ NPs@APTES

SEE CHAPTER II, II.I: MATERIAL AND METHODS, Fe₃O₄ NPs@APTES.

Fe₃O₄ NPs@CMCS

The covalent immobilization of CMCS on Fe₃O₄ NPs was conducted following Liang and Zhang's method [107] with some modifications.

75mg of Fe₃O₄ NPs were sonicated for 30min with 4ml of 200mM sodium phosphate buffer (pH 5) containing 25mg of EDC•HCl (1-Ethyl-3-(3-dimethylaminopropyl)carbodiimide, Sigma n.cat: 03450) and 20mg of N-Hydroxysuccinimide (NHS, Sigma, n.cat: 130672).

Activated Fe₃O₄ NPs were separated from supernatant by magnetic decantation and suspended in 3mL of 200mM sodium phosphate buffer (pH 7) by sonication for 10min. 1mL of CMCS solution (25mg/mL in 200mM sodium phosphate buffer, pH 7) was added and the reaction was sonicated for 3h. Finally, Fe₃O₄ NPs@CMCS were washed with water, and dried overnight at 50°C.

Fe₃O₄ NPs@APTES-Teicoplanin (electrostatic)

4mg of Fe₃O₄ NPs@APTES were suspended in H₂O by sonication for 15min. 1mg of teicoplanin was added in a

final volume of 1ml or 2ml. The reaction was carried out for a period of time between 2 and 3.5 h, in relation to the reaction considered, at room temperature using a rotating plate tube stirrer.

Subsequently, Fe_3O_4 NPs@APTES-Teicoplanin were collected by a magnet and washed twice with 500µl of H_2O. The supernatant was stored for further analysis.

Fe_3O_4 NPs@APTES-Teicoplanin (covalent)

4mg of Fe_3O_4 NPs@APTES were suspended in H_2O by sonication for 15min and then 3mg of EDC and 2mg of NHS were added. 1mg of teicoplanin was added to a final volume of 1ml. The reaction was carried out for 3.5h at room temperature using a rotating plate tube stirrer.

Subsequently, Fe_3O_4 NPs@APTES-Teicoplanin were collected by a magnet and washed twice with 500µl of H_2O. The supernatant was stored for further analysis.

Fe_3O_4 NPs@Teicoplanin

4mg of Fe_3O_4 NPs were suspended in H_2O by sonication for 15min. 1mg of teicoplanin was added in a final volume of 1ml. The reaction was carried out for 2h, at room temperature using a rotating plate tube stirrer.

Subsequently, Fe_3O_4 NPs@Teicoplanin were collected by a magnet and washed twice with 500ml of H_2O. The supernatant was stored for further analysis.

Fe_3O_4 NPs@CMCS-Teicoplanin (electrostatic)

4mg of Fe_3O_4 NPs@CMCS were suspended in H_2O or PBS (depending on the reaction considered) by sonication for 15min. 500µg of teicoplanin were added to a final volume of 1ml. The reaction was carried out for 5h, at room temperature using a rotating plate tube stirrer.

Subsequently, Fe_3O_4 NPs@CMCS-Teicoplanin were collected by a magnet and washed twice with 500ml of H_2O or PBS. The supernatant was stored for further analysis.

Fe_3O_4 NPs@CMCS-Teicoplanin (covalent)

4mg of Fe_3O_4 NPs@APTES were suspended in H_2O or PBS by sonication for 15min with 3mg of EDC and 2mg of NHS. 500µg of teicoplanin were added to a final volume of 1ml. The reaction was carried out for 5h, at room temperature using a rotating plate tube stirrer.

Subsequently, Fe_3O_4 NPs@CMCS-Teicoplanin were collected by a magnet and washed twice with 500ml of H_2O or PBS. The supernatant was stored for further analysis.

Quantification of conjugated teicoplanin

The amount of antibiotic bound to NPs was determined as the difference between the starting amount of teicoplanin and the antibiotic recovered in the supernatant at the end of reaction. Quantification was performed using a calibration line. Fixed wavelength measurements were taken using emission wavelength of 330nm and excitation wavelength of 280nm by a JascoFP-750 spectrofluorometer, equipped with a software-driven Peltier system.

Determination of the biological activity: microbiological assay

Microbiological assays using *Sarcina lutea* ATCC9341 were done, using the medium V0.1 (MV0.1) whose composition is: 2.4g/L soluble starch (Difco), 0.1g/L dextrose (A.D.E.A), 0.3g/L malt extract (Constantine), 0.5 g/L yeast extract (Constantine); 0.5g/L triptose (Difco), 15g/L Agar (Sigma), 1L of deionized water, pH 7.2.

For the overlay of the microbiological assay, 100μl of *S. lutea* glycerinate were pre-inoculated in 10ml of medium AM1 (30.5g/L Antibiotic Medium A, Difco) at 37°C at 200rpm over-night. 2ml of this pre-culture were inoculated in 50ml of LB and incubated at 200rpm at

37°C until reaching an OD600 of around 0.4-0.6. 10% (v/v) of the *S. lutea* culture was added to the SNA (Soft Nutrient Agar) medium (5g/L peptone, Costantino, 3g/L beef extract, Costantino, 5g/L agar, Sigma) and 10ml of this solution are used for the overlay on the plates with teicoplanin.

For the microbiological assay, plates with MV0.1 were prepared and a drop of Fe_3O_4 NPs@CMCS-Teicoplanin was plated in the center and allowed to dry. The plates were placed at 37°C over-night and the zone of inhibition was measured for the assessment of microbiological activity. Control experiment plating a drop of free teicoplanin, Fe_3O_4 NPs, Fe_3O_4 NPs@CMCS and Fe_3O_4 NPs@APTES were done.

III.II: Results and Discussion

Teicoplanin conjugation and quantification

Several attempts were done for teicoplanin immobilization. Three different nanoparticle supports were used: Fe_3O_4 NPs@APTES, Fe_3O_4 NPs and Fe_3O_4 NPs@CMCS. Moreover a number of different reaction conditions were tried. Table 10 summarizes reactions carried out.

NPs	mg NPs	solvent	EDC	NHS	Teicoplanin (mg)	fV (ml)	h	T°C	µg bound	% Teico Bound
Fe_3O_4 NPs@APTES	4	H_2O	3mg	2mg	1	1	3.30	RT	823	82
Fe_3O_4 NPs@APTES	4	H_2O	//	//	1	2	3.30	RT	643	64
Fe_3O_4 NPs@APTES	4	H_2O	//	//	1	1	2	RT	706	71
Fe_3O_4 NPs	4	H_2O	//	//	1	1	2	RT	669	67
Fe_3O_4 NPs@CMCS	4	H_2O	//	//	0,5	1	5	RT	252	50
Fe_3O_4 NPs@CMCS	4	PBS	//	//	0,5	1	5	RT	75	15
Fe_3O_4 NPs@CMCS	4	H_2O	3mg	2mg	0,5	1	5	RT	402	80
Fe_3O_4 NPs@CMCS	4	PBS	3mg	2mg	0,5	1	5	RT	460	92
Fe_3O_4 NPs@CMCS	4	PBS	3mg	2mg	0,5	1	5	RT	456	91
Fe_3O_4 NPs@CMCS	4	PBS	3mg	2mg	0,5	1	5	RT	455	91
Fe_3O_4 NPs@CMCS	4	PBS	3mg	2mg	0,5	1	5	RT	459	92
Fe_3O_4 NPs@CMCS	4	PBS	3mg	2mg	0,5	1	5	RT	464	93
Fe_3O_4 NPs@CMCS	4	PBS	3mg	2mg	0,5	1	5	RT	458	92

Tab 10 Summary of reaction conditions of Teicoplanin immobilization on NPs with spectrofluorometer quantification of antibiotic bound.

Despite Fe_3O_4 NPs@APTES conjugate with covalent bound over 80% of the enzyme, no activity was recovered with microbiological assay. Also electrostatic reaction on Fe_3O_4 NPs@APTES and Fe_3O_4 NPs was quite satisfactory in term of quantity of bound enzyme (mean of 67%), but NPs does not have activity. As what concern electrostatic reaction on Fe_3O_4 NPs@CMCS, a very low

quantity of antibiotic conjugates on NPs: 50% in H_2O and 15% in PBS. Moreover microbiological analysis does not show any activity. With covalent reaction over 80% of antibiotic is able to conjugate on Fe_3O_4 NPs@CMCS both in H_2O and PBS. However only antibiotic conjugated in PBS has activity (table 11).

NPs	SOLVENT	BOUND	Activity MIC
Fe_3O_4 NPs@APTES	H_2O	covalent	NO
Fe_3O_4 NPs@APTES	H_2O	electrostatic	NO
Fe_3O_4 NPs@APTES	H_2O	electrostatic	NO
Fe_3O_4 NPs@CMCS	H_2O	electrostatic	NO
Fe_3O_4 NPs@CMCS	PBS	electrostatic	NO
Fe_3O_4 NPs@CMCS	H_2O	covalent	NO
Fe_3O_4 NPs@CMCS	PBS	covalent	YES

Tab 11 Summary of reactions with MIC results

Being that the only positive activity result was seen with Fe_3O_4 NPs@CMCS-Teicoplanin prepared in PBS with covalent bound, the reaction was repeated several times. Unfortunately the reaction is not reproducible. In fact, though unchanged reaction conditions, Fe_3O_4 NPs@CMCS-Teicoplanin do not always show activity. This probably because the conjugation reaction is difficult to manage and, sometimes, conjugation with the NPs may occur in or near the active site of the antibiotic, compromising activity. Moreover, even if Fe_3O_4 NPs@CMCS-Teicoplanin possess activity at the end of

reaction, this is lost during storage at 4°C. Several attempt of storage in different condition (H_2O or PBS, -20°C or 4°C) have been made but no correlation can be seen.

III.III: CONCLUSIONS

Teicoplanin has been conjugated on Fe$_3$O$_4$ NPs@CMCS with efficiency in term of quantity over the 90%. Unfortunately, the reaction was not reproducible and some problems are associated with storage. The main problem is probably due to the wide active site of teicoplanin: interactions with NPs may affect some of the residues involved in substrate recognition, leading to a loss of activity. To overcome this problem, future goals relate to the optimization of reaction conditions, trying to protect the active site function.

CHAPTER IV

SYNTHESIS OF Fe$_3$O$_4$ NPs@APTES-ACYLASE

IV.I: Materials and Methods

Fe₃O₄ NPs@APTES

See Chapter II, Section II.I: Material and Methods, Fe_3O_4 NPs@APTES.

Fe₃O₄ NPs@APTES-VAC

24mg of Fe_3O_4 NPs@APTES were suspended by sonication for 15min with 1-Ethyl-3-(3-dimethylaminopropyl)carbodiimide (EDC, Sigma n.cat: 03450) and N-Hydroxysuccinimide (NHS, Sigma, n.cat: 130672) in 3:2 ratio in buffer 20mM KH_2PO_4 pH 8. 560µg of VAC were added and the reaction (in a final volume of 2ml) was carried out for 24h at 4°C using a rotating plate tube stirrer.

Subsequently, Fe_3O_4 NPs@APTES-VAC were collected by a magnet and washed twice with 1ml of 20mM KH_2PO_4 pH 8. The supernatant was stored for further analysis.

Fe₃O₄ NPs@APTES-VAC activity assay

VAC catalyzes the hydrolysis of CephC to 7-ACA. The primary amino group of 7-ACA reacts with pDMAB, giving a yellow Schiff's base with a maximum of absorbance at 415nm [108]. In detail: 5µl of enzyme (in a phosphate buffer at pH 8.0) were incubated with 100µl of 2% (w/v) CephC (pH 8.0) for 10 min at 25°C. The

reaction was stopped with 600μl of 20% acetic acid, and then 133μl of 0.5% (w/v) pDMAB (dissolved in methanol) were added and the reaction was incubated for 10min at 25°C, before measuring the absorbance at 415nm.

Fe_3O_4 NPs@APTES-VAC BIOCONVERSION

The time course of bioconversion was determined by a pH-stat assay. The reaction mixture contained 50mM CephC (pH 8.0) and 0.48U of Fe_3O_4 NPs@APTES-VAC in a final volume of 20ml of H_2O or 0.48U of free VAC in a final volume of 10ml of H_2O. Reaction was incubated at 25°C, and aliquots were drawn at different times (up to 70h). Fe_3O_4 NPs@APTES with 50mM CephC and Fe_3O_4 NPs@APTES with water were used as control.

IV.II: Results and Discussion

VAC conjugation on Fe₃O₄ NPs@APTES

Several attempts were made in order to find better condition for VAC conjugation. Figure 43 summarizes reaction performed in different conditions.
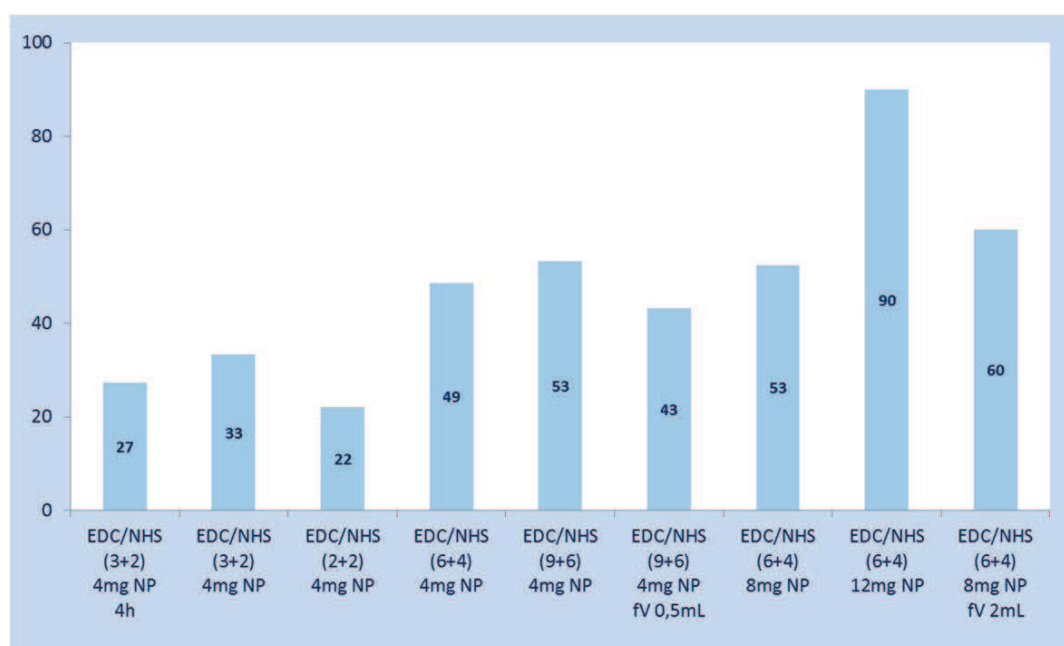

Fig. 43 Summary of VAC conjugation reactions on Fe₃O₄ NPs@APTES with % of immobilized units. Where not specified, the duration of the reaction is 24h and the final volume (fV) is 1ml. For all experiments 300μg of enzyme were used corresponding to 0.27U.

In best experimental conditions 90% of units are conjugated on Fe₃O₄ NPs@APTES, the reaction is reproducible and activity is stable for several weeks. Moreover Fe₃O₄ NPs@APTES-VAC can be used several

times (4/5 times) before a loss in catalytic efficiency may occur. It must be noted that free VAC possesses a specific activity of 0.9U/mg, this means that Fe_3O_4 NPs@APTES-VAC have maximum activity of 0.24U. In light of all these results we decided to increase the activity of the system by scale-up. Characteristics of the new system are summarized in table 12.

	free VAC		System	Scale-up
U/mg	0,9	mg NP	12	24
		U	0,24	0,48

Tab 12 Characteristics of Fe_3O_4 NPs@APTES-VAC and its scale up.

Fe_3O_4 NPS@APTES-VAC BIOCONVERSION OF CephC

The ability of the system to convert CephC to 7-ACA was investigated using a stirred reactor in comparison to the enzymes in the free form.

Theoretical calculations for the bioconversion with the free enzyme indicate that the reaction should be completed in 17.4h, while the Fe_3O_4 NPs@APTES-VAC should convert all the substrate in 34.7h (see figure 44).

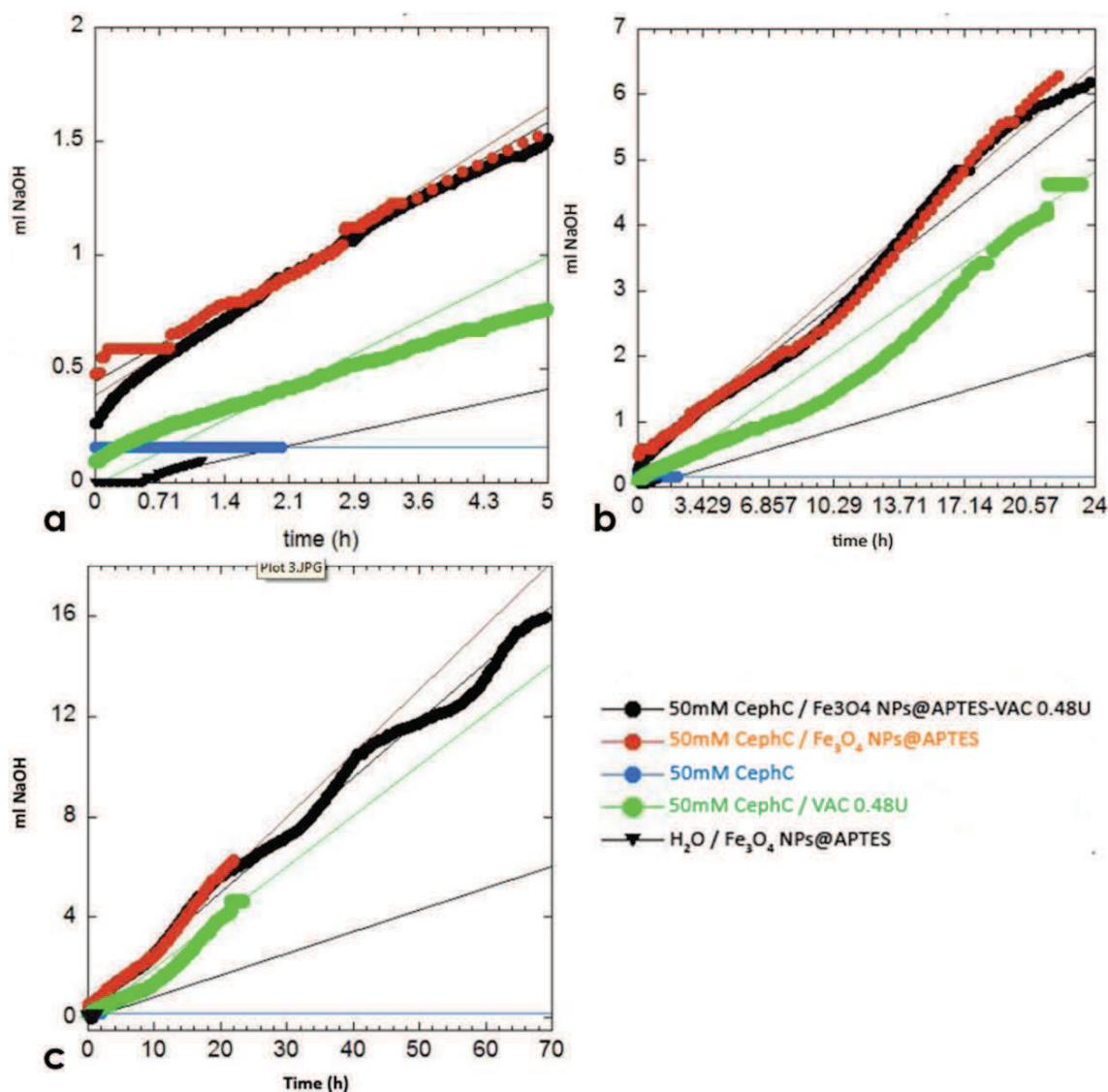The bioconversion time course was followed by the pH-stat assay and results are shown in figure 44.

Fig. 44 CephC bioconversion at 5h (a) 24h (b) and 70h (c). Fe₃O₄ NPs@APTES (in water and 50mM CephC) and CephC alone were used as control. 0.1M NaOH was used to compensate pH variation.

The free enzyme completed the reaction within 22h, confirming theoretical calculations. Unfortunately Fe₃O₄ NPs@APTES-VAC, do not seems to have a specific bioconversion activity. In fact, Fe₃O₄ NPs@APTES-VAC

and Fe₃O₄ NPs@APTES curves overlap and Fe₃O₄ NPs@APTES-VAC reaction continues after 70h (figure 44). This indicates that the pH lowering is nonspecific and caused by NPs.

IV.III: CONCLUSIONS

Despite the efficiency of VAC conjugation on NPs (90%), the low specific activity of the enzyme does not allow to obtain en efficient system on an adequate support (24mg of NPs for 0.48U if VAC). Moreover bioconversion analysis indicates that Fe_3O_4 NPs@APTES interfere with the assay. For this reason there is the need to find other methods to assess the bioconversion ability of the enzyme (for example by HPLC).

Moreover in order to make the system more efficient, efforts will be done in order to find a VAC mutant with a higher specific activity. Future goals relate precisely this last point, so as to increase the specific activity of the system.

CHAPTER IV

SYNTHESIS OF Fe₃O₄ NPs@APTES-LASPO

V.I: MATERIALS AND METHODS

Fe₃O₄ NPs@APTES

SEE CHAPTER II, SECTION II.I: MATERIAL AND METHODS, Fe_3O_4 NPS@APTES.

Fe₃O₄ NPs@APTES-LASPO

8mg of Fe_3O_4 NP@APTES were sonicated for 15min in 5mM NaPPi pH 8.0. 12mg of EDC (1-Ethyl-3-(3-dimethylaminopropyl)carbodiimide, Sigma n.cat: 03450) and 8mg of NHS (N-Hydroxysuccinimide, Sigma, n.cat: 130672) were added under sonication. About 0.06U of StLASPO were added and the reaction was carried out for 2h at room temperature on a rotating plate tube stirrer. The final volume of the reaction was 2ml. Subsequently, Fe_3O_4 NPs@APTES–LASPO were collected by a magnet and washed twice with 1ml of 5mM NaPPi pH 8.0. The supernatant was stored for further analysis.

ACTIVITY ASSAY

The LASPO activity was assayed by measuring the initial rate of production of hydrogen peroxide with a coupled peroxidase/dye assay. The dye produced by the horseradish peroxidase from H_2O_2 and 4-aminoantipyrine was detected spectrophotometrically at 505nm

($\varepsilon=6.58mM^{-1}cm^{-1}$) and 25°C. One unit is defined as the amount of enzyme that catalyses the degradation of 1µmol L-aspartate per minute. Unless otherwise stated, the standard assay mixture contained 10mM L-aspartate in 50mM NaPPi pH 8.0, 1.5mM 4-aminoantipyrine, 10mM phenol, 20µM FAD, 2.5U horseradish peroxidase in a total volume of 1ml. 5µl of free LASPO, 40µl of Fe_3O_4 NPs@APTES-LASPO and 80µl of reaction supernatant were assayed.

EFFECT OF SUBSTRATE CONCENTRATION ON CATALYTIC ACTIVITY OF Fe_3O_4 NPS@APTES-LASPO

The resolution of D,L-Aspartate was carried out at pH 10. Fe_3O_4 NPs@APTES-LASPO were stored in phosphate buffer 50mM pH 7.5 at 4°C. After each enzymatic reaction the NPs were washed twice with deionized water and reused with the opportune reaction solution.

1U (216mg) of Fe_3O_4 NPs@APTES-LASPO were suspended in a solution of in 0.5ml D,L-Aspartic (50mM, 150mM and 250mM) pH 10, 200µl of H_2O and 2µL of catalase. The reaction was conducted at 70°C at 600rpm for 2.30h. Every 30min, 40µl were taken from the supernatant, derivatized with the OPA-NAC reagent and analyzed by high-performance liquid chromatography (HPLC, Zorbax

SB-Aq Analitic Column; eluent 100mM sodium acetate pH 5,2; flux 0.6mL/min).

EFFECT OF THE **pH** ON THE RESOLUTION OF **D,L-A**SPARTIC ACID **150mM**

The resolution of 150mM D,L-Aspartic (final concentration of 100mM) at different pH values was carried out. 1U (216mg) of Fe_3O_4 NPs@APTES-LASPO were suspended in a solution of 0.5ml 150mM D,L-Aspartic at different pH (8, 9, 10), 200µl of H_2O and 2µL of catalase. The reaction was conducted at 70°C at 600rpm for 2.30h. Every 30min, 40µl were taken from the supernatant, derivatized with the OPA-NAC reagent and analyzed by high-performance liquid chromatography (HPLC, Zorbax SB-Aq Analitic Column; eluent 100mM sodium acetate pH 5,2; flux 0.6mL/min).

V.II: RESULTS AND DISCUSSION

LASPO CONJUGATION ON Fe₃O₄ NPS@APTES

Several reactions were performed to find the best conditions for LASPO conjugation. Figure 45 summarizes the reactions executed, highlighting the percentage efficiency of immobilization in terms of units.
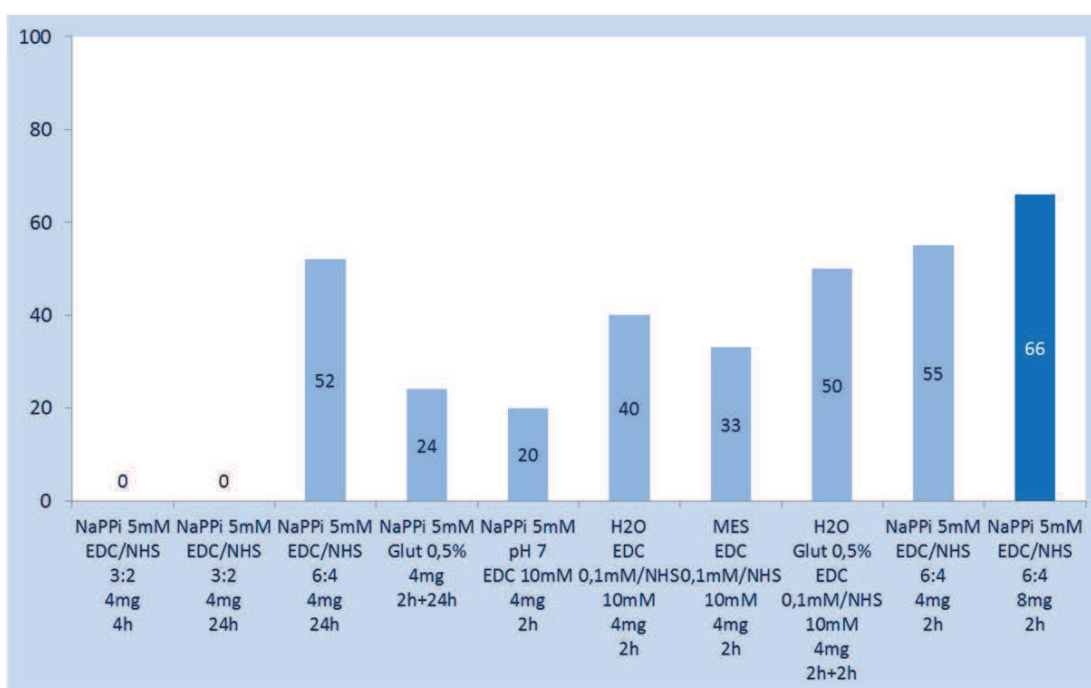

Fig. 45 Summary of LASPO conjugation reactions on Fe₃O₄ NPs@APTES with % of immobilized units. The final volume is 1ml for all reactions except for the last, for which is 2ml. Dark blue indicates the best experimental condition, used for Fe₃O₄ NPs@APTES-LASPO preparation for kinetics experiments.

In best experimental condition about 60% of LASPO is conjugated on NPs. This means that on 8mg of Fe₃O₄

NPs@APTES about 0.4U of LASPO are conjugated. A scale-up was tried, but unfortunately the operation was difficult. To avoid excessive waste of the enzyme, it was decided to get the required amount (1U immobilized) for subsequent experiments performing multiple reactions simultaneously, bringing them all together. For this purpose 27 conjugation reactions were performed, immobilizing about 1U on approximately 216mg of NPs.

CATALYTIC ACTIVITY

The ability of the system in the deracemization of D,L-aspartate mixture was investigated with different substrate concentrations. The conversion of the L-enantiomer was quantified by HPLC. Results are reported in table 13 as percentage of enantiomeric excess (ee).

D, L-Asp Concentration	Final [D, L-Asp]	30' ee %	60' ee %	90' ee %	120' ee %	150' ee %	180' ee %	240' ee %
50mM	35mM	100						
150mM	107mM	25	46	67	85	100		
250mM	178mM		32		57		94	100

Tab 13 Conversion of D, L-aspartate in function of time

With 50mM D,L-aspartate as substrate the reaction reaches the 100% of conversion within 30 minutes, while with 150mM and 250mM within 150 and 240 minutes respectively. Deracemization time is directly proportional to the concentration with an R^2 of 0.9934. Then the

activity of the conjugated enzyme was tested at three different pH values (figure 46). The system seems to be more active at pH 9 whereas the free enzyme prefers pH 10 [96]. No differences can be noted between pH 8 and 9.
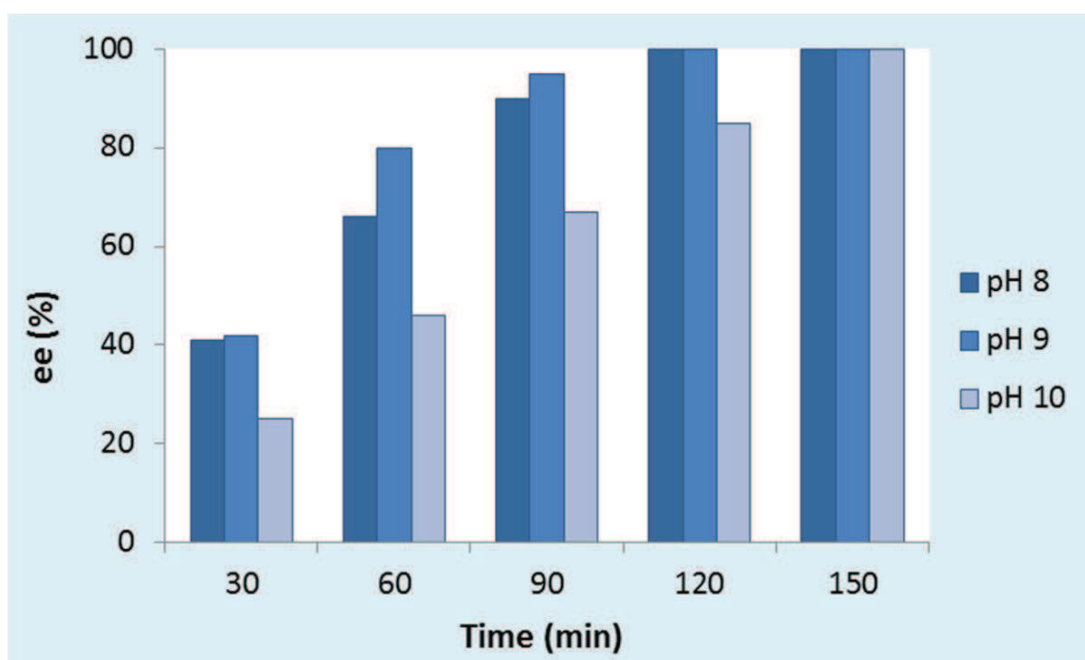

Fig. 46 Conversion of 150mM D, L-aspartic acid at pH 8, 9 and 10.

For all these experiment Fe_3O_4 NPs@APTES-LASPO were reutilized several times, collecting them with the magnet and then bringing them back into suspension by shaking. Despite this, the NPs do not seem to have lost activity, indicating that they are very stable.

V.III: CONCLUSIONS

In this work a StLASPO was conjugated on Fe_3O_4 magnetic NPs with an efficiency in term of unit of 60%. 1U of enzyme was conjugated on 216mg of NPs. The system was efficiently used for the resolution of a racemic mixture of D,L-aspartate: 1U converts 250mM of D,L-aspartate in 240min. Moreover Fe_3O_4 NPs@APTES-LASPO seems to have a stable activity in a wide pH range (8-10), with an optimum around pH 9. Indeed and because of the high stability of the system, Fe_3O_4 NPs@APTES-LASPO can be used for additional cycles of bioconversion.

StLASPO with its extraordinary properties, represents an appropriate biocatalyst for the resolution of racemic resolution of D,L-aspartate and its conjugation on magnetic NPs increases its industrial value.

Future goals will be to repeat the experiments in order to confirm the results. Moreover the kinetic properties of the immobilized enzyme will be characterized, investigating the range of temperature and pH with higher performances in terms of activity and stability. Finally, the characteristics of immobilized LASPO with those of the free enzyme will be compared.

BIBLIOGRAPHY

1- "Nanoparticles and Catalysis". Chapter 1 "Transition metal Nanoparticles in Catalysis: From Historical Background to the State of the Art". Edited by Didier Astruc. WILEY-VCH Verlag GmbH & Co. KGaA, Weinheim; 2008.

2- Saha K, Agasti SS, Kim C, Li XN, Rotello VM. "Gold Nanoparticles in Chemical and Biological Sensing". *Chemical Reviews* 112:2739-2779, 2012.

3- Stratakis E, Kymakis E. "Nanoparticle-based plasmonic organic photovoltaic devices". *Materials Today* 16:133–146, 2013.]

4- Saroja C, Lakshmi P, Bhaskaran S. "Recent trends in vaccine delivery systems: a review". *Journal of Pharmaceutical Investigation* 1:64–74, 2011.

5- Meng FH, Cheng R, Deng C, Zhong ZY. "Intracellular drug release nanosystems". *Materials Today* 15:436–442, 2012.

6- Yoo JW, Irvine DJ, Discher DE, Mitragotri S. "Bio-inspired, bioengineered and biomimetic drug delivery carriers". *Nature Reviews Drug Discovery* 10:521–535, 2011.

7- Pan Y, Neuss S, Leifert A, Fischler M, Wen F, Simon U, Schmid G, Brandau W, Jahnen-Dechent W. "Size-dependent cytotoxicity of gold nanoparticles".

Small 3:1941-1949, 2007.

8-   Albanese A, Tang PS, Chan WCW. "The Effect of Nanoparticle Size, Shape, and Surface Chemistry on Biological Systems". *Annual Review of Biomedical Engineering* 14:1–16, 2012.

9-   Crespo P, de la Presa P, Marın P, Multigner M, Alonso JM, Rivero G, Yndurain F, Gonzalez-Calbet JM, Hernando A. "Magnetism in nanoparticles: tuning properties with coating". *Journal of Physics: Condensed Matter* 25:484006, 2013.

10-   Sun S, Murray CB, Weller D, Folks L, Moser A. "Monodisperse FePt nanoparticles and ferromagnetic FePt nanocrystal superlattices". *Science* 287:1989-1992, 2000.

11-   "Advanced Magnetic Nanostructures". Chapter 7 Bonder MJ, Huang Y, Hadjipanayis GC "Magnetic nanoparticles" 183-206. Edited by Sellmyer D, Skomski R. Springer US 2006.

12-   Terris BD, Thomson T "Nanofabricated and self-assembled magnetic structures as data storage media". *Journal of Physics D: Applied Physics* 38:R199-R222, 2005.

13-   Jin Y, Jia C, Huang SW, O'Donnell M, Gao X. "Multifunctional nanoparticles as coupled contrast

agents". *Nature Communications* 1:41, 2010.

14- Tsang SC, Caps V, Paraskevas I ,Chadwick D, Thompsett D. "Magnetically Separable, Carbon-Supported Nanocatalysts for the Manufacture of Fine Chemicals". *Angewandte Chemie International Edition in English* 43:5645-5649, 2004

15- Lu AH, Schmidt W, Matoussevitch N, Bonnemann H, Spliethoff B, Tesche B, Bill E, Kiefer W, Schuth F. "Nanoengineering of a magnetically separable hydrogenation catalyst". *Angewandte Chemie International Edition in English* 43:4303-4306, 2004.

16- Beveridge JS, Stephens JR, Williams ME. "Differential Catch and Release: Experimental Parameters for Controlled Separation of Magnetic Nanoparticles". *Analyst* 136:2564-2571, 2011.

17- Jun YW, Seo JW, Cheon J. "Nanoscaling laws of magnetic nanoparticles and their applicabilities in biomedical science". *Accounts of Chemical Research* 41:179-189, 2008.

18- Hofmann-Amtenbrink M, von Rechenberg B, Hofmann H. "Superparamagnetic nanoparticles for biomedical applications". Nanostructured Materials for Biomedical Applications. Edited by Tan MC, pp. 119-148. 2009.

19- Indira TK, Lakshmi PK. "Magnetic Nanoparticles – A Review". *International Journal of Pharmaceutical Sciences and Nanotechnology* 3:1035-1042, 2010

20- Chen Y, Chen BA. "Application and development of magnetic iron-oxide nanoparticles in tumor-targeted therapy". *Chinese Journal of Cancer* 29:118-121, 2010.

21- Wu W, He Q, Jiang C. "Magnetic iron oxide nanoparticles: synthesis and surface functionalization strategies" *Nanoscale Research Letters* 3:397-415, 2008.

22- Laurent S, Forge D, Port M, Roch A, Robic C, Elst LV,RN Muller. "Magnetic iron oxide nanoparticles: synthesis stabilization vectorization physicochemical characterizations and biological applications" *Chemical Reviews* 108:2064-2110, 2008.

23- Subbiah R, Veerapandian M, Yun KS. "Nanoparticles: Functionalization and Multifunctional Applications in Biomedical Sciences". *Current Medicinal Chemistry* 17:4559-4577, 2010.

24- del Campo A, Sen T, Lellouche JP, Bruce IJ. "Multifunctional magnetite and silica–magnetite nanoparticles: Synthesis,surface activation and

applications in life sciences". *Journal of Magnetism and Magnetic Materials* 293:33–40, 2005.

25- Feng B, Hong RY, Wang LS, Guo L, Li HZ, Ding J, Zheng Y, Wei DG. "Synthesis of Fe3O4/APTES/PEG diacid functionalized magnetic nanoparticles for MR imaging". Colloids and Surfaces A: Physicochemical and Engineering Aspects 328:52–59, 2008.

26- Laurencin CT, El-Amin SF, Ibim SE, Willoughby DA, Attawia M, Allcock HR, Ambrosio AA. "A highly porous 3-dimensional polyphosphazene polymer matrix for skeletal tissue regeneration". *Journal of Biomedical Materials Research Part A* 30:133–138, 1996.

27- Zhua A, Chan-Park MB, Dai S, Li L. "The aggregation behavior of O-carboxymethylchitosan in dilute aqueous solution". *Colloids and Surfaces B: Biointerfaces* 43:143–149. 2005.

28- Chatterjee K, Sarkar S, Rao KJ, Paria S. "Core/shell nanoparticles in biomedical applications". *Advances in Colloid and Interface Science*, 2014

29- Pinho SLC, Pereira GA, Voisin P, Kassem J, Bouchaud V, Etienne L, Peters JA, Carlos L, Mornet S, Geraldes CFGC, Rocha J, Delville MH. "Fine

tuning of the relaxometry of γ-Fe2O3@SiO2 nanoparticles by tweaking the silica coating thickness". *ACS Nano* 4:5339–5349, 2010.

30- Shang L, Nienhaus K, Nienhaus GU. "Engineered nanoparticles interacting with cells: size matters" *Journal of Nanobiotechnology* 12:5, 2014.

31- Iseult L, Dawson KA. "Protein-nanoparticle interactions". *Nanotoday* 3:40-47, 2008.

32- Verma A, Stellacci F. "Effect of surface properties on nanoparticle-cell interactions". *Small* 6:12–21, 2010.

33- Mahmoudi M, Saeedi-Eslami SN, Shokrgozar MA, Azadmanesh K, Hassanlou M, Kalhor HR, Burtea C, Rothen-Rutishauser B, Laurent S, Sheibani S, Vali H. "Cell vision: complementary factor of protein corona in nanotoxicology". *Nanoscale* 4:5461–5468, 2012.

34- Malugin A, Ghandehari H. "Cellular uptake and toxicity of gold nanoparticles in prostate cancer cells: a comparative study of rods and spheres". *Journal of Applied Toxicology* 30:212–217, 2010.

35- Chithrani BD, Ghazani AA, Chan WCW. "Determining the size and shape dependence of gold nanoparticle uptake into mammalian cells".

Nano Letters 6:662–668, 2006.

36- Wang SH, Lee CW, Chiou A, Wei PK. "Size-dependent endocytosis of gold nanoparticles studied by three-dimensional mapping of plasmonic scattering images". *Journal of Nanobiotechnology* 8:33, 2010.

37- Lu F, Wu SH, Hung Y, Mou CY. "Size effect on cell uptake in well-suspended, uniform mesoporous silica nanoparticles". *Small* 5:1408–1413, 2009.

38- Varela JA, Bexiga MG, Aberg C, Simpson JC, Dawson KA. "Quantifying size dependent interactions between fluorescently labeled polystyrene nanoparticles and mammalian cells". *Journal of Nanobiotechnology* 10:39, 2012.

39- Huang J, Bu L, Xie J, Chen K, Cheng Z, Li X, Chen X. "Effects of nanoparticle size on cellular uptake and liver MRI with polyvinylpyrrolidone-coated iron oxide nanoparticles". *ACS Nano* 4:7151–7160, 2010.

40- Walkey CD, Olsen JB, Guo H, Emili A, Chan WC. "Nanoparticle size and surface chemistry determine serum protein adsorption and macrophage uptake". *Journal of the American Chemical Society* 134:2139–2147, 2012.

41- Shang L, Yang L, Seiter J, Heinle M, Brenner-Weiss G,

Gerthsen D, Nienhaus GU. "Nanoparticles interacting with proteins and cells: a systematic study of protein surface charge effects". *Advanced Materials Interfaces* 10.1002/admi.201300079, 2014.

42- Lovrić J, Bazzi H, Cuie Y, Fortin GA, Winnik F, Maysinger D. "Differences in subcellular distribution and toxicity of green and red emitting CdTe quantum dots". *Journal of Molecular Medicine* 83:377–385, 2005.

43- Nel A, Xia T, Madler L, Li N. "Toxic potential of materials at the nanolevel". *Science* 311:622–627, 2006.

44- Barkalina N, Charalambous C, Jones C, Coward K. "Nanotechnology in reproductive medicine: Emerging applications of nanomaterials". *Nanomedicine: Nanotechnology, Biology and Medicine* 5:921-938, 2014.

45- Bromley DA. Letter from Dean D. Allan Bromley sent to President Clinton. In: Roco MC, Bainbridge WS editors. Societal implications of nanoscience and nanotechnology. Arlington, VA: International Technology Research Institute, World Technology (WTEC) Division, Loyola College; 2001. p. 269-70.

46- Velez JM, Velez JJ. "The eminent need for an

academic program in universities to teach nanomedicine". *International Journal of Nanomedicine* 6:1733-8, 2011.

47- Emerich DF. "Nanomedicine — prospective therapeutic and diagnostic applications". *Expert Opinion on Biological Therapy* 5:1-5, 2005.

48- Antunes AMD, Alencar MSD, da Silva CH, Nunes J, Mendes FML. "Trends in nanotechnology patents applied to the health sector". *Recent Patents on Nanotechnology* 6:29-43, 2012.

49- Kemp KC, Seema H, Saleh M, Le NH, Mahesh K, Chandra V, Kim KS. "Environmental applications using graphene composites: water remediation and gas adsorption". *Nanoscale* 5:3149-3171, 2013.

50- Raychoudhury T, Scheytt T. "Potential of zerovalent iron nanoparticles for remediation of environmental organic contaminants in water: a review". *Water Science and Technology* 68:1425-39, 2013.

51- Sekhon BS. "Food nanotechnology – an overview". *Nanotechnology, Science and Applications* 3:1-15, 2010.

52- Lav R. Khot a, Sankaran S, Maja JM, Ehsani R, Schuster EW. "Applications of nanomaterials in agricultural production and crop protection: A

review". *Crop Protection* 35:64-70, 2012

53- Gilmore JL, Yi X, Quan L, Kabanov AV. "Novel Nanomaterials for Clinical Neuroscience.", *Journal of NeuroImmune Pharmacology* 3: 83–94, 2008.

54- Boyd BJ. "Past and future evolution in colloidal drug delivery systems". *Expert Opinion on Drug Delivery* 5:69-85, 2008.

55- Duncan R. "Designing polymer conjugates as lysosomotropic nanomedicines", *Biochemical Society Transactions* 35:56-60, 2007.

56- Jain KK. "Advances in the field of nanooncology". *BMC Medicine* 8:83-94, 2010.

57- "Advances in nanoscience and nanotechnology" Volume 2 - Nanomedicne and cancer therapies". Chapter 1 "Nanotechnological based system for cancer". Edited By Apple Academic Press, Oakville 2013

58- Lim EK, Jang E, Lee K, Haam S, Huh YM. "Delivery of Cancer Therapeutics Using Nanotechnology". *Pharmaceutics* 5:294-317, 2013

59- Gang J, Park SB, Hyung W, Choi EH, Wen J, Kim HS, Shul YG, Haam S, Song SY. "Magnetic poly ε-caprolactone nanoparticles containing Fe_3O_4 and gemcitabine enhance anti-tumor effect in

pancreatic cancer xenograft mouse model". *Journal of Drug Targeting* 15:445–453, 2007.

60- Lee JH, Chen KJ, Noh SH, Garcia MA, Wang H, Lin WY, Jeong H, Kong BJ, Stout DB, Cheon J, Tseng HR. "On-demand drug release systems for in vivo cancer treatment through self-assembled magnetic nanoparticles". *Angewandte Chemie International Edition* 52:1–6, 2013.

61- Cho MH, Lee EJ, Son M, Lee JH, Yoo D, Kim JW, Park SW, Shin JS, Cheon J. "A magnetic switch for the control of cell death signaling in in vitro and in vivo systems". *Nature Materials* 11:1038–1043, 2012.

62- Thomas CR, Ferris DP, Lee JH, Choi E, Cho MH, Kim ES, Stoddart JF, Shin JS, Cheon J, Zink JI. "Noninvasive remote-controlled release of drug molecules in vitro using magnetic actuation of mechanized nanoparticles". *Journal of the American Chemical Society* 132:10623–10625, 2010.

63- Katagiri K, Imai Y, Kounoto K, Kaiden T, Kono K, Aoshima S. "Magnetoresponsive on-demand release of hybrid liposomes formed from Fe3O4 nanoparticles and thermosensitive block copolymer". *Small* 7:1683–1689, 2011.

64- "Technology analysis – industrial application of

nanomaterials, chances and risks". Edited by Luter W. Future Technologies Division of VDI Technologiezentrum GmbH, Düsseldorf, Germany

65- Liu W, Wang L, Jiang R. "Specific Enzyme Immobilization Approaches and Their Application with Nanomaterials". *Topics in Catalysis* 55:1146–1156, 2012.

66- Yu CC, Kuo YY, Liang CF, Chien WT, Wu HT, Chang TC, Jan FD, Lin CC. "Site-Specific Immobilization of Enzymes on Magnetic Nanoparticles and Their Use in Organic Synthesis". *Bioconjugate Chemistry* 23:714–724, 2012.

67- Meridor D, Gedanken A. "Preparation of enzyme nanoparticles and studying the catalytic activity of the immobilized nanoparticles on polyethylene films". *Ultrasonic sonochemistry* 20:425-431, 2013.

68- Liu Y, Wang S, Zhang C, Su X, Huang S, Zhao M. "Enhancing the Selectivity of Enzyme Detection by Using Tailor-Made Nanoparticles". *Analytical Chemistry* 85:4853–4857, 2013.

69- Wu CS, Lee CC, Wu CT, Yang YS, Ko FH. "Size-modulated catalytic activity of enzyme nanoparticle conjugates: a combined kinetic and theoretical study". *Chemical Communications*

47:7446–7448, 2011.

70- Wang W, Xu Y, Wang DIC, Li Z. "Recyclable nanobiocatalyst for enantioselective sulfoxidation: facile fabrication and high performance of chloroperoxidase-coated magnetic nanoparticles with iron oxide core and polymer shell". *Journal of the American Chemical Society* 131:12892–12893, 2009.

71- Jin MJ, Lee DH. "A Practical Heterogeneous Catalyst for the Suzuki, Sonogashira, and Stille Coupling Reactions of Unreactive Aryl Chlorides". *Angewandte Chemie International Edition* 49:1119 – 1122, 2010

72- Sacchi S, Rosini E, Molla G, Pilone MS, Pollegioni L. "Modulating D-amino acid oxidase substrate specificity: production of an enzyme for analytical determination of all D-amino acids by directed evolution". *Protein Engineering, Design & Selection* 17:517–525, 2004.

73- Pollegioni L, Piubelli L, Sacchi S, Pilone MS, Molla G. "Physiological functions of D-amino acid oxidases: from yeast to humans". *Cellular and Molecular Life Sciences* 64:1373–1394, 2007.

74- Olsiewski PJ, Kaczorowski GJ, Walsh C. "Purification

and properties of D-amino acid dehydrogenase, an inducible membrane-bound iron-sulfur flavoenzyme from Escherichia coli B". *The Journal of Biological Chemistry* 255:4487–4494, 1980.

75- Pollegioni L, Diederichs K, Molla G, Umhau S, Welte W, Ghisla S, Pilone MS. "Yeast D-amino acid oxidase: structural basis of its catalytic properties". *Journal of Molecular Biology* 324:535-546, 2002.

76- D'Aniello A, D'onofrio G, Pischetola M, D'aniello G, Vetere A, Petrucelli L, Fisher GH. "Biological role of D-amino acid oxidase and D-Aspartate Oxidase". *The American Society for Biochemistry and Molecular Biology* 268:26941-26949, 1993.

77- Tishkov VI, Khoronenkova SV. "D-amino acid oxidase: structure, catalytic mechanism, and pratical application". *Biochemistry* 70:40-54, 2005.

78- Hsieh HC, Kuan IC, Lee SL, Tien GY, Wang YJ, Yu CY. "Stabilization of D-amino acid oxidase from Rhodosporidium toruloides by immobilization onto magnetic nanoparticles". *Biotechnology Letters* 31:557-563, 2009.

79- Fang J, Sawa T, Akaike T, Maeda H. "Tumor-targeted delivery of polyethylene glycol-conjugated D-amino acid oxidase for antitumor

therapy via enzymatic generation of hydrogen peroxide". *Cancer Research* 62:3138–3143, 2002.

80- El Sayed SM, Abou El-Magd RM, Shishido Y, Chung SP, Diem TH, Sakai T, Watanabe H, Kagami S, Fukui K. "3-Bromopyruvate antagonizes effects of lactate and pyruvate, synergizes with citrate and exerts novel anti-glioma effects". *Journal of Bioenergetics and Biomembranes* 44:61–79, 2012b.

81- El Sayed SM, Abou El-Magd RM, Shishido Y, Yorita K, Chung SP, Tran DH, Sakai T, Watanabe H, Kagami S, Fukui K. "D-Amino acid oxidase-induced oxidative stress, 3-bromopyruvate and citrate inhibit angiogenesis, exhibiting potent anticancer effects". *Journal of Bioenergetics and Biomembranes* 44:513–523, 2012.

82- Divakaran SA, Sreekanth KM, Nair KV, CKK. "D-Aminoacid Oxidase-Fe2O3 Nanoparticle Complex Mediated Antitumor Activity in Swiss Albino Mice". *Journal of Cancer Therapy* 2:666-674, 2011.

83- Stegman LD, Zheng H, Neal ER, Ben-Yoseph O, Pollegioni L, Pilone MS, Ross BD. "Induction of cytotoxic oxidative stress by D-Alanine in brain tumor cells expressing Rhodotorula gracilis D-amino acid oxidase: a cancer gene therapy strategy".

Human Gene Therapy 9:185-193, 1998.

84- Matthews L, Kanwar RK, Zhou S, Punj V, Kanwar JR. "Applications of Nanomedicine in Antibacterial Medical Therapeutics and Diagnostics". *The Open Tropical Medicine Journal* 3:1-9, 2010.

85- Bhattacharya D, Saha B, Mukherjee A, Santra CR, Karmakar P. "Gold nanoparticles conjugated antibiotics: stability and functional evaluation". *Nanoscience and Nanotechnology* 2:14-21, 2012.

86- Grace AN, Pandian K. "Antibacterial efficacy of aminoglycosidic antibiotics protected gold nanoparticles. A brief study". *Colloids and Surfaces A: Physicochemical Engineered Aspects* 297:63-70, 2007.

87- Fattal E, Youssed M, Couvreur P, Andremont A. "Treatment of Experimental salmonellosis in mice with ampicillin-bound nanoparticles". *Antimicrobial Agents and Chemotherapy* 33:1540-1543, 1989.

88- Kora AJ, Rastogi L. "Enhancement of antibacterial activity of capped silver nanoparticles in combination with antibiotics, on model gram-negative and gram-positive bacteria". *Bioinorganic Chemistry and Applications* 2013:7 pages, 2013.

89- Zhang L. Pornpattananangkul D, Hu CMJ, Huang

CM. "Development of nanoparticles for antimicrobial drug delivery". *Current Medicinal Chemistry* 17:585-594, 2010.

90- Piyasena ME, Real LJ, Diamond RA, Xu HH, Gomez FA. "Magnetic microsphere-based methods to study the interaction of teicoplanin with peptides and bacteria". *Analytical and Bioanalytical Chemistry* 392:877-886, 2008.

91- Economou NJ, Zentner IJ, Jakoncic J, Stajanoff V, Weeks SD, Grasty KC, Cocklin S, Loll PJ. "Structure of the complex between teicoplanin and a bacterial cell-wall peptide: use of a carrier-protein approach". *Acta Crysrallographica Section D* 69:520-533, 2013.

92- Zhu X, Luo H, Chang Y, Su H, Li Q, Yu H, Shen Z. "Characteristic of immobilized cephalosporin C acylase and its application in one-step enzymatic conversion of cephalosporin C to 7-aminocephalosporanic acid". *World Journal of Microbiology and Biotechnology* 27:823-829, 2011.

93- Pollegioni L, Lorenzi S, Rosini E, Marcone GL, Molla G, Verga R, Cabri W, Pilone MS. " Evolution of an acylase active on cephalosporin C". *Protein Science* 14:3064-3076, 2005.

94- Pollegioni L, Rosini E, Molla G. "Chephalosporin C acylase: dream and(/or) reality". *Applied Microbiology and Biotechnology* 97:2341-2355, 2013.

95- Pollegioni L, Motta P, Molla G. "L-amino acid oxidase as biocatalyst: a dream too far?". *Applied Microbiology and Biotechnology* 97:9323-9341, 2013.

96- Bifulco D, Pollegioni L, Tessaro D, Servi S, Molla G. "A termostabile L-aspartate oxidase: a new tool for biotechnologial applications". *Applied Microbiology and Biotechnology* 97:7285-7295, 2013.

97- Sakuraba H, Yoneda K, Asai I, Tsuge H, Katunama N, Ohshima T. "Structure of L-aspartate oxidase from the hyperthermophilic archaeon Sulfolobus tokodaii". *Biochimica et Biophysica Acta* 1784:563-571, 2008.

98- Molla G, Porrini D, Job V, Motteran L, Vegezzi C, Campaner S, Pilone MS, Pollegioni L. "Role of arginine 285 in the active site of Rhodotorula gracilis D-amino acid oxidase. A site-directed mutagenesis study". *Journal of biological chemistry* 275: 24715-24721, 2000.

99- Rosini E, Pollegioni L, Ghisla S, Orru R, Molla G. "Optimization of D-amino acid oxidase for low substrate concentrations--towards a cancer enzyme therapy". *The FEBS journal* 276:4921-4932, 2009.

100- Sacchi S, Bernasconi M, Martineau M, Mothet JP, Ruzzene M, Pilone MS, Pollegioni L, Molla G. "pLG72 modulates intracellular D-serine levels through its interaction with D-amino acid oxidase: effect on schizophrenia susceptibility". *The Journal of biological chemistry* 283:22244-22256, 2008.

101- Irwin S. "Comprehensive observational assessment: Ia. A systematic, quantitative procedure for assessing the behavioral and physiologic state of the mouse". *Psychopharmacologia* 13:222-257, 1968

102- Siegel R, Naishadham D, Jemal A. "Cancer statistics, 2013". *CA: A Cancer Journal for Clinicians* 63:11-30, 2013.

103- Pollegioni L, Sacchi S. "Methabolism of the neuromodulator D-serine". *Cellular and Molecular Life Science* 67:2387-2404, 2010.

104- Divakaran SA, Streekanth KM, Rao KV, Nair CKK. "D-aminoacid oxidase-Fe_2O_3 nanoparticle complex

mediated antitumor activity in swiss albino mice". *Journal of Cancer Therapy* 2:666-674, 2011.

105- Hsieh HC, Kuan IC, Lee SL, Tien GY, Wang YJ, Yu CY. "Stabilization of D-amino acid oxidase from Rhodosporidium toruloides by immobilization onto magnetic nanoparticles". *Biotechnology Letters* 31:557-563, 2009.

106- Chien LJ, Lee CK. "Biosilicification of dual-fusion enzyme immobilized on magnetic nanoparticles". *Biotechnology and bioengineering* 100:223-230, 2008.

107- Liang YY, Zhang LM. "Bioconjugation of papain on superparamagnetic nanoparticles decorated with carboxyme-   thylated   chitosan". *Biomacromolecules* 8:1480–1486, 2007.

108- Balasingham K, Warburton D, Dunnill P, Lilly MD. "The isolation and kinetics of penicillin amidase from Escherichia coli". *Biochimica et Biophysica Acta* 276:50–256, 1972.

PAPERS
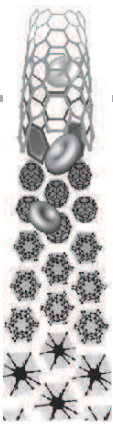
D-amino acid oxidase–nanoparticle system: a potential novel approach for cancer enzymatic therapy

Aim: The authors propose a new magnetic nanoparticle–enzyme system for cancer therapy capable of targeting the enzyme and consequently decreasing the adverse effects, meanwhile improving the patient's life quality. **Materials & methods:** The authors have functionalized Fe_3O_4 nanoparticles with 3-aminopropyltriethoxysilane (APTES) and conjugated it to yeast D-amino acid oxidase (DAAO) by coupling this with glutaraldehyde. **Results & conclusion:** The authors have tested the Fe_3O_4-APTES–DAAO system on three tumor cell lines. Exposed cells show, at the electron microscope level, nanoparticles on the surface of the plasma membrane and inside endocytic vesicles. Fe_3O_4-APTES–DAAO caused a substantial decrease of cell viability greatly augmented when D-alanine, a DAAO substrate, was added. Fe_3O_4-APTES–DAAO was demonstrated to be more effective than free DAAO, confirming the validity of the system in cancer therapy.

Adriana Bava[1], Rosalba Gornati*[1,2], Francesca Cappellini[1], Laura Caldinelli[1,2], Loredano Pollegioni[1,2] & Giovanni Bernardini[1,2]

[1]Dipartimento di Biotecnologie e Scienze della Vita, Università degli Studi dell'Insubria, Via Dunant 3, Varese, Italy
[2]'The Protein Factory' Research Center, Politecnico di Milano, ICRM-CNR Milano & Università dell'Insubria, Via Mancinelli 7, Milano, Italy
*Author for correspondence:
Tel.: +39 033 242 1314
Fax: +39 033 242 1500
rosalba.gornati@uninsubria.it

Nano-oncology, the application of nanobiotechnology to the management of cancer, is currently a promising issue in nanomedicine. Nanoparticles (NPs) enable the targeted delivery of drugs to cancer cells [1–3]. This localized therapy improves efficacy and, at the same time, decreases adverse effects by reducing the dosage of anticancer drugs resulting in ameliorating the patient's quality of life [3]. Moreover, NPs are often capable of crossing various biological barriers [4–6] such as the blood–brain barrier, which limits the access to brain tumors. NPs can also penetrate solid tumors, where the access of drugs to malignant cells is often limited by the abnormal organization, structure and function of the blood vessels that form a barrier [7–11]. Several drugs, some of these already approved for human treatment, are based on nanobiotechnology and comprise different formulations of active principles. Liposomes (DaunoXome® [Gilead Sciences, CA, USA; daunorubicin], Doxil® [Janssen Biotech, Inc., PA, USA]/Caelyx® [Janssen, NSW, Australia] [doxorubicin]), polymer–protein conjugates (Oncaspar® [Enzon Pharmaceuticals, Inc., NJ, USA; polyethylene glycol–L-asparaginase], SMANCS [Astellas Pharma, Inc., Tokyo, Japan; zinostatin]) and radioimmunoconjugates (Bexxar® [GlaxoSmithKline, Brentford, UK; anti-CD20 conjugated to iodine-131], Zevalin® [Spectrum Pharmaceuticals, NV, USA; anti-CD20 conjugated to yttrium-909])

are some examples of approved anticancer nanodrugs [1,12].

Among the innumerable approaches that can be used in the treatment of cancer, one of the oldest is based on the oxidative stress caused by reactive oxygen species. Radiation generates oxygen-derived free radicals and excited states; therefore, radiotherapy is one of the most common treatments of cancers [13]. On the other hand, radiotherapy poses the risk of secondary malignancy in the radiated area and its efficacy is often hindered by the emergence of radiation-resistant populations [14]. From the late 1950s to the early 1970s, injections of H_2O_2 into the tumor were performed, but this approach showed little therapeutic success [15]. Later, H_2O_2-generating enzymes, such as glucose oxidase or xanthine oxidase, were delivered in experimental tumors [16]. Unfortunately, the stability of the enzymes was low *in vivo* and, furthermore, their substrates (glucose, xanthine and oxygen) were endogenous molecules whose concentration could not be adequately modulated [17]. Therefore, there was a rationale for the use of other oxidizing enzymes whose activity could be regulated. D-amino acid oxidase (DAAO; EC 1.4.3.3) represents a good choice: its favorite substrate, D-Ala, can be found endogenously in very small amounts; therefore, H_2O_2 production can be modulated by the delivery of an appropriate dose of D-amino acids. Owing to its availability as a recombinant

Future Medicine
fsg part of

protein and peculiar biochemical characteristics, such as high specific activity, tight binding with the flavin adenine dinucleotide cofactor and good thermal stability [18], *Rhodotorula gracilis* DAAO (RgDAAO) was proposed as a suitable candidate to produce reactive oxygen species in tumors [19]. A main drawback in the use of native RgDAAO is the comparatively high K_m for oxygen ($\sim$2 mM) [20] versus the local oxygen concentration (estimated at $\sim$25 μM in growing tumors). A RgDAAO variant possessing a tenfold lower $K_{m,O2}$ was produced by a directed evolution approach. This evolved enzyme, containing five point mutations, induced remarkably increased cytotoxicity effects on mouse tumor cells [21].

In this context, a possibility to improve the efficacy of cancer therapy would also be to combine the advantages of using NPs, especially magnetic NPs such as magnetite and maghemite, with those of an enzyme with a well-known and controlled anticancer effect, such as DAAO. The authors have chosen magnetic NPs as they offer some attractive possibilities in biomedicine for a variety of important reasons. First, they have controllable sizes in the range of those of a virus, which can be exploited to reach poorly accessible districts. Second, they can be manipulated by a magnetic field. This property, combined with the intrinsic penetrability of magnetic fields into human tissue, makes them particularly interesting in guiding an anticancer drug directly to a tumor. Third, magnetic NPs can be heated by a magnetic field to trigger drug release or to produce hyperthermia and tissue ablation [22–24]. Fourth, magnetic NPs can be efficiently visualized by MRI giving the same system both therapeutic and diagnostic (theranostic) functions [25].

To optimize this oxystress-based cancer therapy, Fe_3O_4 NPs were functionalized with 3-aminopropyltriethoxysilane (APTES) and conjugated to RgDAAO to produce Fe_3O_4-APTES–DAAO. This system has been studied by *in vitro* tests of cytotoxicity and uptake to check for its capability to kill human cancer cells. To this aim, three different tumor cell lines (human ovary adenocarcinoma SKOV-3, human glioblastoma U87 and human colorectal carcinoma HCT116) have been used. This investigation could help to develop a new, more effective treatment especially for brain tumors, which are isolated by the blood–brain barrier, and for solid tumors where the access of drugs is often limited by poor vascularization and areas of necrosis [7]. In particular, brain tumors are intrinsically more complicated to treat than systemic malignancies; this depends on the type, location and size of the tumor, the patient's age and general health, as well as the blood–brain barrier-induced diffusion limitation, which impedes chemotherapeutic agents from reaching brain neoplasms. For all of these reasons, brain tumors are treated with surgery, radiation therapy and chemotherapy with a low recovery rate [26]. In this context, an alternative system for cancer therapy is desiderable and nanosystems can bring significant innovations over conventional formulations with respect to decreased toxicity and improved pharmacokinetic and pharmacodynamic properties [27–29].

Materials & methods
■ Chemicals
Iron oxide NPs, Fe_3O_4 NPs (nanopowder: <50 nm particle size), APTES (purity: >98%) and all other reagents (cell culture grade) were purchased from Sigma-Aldrich (Milan, Italy). Horseradish peroxidase was purchased from Roche (Milano, Italy), CellTiter-Glo® Luminescent Cell Viability Assay was purchased from Promega (WI, USA). RgDAAO variants were produced as recombinant proteins in *Escherichia coli* and purified as stated in [30]. The final enzyme preparation equilibrated in 50 mM potassium phosphate buffer at pH 7.5, 2 mM EDTA, 10% v/v glycerol and 5 mM 2-mercaptoethanol, had a specific activity of approximately 90 U/mg protein at 25°C, 21% oxygen and on D-Ala as a substrate. Milli-Q Ultrapure Water System (Millipore, MA, USA) was used.

■ Coating of magnetic NPs
Fe_3O_4-APTES
A 5-ml APTES solution (2% w/v final concentration) was added to a well-dispersed suspension of 150 mg of Fe_3O_4 NPs in 10 ml water, and maintained under mechanical stirring at 50°C for 5 h according to del Campo *et al.* [31]. The Fe_3O_4-APTES were separated from unbound APTES by a commercial parallelepiped neodymium magnet (Webcraft GmbH, Uster, Switzerland; Ni–Cu–Ni plated; magnetization: N45; size: 30 × 30 × 15 mm), washed several times with water, anhydrificated with ethanol and dried overnight at 50°C.

Fe_3O_4-APTES–DAAO
A suspension of 4 mg of Fe_3O_4-APTES in 2 ml glutaraldehyde (0.5% v/v) obtained by ultrasonication for 1 min (Sonica® 5300MH; Soltec, Milano, Italy) was allowed to react for 2 h using a rotating plate tube stirrer at room temperature. The produced adduct was separated

from the supernatant with a neodymium magnet, washed three times with 500 μl of distilled water, then with 500 μl 5 mM sodium pyrophosphate buffer (NaPPi) at pH 8.5. Functionalized Fe_3O_4 NPs were resuspended in 5 mM NaPPi at pH 8.5 and the mixture sonicated for 1 min. Finally, 250 μg of pure RgDAAO was added (1 ml of final volume) and the reaction was carried out for 4 h at 4°C using a rotating plate tube stirrer. Subsequently, Fe_3O_4-APTES–DAAO were collected by a magnet and washed twice with 500 μl of 5 mM NaPPi. The supernatant was stored for further analysis.

The same procedure has been used to prepare the system Fe_3O_4-APTES–DAAO(R285A), in which the Arg (R) 285 in the active site has been substituted with an Ala (A) generating a nonactive RgDAAO mutant [32].

■ Spectra analysis
The amount of protein bound to Fe_3O_4 NPs was determined as the difference between the starting amount of RgDAAO and the protein recovered in the supernatant at the end of reaction. Quantification was performed using the extinction coefficient at 455 nm ($\sim$12.6 $mM^{-1}cm^{-1}$) using an UV-Vis V-560 Spectrophotometer (JASCO, MD, USA).

Characterization of the NP-coated samples was performed using the solid phase Fourier transform infrared spectroscopy: spectra were collected on a Nicolet Avatar 360 Spectrometer (JASCO). Samples were mixed with infrared grade KBr in a proportion of 2:100 (w/w).

■ RgDAAO activity assay
The activity of Fe_3O_4-APTES–DAAO and Fe_3O_4-APTES–DAAO(R285A) was determined by measuring the absorbance increase accompanying the H_2O_2-induced oxidation of o-dianisidine. One DAAO unit corresponds to the amount of enzyme that converts 1 μmol of substrate per min at 25°C and at 0.253 mM oxygen concentration [33]. The standard assay mixture contained 890 μl of 100 mM D-Ala in 100 mM NaPPi buffer, pH 8.5, 100 μl 3.2 mg/ml o-dianisidine in water, 10 μl of 0.4 mg/ml horseradish peroxidase in 100 mM NaPPi buffer, pH 8.5, and 10 μl of 0.4 mg/ml Fe_3O_4-APTES–DAAO in the same buffer. The reaction was initiated by the addition of the enzyme and the absorbance increase was monitored at 440 nm for 1 min using an UV-Vis V-560 Spectrophotometer. The initial velocity at different substrate concentrations (0.1–100 mM) were recorded and used to calculate the apparent

kinetic parameters using the KaleidaGraph 4.0 software (Synergy Software, PA, USA).

■ HPLC measurements
D- and L-serine cellular concentrations were determined according to Sacchi et al. [34]. In detail, a fixed amount (5×10^5 cells) of SKOV-3 or U87 cells were homogenized in 1 ml of 5% cold trichloroacetic acid and then centrifuged at $16,000 \times g$ for 45 min at 4°C. Trichloroacetic acid was stripped six times from the supernatant using diethylether before lyophilization and storage at -20°C. Lyophilized cell samples were dissolved in 90 μl of 0.1 M sodium borate buffer, pH 10.4. For amino acid derivatization, 3 μl of U87 or 15 μl of SKOV-3 samples were treated with 24 μg of N-acetyl-cysteine and 7.5 μg of o-phthaldialdehyde in 0.1 M sodium borate buffer, pH 10.4.

HPLC separations were performed on a Symmetry® Column C8 (Waters, Milano, Italy; 5 μm) kept at 30°C using a JASCO HPLC system. Flow rate was set at 1 ml/min; L- and D-serine were eluted with an isocratic method using 0.1 M sodium acetate and 1% tetrahydrofuran at pH 6.2. Derivatized amino acids were detected using a fluorescence detector: excitation at 344 nm and emission at 443 nm. D- and L-serine quantification was performed by a calibration curve set up using increasing concentrations of standard D-serine (0.25–10 pmol) and L-serine (10–200 pmol).

■ Cell culture test
SKOV-3 and HCT116 cell lines were maintained as adherent cells in RPMI1640 medium, while U87 cell lines were maintained in DMEM medium, at 37°C in a humidified 5% CO_2 atmosphere. RPMI1640 medium was supplemented with 10% fetal bovine serum, 1% L-glutamine and 1% penicillin/streptomycin solution, whereas DMEM medium was supplemented with 10% fetal bovine serum, 1% L-glutamine, 1% penicillin/streptomycin and 1% sodium pyruvate. Cells were passaged as needed using 0.25% trypsin–EDTA.

■ Cell viability
Cell viability was determined as ATP content by using the CellTiter-Glo Luminescent Cell Viability Assay according to the manufacturer's instruction. In detail, 200 μl of cell suspension (containing 2×10^4, 1×10^4, 5×10^3 or 25×10^2 cells, depending of the exposure time) were seeded into 96-well assay plates and cultivated for 24 h at 37°C in 5% CO_2 to equilibrate and
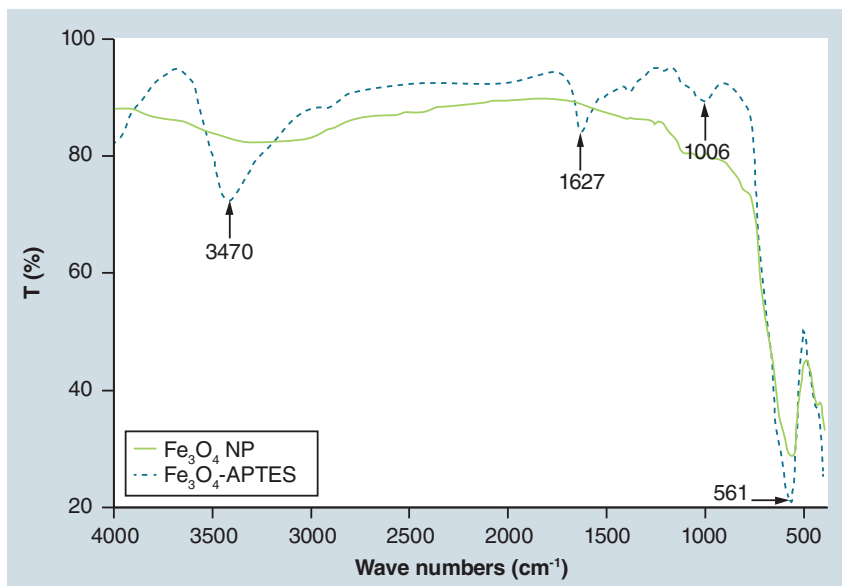
Figure 1. Fourier transform infrared spectra. The peak at 561 cm^{-1} indicates the Fe-O bond, the peak at 1006 cm^{-1} indicates the Si-O bond and the peak at 1627 cm^{-1} is assigned to the bending N-H bond. The peak at 3470 cm^{-1} corresponds to the N-H stretching vibrations of the -NH$_2$ group overlapped to hydrogen-bonded silanols.

NP: Nanoparticle; Fe$_3$O$_4$-APTES: Fe$_3$O$_4$ nanoparticles functionalized with 3-aminopropyltriethoxysilane.

become attached prior the treatment. Cells were then exposed to increasing amounts of naked Fe$_3$O$_4$ NPs for 0.5, 1, 2, 24, 48 and 72 h. In another series of experiments, 1 × 10^4 cells were exposed to increasing amounts of free DAAO or Fe$_3$O$_4$-APTES–DAAO for 24 h. Following the treatment, plates were equilibrated for 30 min at
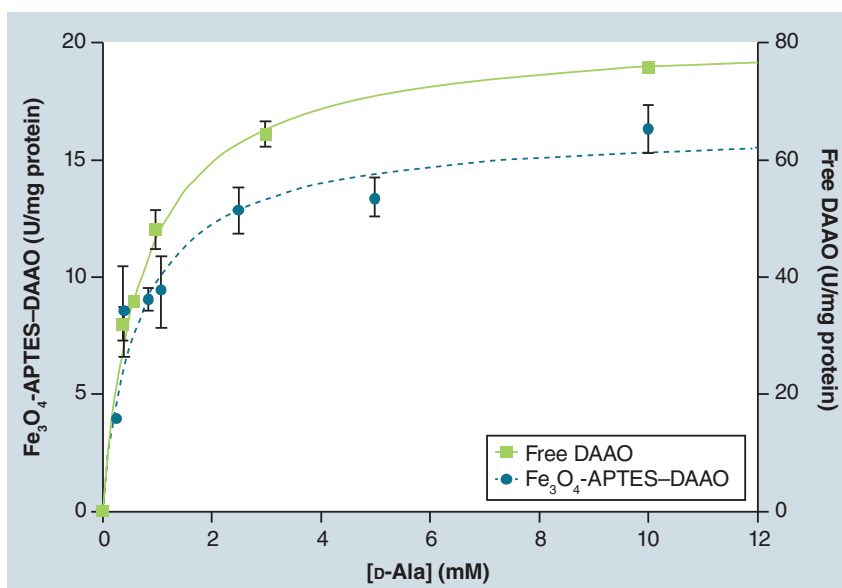
Figure 2. Michaelis–Menten plot of the activity measured for Fe$_3$O$_4$-3-aminopropyltriethoxysilane-D-amino acid oxidase and free D-amino acid oxidase at increasing D-Ala concentrations.

DAAO: D-amino acid oxidase; Fe$_3$O$_4$-APTES: Fe$_3$O$_4$ nanoparticles functionalized with 3-aminopropyltriethoxysilane.

room temperature and 100 µl of CellTiter-Glo Reagent was then added to each well. Plates were shaken for 2 min and left at room temperature for 10 min prior to the recording of luminescent signals using the Infinite F200 plate reader (Tecan Group, Männedorf, Switzerland). For all cell lines, experiments were performed in triplicate. Cell viability, expressed as ATP content, was normalized against control values. The same procedure has been used for free DAAO(R285A) and Fe$_3$O$_4$-APTES–DAAO(R285A).

■ Cellular uptake

Cellular uptake and localization was determined on SKOV-3, U87 and HCT116 cells exposed to Fe$_3$O$_4$-APTES–DAAO for 24 h and analyzed by transmission electron microscopy. For transmission electron microscopy studies, exposed cells were harvested, fixed in 2% glutaraldehyde in 0.1 M sodium cacodylate buffer (pH 7.2) for 10 min on ice and for 30 min at room temperature, washed in the same buffer, and postfixed in dark for 1 h with 1% osmiun tetroxide in 0.1 M sodium cacodylate buffer (pH 7.2) at room temperature. After standard steps of serial ethanol dehydration, samples were embedded in an Epon-Araldite 812 1:1 mixture (Sigma-Aldrich). Thin sections (80 nm) were obtained with a ReichertUltracut S ultratome (Leica, Wetzlar, Germany), stained by standard methods with uranyl acetate and lead citrate, and observed with a JEOL 1010 electron microscope (JEOL, Tokyo, Japan) operated at 90 kV.

■ Statistics

Kinetic data and cell viability values were expressed as mean ± standard deviation. Statistical tests were performed using KaleidaGraph 4.0 software (Synergy Software).

Results

■ Sample characterization

Fe$_3$O$_4$-APTES were produced by a simple and fast procedure described in the 'Materials & Methods' section. FIGURE 1 reports Fourier transform infrared spectra of Fe$_3$O$_4$ NPs and Fe$_3$O$_4$-APTES. The peak within 550–570 cm^{-1} is characteristic of Fe-O vibrations related to the magnetite core. The presence of silane on the surface of NPs (FIGURE 1) is confirmed by the presence of characteristic peaks; the peak at 1006 cm^{-1} is indicative of the Si-O bond; the peaks at 3470 and 1627 cm^{-1} are indicative of the N-H stretching and bending vibrations overlapped with those of vibration bands of hydrogen-bonded silanols (SiOH groups).

Fe_3O_4-APTES expose the -NH_2 groups, allowing NPs to remain dispersed in the medium.

■ Assessment of binding efficiency

RgDAAO was conjugated to Fe_3O_4-APTES by means of glutaraldehyde. Under the authors' best experimental conditions, the amount of enzyme bound to NPs, determined as the difference between the protein amount added and that recovered in the supernatant, is approximately 70%, with an enzymatic activity of approximately 4.5 U/mg NP. DAAO activity remained stable for 2 weeks at 4°C and a 20% decrease was observed after 2 months. The coating procedure did not affect the kinetic properties of RgDAAO. In fact, the apparent K_m of the immobilized enzyme for D-Ala was identical to that of the free enzyme (0.9 vs 1 mM, see FIGURE 2) [18]. Altogether, this conjugation procedure does not seem to alter the flavoenzyme conformation and its binding with the flavin adenine dinucleotide cofactor, which is absolutely required for its catalytic activity.

■ Cytotoxicity studies

Cytotoxicity was tested on three different tumor cell lines, that is, SKOV-3 (ovarian adenocarcinoma), HCT116 (colorectal carcinoma) and U87 (glioblastoma and astrocytoma). The effects of the different forms of DAAO on cell viability, expressed as ATP content, are reported in FIGURE 3. In absence of the D-Ala addition, free DAAO, at the tested doses, did not affect viability of the three tested cell lines. To induce the cytotoxic stress, D-Ala was used since it represents the reference substrate for DAAO [18]. Noteworthily, D-Ala itself had no effect on cell viability at the used concentrations [BAVA, GORNATI, CAPPELLINI ET AL., UNPUBLISHED DATA]. When D-Ala was added, a clear effect was seen in SKOV-3 (FIGURE 3A) and HCT116 (FIGURE 3B) cell lines, while U87 glioblastoma cells were insensitive to the treatment (FIGURE 3C).

Fe_3O_4-APTES–DAAO, with and without its substrate, was also tested. As far as it concerns cytotoxic effects, the effect of Fe_3O_4 NPs at the concentrations used in these experiments is negligable (SUPPLEMENTARY DATA; see online at www.futurescience.com/doi/suppl/10.2217/NNM.12.187). As shown in FIGURE 3, Fe_3O_4-APTES–DAAO also exert a certain degree of toxicity in the absence of the substrate addition. In all cases, however, the cytotoxicity is increased by D-Ala addition. It is noteworthy that Fe_3O_4-APTES–DAAO in the presence of 1 mM D-Ala completely depletes the ATP
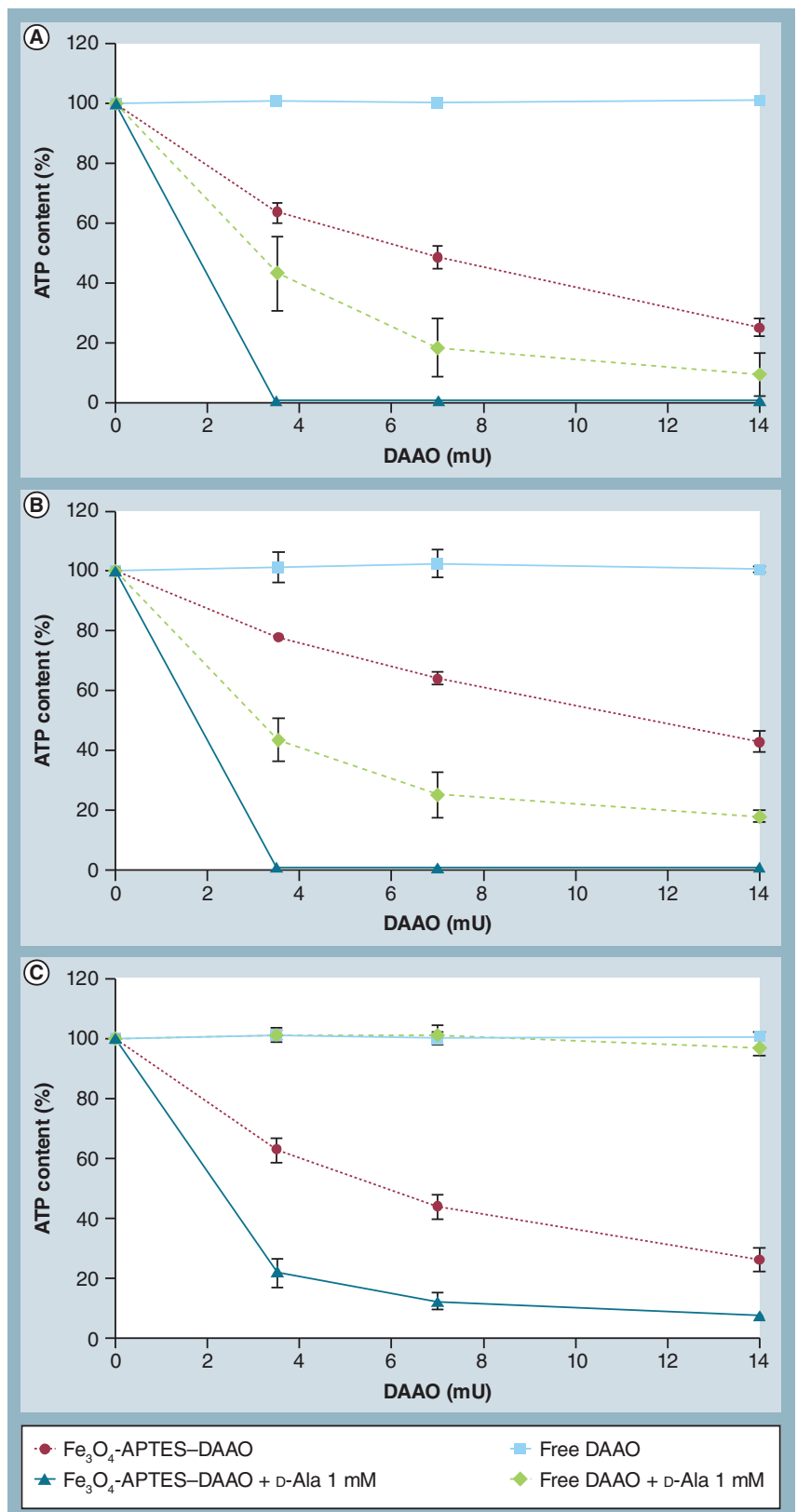

Figure 3. Cell viability. (A) SKOV-3; **(B)** HCT116; and **(C)** U87 cell lines. Cell viability is expressed as a percentage of ATP content compared with control after a 24-h exposure to 3.5, 7 and 14 mU of Fe_3O_4-APTES–DAAO and free DAAO, with and without the substrate D-Ala.
DAAO: D-amino acid oxidase; Fe_3O_4-APTES-DAAO: Fe_3O_4 nanoparticles functionalized with 3-aminopropyltriethoxysilane and bound to D-amino acid oxidase.

Legend (bottom of figure):
- Fe$_3$O$_4$-APTES–R285A
- Fe$_3$O$_4$-APTES–R285A + D-Ala 1 mM
- Free R285A
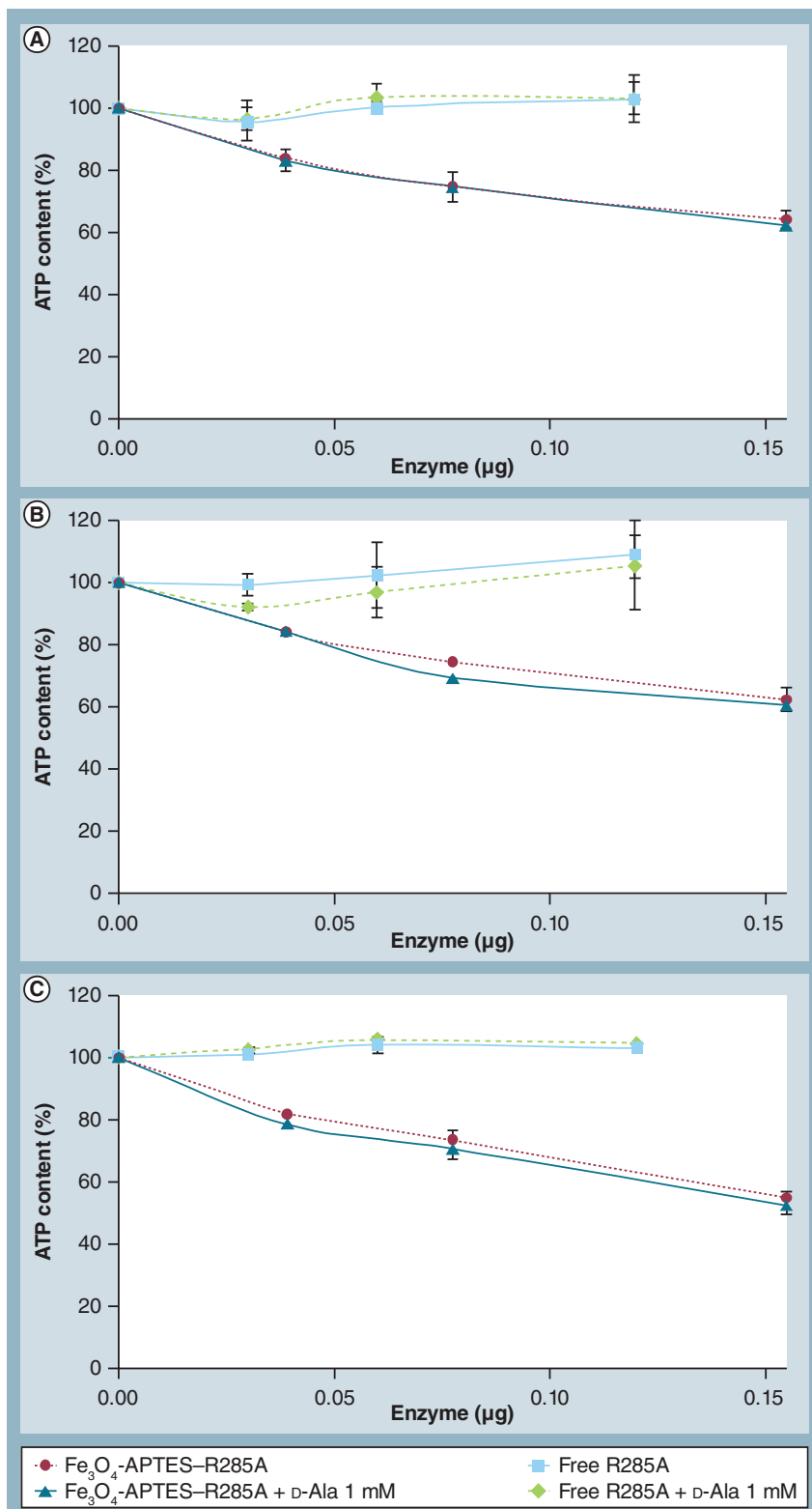- Free R285A + D-Ala 1 mM

Figure 4. Cell viability expressed as percentage of ATP content compared with control. (A) SKOV-3; **(B)** HCT116; and **(C)** U87 cell lines after a 24-h exposure to the nonactive D-amino acid oxidase mutant R285A, with and without the substrate D-Ala. The mutant was either free (0.03, 0.06 and 0.012 µg of enzyme) or bound to Fe$_3$O$_4$-APTES (0.04, 0.08 and 0.015 µg of enzyme).
Fe$_3$O$_4$-APTES–R285A: Fe$_3$O$_4$ nanoparticles functionalized with 3-aminopropyltriethoxysilane and bound to D-amino acid oxidase mutant R285A.

content already at 3.5 mU of the enzyme.

U87 glioblastoma cells were generally less sensitive to the treatment (**Figure 3C**). To check for a possible presence of endogenous D-amino acids, D-Ser in U87 was measured and compared with its presence in SKOV-3. D-Ser is a well-known neuromodulator, which represents the most abundant natural D-amino acid in different brain cells [35]. HPLC analysis showed that the cellular D-Ser content was approximately 1% of the total (L- and D-) serine levels in both cell lines. Accordingly, if oxidized by DAAO, the natural content in D-Ser should result in the same H$_2$O$_2$ production and, thus, should similarly affect the viability of cell lines during treatment.

To confirm that the toxicity was mainly due to the enzyme activity, cells were also exposed, in the same conditions previously used, to DAAO(R285A), a nonactive mutant. The results, reported in **Figure 4**, confirmed that the free DAAO(R285A) in presence or not of 1 mM of D-Ala does not affect ATP content, while the system Fe$_3$O$_4$-APTES–DAAO(R285A), even at the highest dose, accounts, at most, for 40% of ATP reduction.

■ **NP uptake**
As already reported [36], NPs are able to enter the cells by endocytosis, probably by binding to the membrane (**Figures 5 & 6**). Cañete *et al.* have demonstrated that iron oxide NPs enter the cells mainly by a macropinocytosis process and not by a clathrin-mediated endocytosis [37]. NP uptake seems a requisite to exert their maximum toxicity. Internalization of the particles was rapid, aspecific and concentration dependent [Bava, Gornati, Cappellini *et al.*, Unpublished Data]. In **Figures 5 & 6**, where SKOV-3 and U87 cells exposed to Fe$_3$O$_4$-APTES–DAAO for 24 h are reported as examples, cellular pseudopodes, characteristic structures of the endocytosis pathway, are particularly evident. Once entered into the cell, the majority of NPs remain in the cytoplasm inside the endocytic vesicles. Nevertheless, vesicles may undergo mechanical damage, freeing NPs, which could reach different cell districts such as mitochondria where they are seen by transmission electron microscopy (**Figure 5B**).

Discussion
The authors have focused their research on the synthesis and characterization of magnetic NPs combined with the enzyme DAAO as a potential drug for cancer treatment. They took
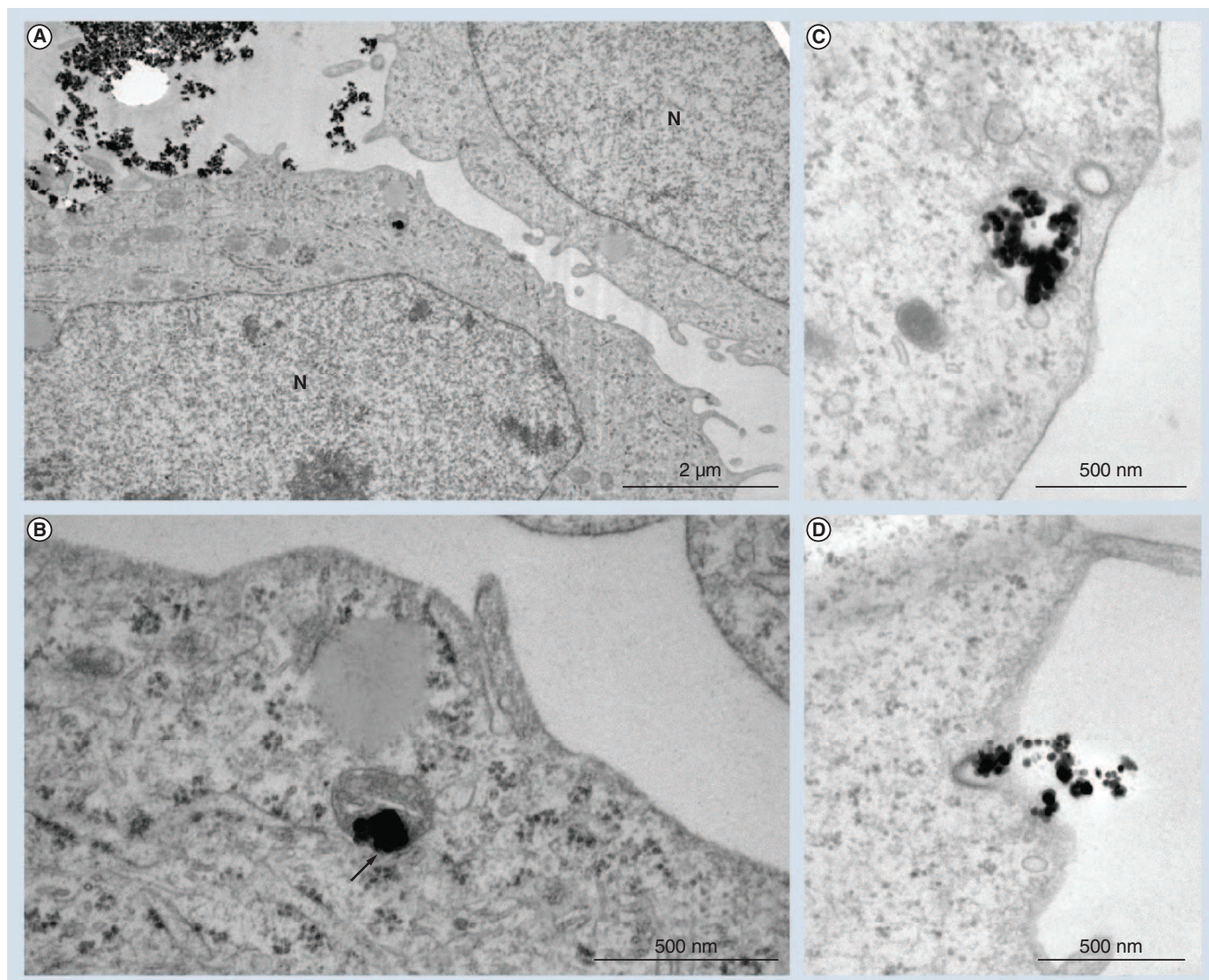
Figure 5. Transmission electron microscopy pictures of SKOV-3 cells exposed to Fe₃O₄ nanoparticles functionalized with 3-aminopropyltriethoxysilane for 24 h. (A) Several electron opaque particles in the extracellular space and adhering to the plasma membrane. Particles are also visible inside the cell. **(B)** The enlargement of **(A)** shows particles in correspondence of a mitochondrion (arrow). Particles are also visible **(C)** inside a vesicle and **(D)** on the surface of the cell in correspondence of a membrane invagination. N: Nucleus.

advantage of the use of a very active flavoenzyme capable of producing H_2O_2 by oxidation of a specific substrate, such as a D-amino acid. These compounds are scarcely present in human tissues, so it is possible to control the production of H_2O_2 by adjusting the concentration of the substrate to be administered [19,21]. For a recent, general review on the use of oxidative stress for cancer therapy, see [7,38,39].

In this work, RgDAAO covalently linked to Fe_3O_4 NPs by free -NH_2 groups of APTES activated by glutaraldehyde was used. The presence of aminosilane has been confirmed by Fourier transform infrared spectroscopy analysis and, as reported in the literature [40,41], the peaks found at 1006, 1627 and 3470 cm^{-1}

are characteristic of the Si-O bond and -NH groups present in the APTES molecule (FIGURE 1). Under the authors' best experimental conditions, they were able to immobilize approximately 70% of the free enzyme. The system (i.e., Fe_3O_4-APTES–DAAO) showed an activity of 4.5 U/mg of NP and an apparent K_m for the substrate D-Ala similar to that determined for the free enzyme. Unfortunately, the results are difficult to compare with the data present in literature [42,43] due to the disparate experimental conditions that were used. However, Hsieh *et al.* reported that they were able to immobilize approximately 80% of the free enzyme, but with a relatively low recovered activity [44]. A problem associated with the use
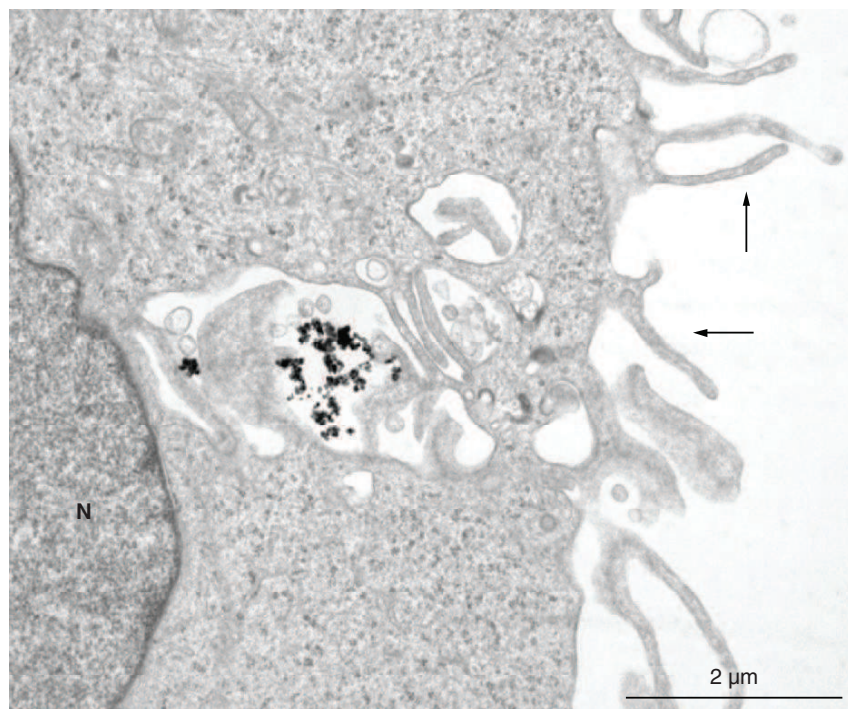
Figure 6. Transmission electron microscopy image of U87 cells exposed to Fe₃O₄ nanoparticles functionalized with 3-aminopropyltriethoxysilane for 24 h. Electron opaque particles are entrapped in intricate membrane morphology. Arrows indicate the pseudopodes.
N: Nucleus.

of magnetic NPs is represented by the safe dose of accumulation to avoid side effects. The system allows for a minimal amount of Fe_3O_4 NPs (~6 µg) to be used, whose intrinsic cytotoxicity is approximately 20% for the examined cell lines (see SUPPLEMENTARY DATA and [45–47]).

NP cellular uptake, studied in a wide variety of cell types, has revealed a conserved mechanism characterized by an inverse relationship between the internalization and NP size; furthermore, the uptake machinery depends on the cell-loading conditions, including surface charge, particle concentration and properties, and incubation time [48,49]. For high concentrations and long exposure times, such as those used in these experiments (system concentration of 80 µg/ml and exposure time of 24 h), the process was not dependent on the aforementioned parameters. This assertion has been confirmed by experiments showing a similar behavior of system Fe_3O_4-APTES–DAAO towards all of the tested cell lines, both in the presence and absence of 1 mM of D-Ala. One advantage of this formulation is its efficacy in killing cells when administered together with its substrate and the relatively less efficacy when the treatment does not include the D-Ala, independently of cell type used. D-amino acids are normally present in the tissues, although at a much lower

concentration than that of the L-amino acids. Therefore, a minimal activity of the enzyme in the absence of the exogenous substrate is also expected. Such activity is augmented by the fact that the system Fe_3O_4-APTES–DAAO probably exerts its function close to the cell membranes or inside the cells (Trojan horse effect). However, the toxicity of the system is dramatically increased by substrate addition and the difference is particularly evident at lower doses. A second main advantage is the very low amount of enzyme required to give maximal toxicity; the system Fe_3O_4-APTES–DAAO appears more efficient compared with that proposed by Divakaran *et al.* [50]. They reported the antitumor activity of a NP-DAAO system, prepared by electrostatically binding pig kidney DAAO to polyvinylpyrrolidone-coated Fe_2O_3 NPs. RgDAAO, in fact, is tenfold more active than pig kidney DAAO and the D-Ala concentration used in these experiments is dramatically lower. Moreover, the covalent link of RgDAAO to the NPs should confer a greater stability to the system.

After the exposure of cells with Fe_3O_4-APTES–DAAO, the NP system is probably confined in endosomal vesicles for a long time without affecting cell phenotype and function, even though long-term biotransformation is supposed to occur [48].

The effect of free RgDAAO whose behavior depends on the cell type is different. In fact, as shown in FIGURES 3A & 3B, significant toxicity is observed with free RgDAAO in the presence of 1 mM of D-Ala on SKOV-3 and HCT116 cell lines, while U87 glyoblastoma cells were totally insensitive (FIGURE 3C).

This behavior can be explained considering that free RgDAAO exerts its action in the extracellular environment, whose characteristics (pH, redox capability and presence of metabolites) can change depending on the cell type. Moreover, cell lines respond differently to reactive oxygen species insults. In any case, the fact that the effect of this nanosystem was due to the enzyme was confirmed by the relative ineffectiveness of the system Fe_3O_4-APTES–DAAO(R285A) (FIGURE 4).

Conclusion

Our experiments demonstrated that Fe_3O_4-APTES–DAAO was more effective than free RgDAAO, and independent of cell type, in inducing cytotoxicity, thus supporting the validity of the combination of Fe_3O_4-APTES–DAAO/D-Ala as a possible treatment in cancer therapy.

Future perspective

The potentiality of this system should be verified by studying tissue distribution, toxicity and clearance after intravenous injection. DAAO is an enzyme that catalyzes the stereoselective deamination of ᴅ-amino acids generating H_2O_2 and, therefore, it may be regarded as a promising anticancer therapeutic. Its combination with magnetic NPs will allow the area of interest to be addressed by applying an external magnetic field. Consequently, the efficacy of the oxystress will be maximized and the general toxicity minimized. The magnetic properties of the system will allow its detection by MRI and, therefore, it can also be exploited as a theranostic.

Ethical conduct of research

The authors state that they have obtained appropriate institutional review board approval or have followed the principles outlined in the Declaration of Helsinki for all human or animal experimental investigations. In addition, for investigations involving human subjects, informed consent has been obtained from the participants involved.

Executive summary

Development of a nanoparticle–enzyme system for cancer therapy
- The method developed for the nanoparticle–enzyme conjugation is reproducible and reliable.

Main characteristics of the nanoparticle–enzyme system
- The system is stable and active for a relatively long time. The use of magnetic nanoparticles allows the system to be directed to the target tissue. The cytotoxicity of the system could be controlled by the addition of appropriate concentrations of the substrate and not strictly dependent on cell type.

Future perspective
- The potentiality of this system should be verified studying tissue distribution, toxicity and clearance after intravenous injection. The efficacy of the oxystress will be maximized addressing Fe_3O_4-3-aminopropyltriethoxysilane–ᴅ-amino acid oxidase in the area of interest by applying an external magnetic field. The system magnetic properties can be exploited also in theranostic.

References

Papers of special note have been highlighted as:
- of interest
- of considerable interest

1   Cattaneo AG, Gornati R, Sabbioni E *et al.* Nanotechnology and human health: risks and benefits. *J. Appl. Toxicol.* 30, 730–744 (2010).
- **Comprehensive review balancing risks and benefits on human health.**

2   Khanna VK. Targeted delivery of nanomedicines. *ISRN Pharmacol.* doi:10.5402/2012/571394 (2012) (Epub ahead of print).

3   Davis ME, Chen ZG, Shin DM. Nanoparticle therapeutics: an emerging treatment modality for cancer. *Nat. Rev. Drug Discov.* 7, 771–782 (2008).

4   De Jong WH, Borm PJ. Drug delivery and nanoparticles: applications and hazards. *Int. J. Nanomedicine* 3(2), 133–49 (2008).

5   Kwon JT, Hwang SK, Jin H *et al.* Body distribution of inhaled fluorescent magnetic nanoparticles in the mice. *J. Occup. Health* 50(1), 1–6 (2008).

6   Lankveld DP, Oomen AG, Krystek P *et al.* The kinetics of the tissue distribution of silver nanoparticles of different sizes. *Biomaterials* 31(32), 8350–8361 (2010).

7   Fang J, Nakamura H, Iyer A. Tumor-targeted induction of oxystress for cancer therapy. *J. Drug Target.* 15, 475–486 (2007).
- **Production of polyethylene glycol-conjugated enzyme for oxystress therapy.**

8   Niculescu-Duvaz I, Springer CJ. Introduction to the background, principles, and state of the art in suicide gene therapy. *Mol. Biotechnol.* 30, 71–88 (2005).

9   Fukumura D, Jain RK. Tumor microenvironment abnormalities: causes, consequences, and strategies to normalize. *J. Cell. Biochem.* 101, 937–949 (2007).

10   Jain RK. Normalization of tumor vasculature: an emerging concept in antiangiogenic therapy. *Science* 307, 58–62 (2005).

11   Nacev A, Kim SH, Rodriguez-Canales J, Tangrea MA, Shapiro B, Emmert-Buck MR. A dynamic magnetic shift method to increase nanoparticle concentration in cancer metastases: a feasibility study using simulations on autopsy specimens. *Int. J. Nanomedicine* 6, 2907–2923 (2011).

12   Jain KK. Advances in the field of nanooncology. *BMC Med.* 8, 83–93 (2010).

13   Barakat IAH, Abbas OA, Ayad S, Hassan AM. Evaluation of radio protective effects of wheat germ oil in male rats. *J. Am. Sci.* 7, 664–673 (2011).

14   Lee Koo YE, Reddy GR, Bhojani M *et al.* Brain cancer diagnosis and therapy with nanoplatforms. *Adv. Drug Deliv. Rev.* 58, 1556–1577 (2006).

15   Paillard F. Cancer gene therapy using oxidative stress. *Hum. Gene Ther.* 9, 159–160 (1998).
- **One of the first examples of enzyme oxystress treatment.**

16   Ben-Yoseph O, Ross BD. Oxidation therapy: the use of a reactive oxygen species-generating enzyme system for tumor treatment. *Br. J. Cancer* 70, 1131–1135 (1994).

17   Connors TA. The choice of prodrugs for gene directed enzyme prodrug therapy of cancer. *Gene Ther.* 2, 702–709 (1995).

18 Pollegioni L, Piubelli L, Sacchi S, Pilone MS, Molla G. Physiological functions of D-amino acid oxidases: from yeast to humans. *Cell. Mol. Life Sci.* 64, 1373–1394 (2007).

■■ **A comprehensive review of structure–function relationships in D-amino acid oxidase.**

19 Stegman LD, Zheng H, Neal ER *et al.* Induction of cytotoxic oxidative stress by D-alanine in brain tumor cells expressing *Rhodotorula gracilis* D-amino acid oxidase: a cancer gene therapy strategy. *Hum. Gene Ther.* 9, 185–193 (1998).

20 Pollegioni L, Langkau B, Tischer W, Ghisla S, Pilone MS. Kinetic mechanism of D-amino acid oxidases from *Rhodotorula gracilis* and *Trigonopsis variabilis. J. Biol. Chem.* 268, 13850–13857 (1993).

21 Rosini E, Pollegioni L, Ghisla S, Orru R, Molla G. Optimization of D-amino acid oxidase for low substrate concentrations – towards a cancer enzyme therapy. *FEBS J.* 276, 4921–4932 (2009).

22 Pankhurst QA, Connolly J, Jones SK, Dobson J. Applications of magnetic nanoparticles in biomedicine. *J. Phys. D. Appl. Phys.* 36, R167–R181 (2003).

23 Arruebo M, Fernández-Pacheco R, Ibarra MR, Santamaría J. Magnetic nanoparticles for drug delivery. *Nano. Today* 2(3), 22–32 (2007).

24 Dobson J. Magnetic nanoparticles for drug delivery. *Drug Dev. Res.* 67, 55–60 (2006).

25 Yoo D, Lee JH, Shin TH, Cheon J. Theranostic magnetic nanoparticles. *Acc. Chem. Res.* 44(10), 863–874 (2012).

26 Harford-Wright E, Lewis KM, Vink R. Towards drug discovery for brain tumors: interaction of kinins and tumors at the blood brain barrier interface. *Recent Pat. CNS Drug Discov.* 6, 31–40 (2011).

27 Rabanel JM, Aoun V, Elkin I, Mokhtar M, Hildgen P. Drug-loaded nanocarriers: passive targeting and crossing of biological barriers. *Curr. Med. Chem.* 19(19), 3070–3102 (2012).

28 Liu Y, Lu W. Recent advances in brain tumor-targeted nano-drug delivery system. *Expert Opin. Drug Deliv.* 9(6), 671–686 (2012).

29 Nair BG, Varghese SH, Nair R, Yoshida Y, Maekawa T, Kumar DS. Nanotechnology platforms; an innovative approach to brain tumor therapy. *Med. Chem.* 7(5), 488–503 (2011)

30 Fantinato S, Pollegioni L, Pilone MS. Engineering, expression and purification of a His-tagged chimeric D-amino acid oxidase from *Rhodotorula gracilis. Enz. Microbiol. Technol.* 29, 407–412 (2001).

31 del Campo A, Sen T, Lellouche JP, Bruce IJ. Multifunctional magnetite and silica–magnetite nanoparticles: synthesis, surface activation and applications in life sciences. *J. Magn. Magn. Mater.* 293, 33–40 (2005).

32 Molla G, Porrini D, Job V *et al.* Role of arginine 285 in the active site of *Rhodotorula gracilis. J. Biol. Chem.* 275, 24715–24721 (2000).

33 Harris CM, Molla G, Pilone MS, Pollegioni L. Studies on the reaction mechanism in *Rhodotorula gracilis* D-amino acid oxidase. *J. Biol. Chem.* 274, 36233–36240 (1999).

34 Sacchi S, Bernasconi M, Martineau M *et al.* pLG72 modulates intracellular D-serine levels through its interaction with D-amino acid oxidase: effect on schizophrenia susceptibility. *J. Biol. Chem.* 283(32), 22244–22456 (2008).

35 Pollegioni L, Sacchi S. Metabolism of the neuromodulator D-serine. *Cell. Mol. Life Sci.* 67, 2387–2404 (2010).

■ **Update on D-serine in the brain.**

36 Papis E, Rossi F, Raspanti M *et al.* Engineered cobalt oxide nanoparticles readily enter cells. *Toxicol. Lett.* 189, 253–259 (2009).

■■ **Clear example of nanoparticle internalization.**

37 Cañete M, Soriano J, Villanueva A *et al.* The endocytic penetration mechanism of iron oxide magnetic nanoparticles with positively charged cover: a morphological approach. *Int. J. Mol. Med.* 26(4), 533–539 (2010).

38 Verrax J, Beck R, Dejeans N *et al.* Redox-active quinones and ascorbate: an innovative cancer therapy that exploits the vulnerability of cancer cells to oxidative stress. *Anticancer Agents Med. Chem.* 11(2), 213–221 (2011).

39 Manthe RL, Foy SP, Krishnamurthy N, Sharma B, Labhasetwar V. Tumor ablation and nanotechnology. *Mol. Pharm.* 7(6), 1880–1898 (2010).

40 Mohapatra S, Pramanik N, Mukherjee S, Ghosh SK, Pramanik P. A simple synthesis of amine-derivatised superparamegnetic iron oxide nanoparticles for bioapplications. *J. Mater. Sci.* 42, 7566–7574 (2007).

41 Yamaura M, Camilo RL, Sampaio LC, Macêdo MA, Nakamura M, Toma HE. Preparation and characterization of (3-aminopropyl)triethoxysilane-coated magnetite nanoparticles. *J. Magn. Magn. Mat.* 279, 210–217 (2004).

42 Kuan IC, Wu JC, Lee SL, Tsai CW, Chuang CA, Yu CY. Stabilization of D-amino acid oxidase from *Rhodosporidium toruloides* by encapsulation in polyallylamine-mediated biomimetic silica. *Biochem. Eng. J.* 49, 408–413 (2010).

43 Chien LJ, Lee CK. Biosilicification of dual-fusion enzyme immobilized on magnetic nanoparticle. *Biotechnol. Bioeng.* 100, 223 (2008).

44 Hsieh HC, Kuan IC, Lee SL, Tien GY, Wang YJ, Yu CY. Stabilization of D-amino acid oxidase from *Rhodosporidium toruloides* by immobilization onto magnetic nanoparticles. *Biotechnol. Lett.* 31, 557–563 (2009).

45 Naqvi S, Samim M, Abdin M *et al.* Concentration-dependent toxicity of iron oxide nanoparticles mediated by increased oxidative stress. *Int. J. Nanomedicine* 5, 983–989 (2010)

46 Prijic S, Scancar J, Romih R *et al.* Increased cellular uptake of biocompatible superparamagnetic iron oxide nanoparticles into malignant cells by an external magnetic field. *J. Membr. Biol.* 236, 167–179 (2010).

47 Xin-li L, Shu-Hua Z, Long Z, Gui-Qin H, Zhi-Wei S, Wen-Sheng Y. Dose dependent cytotoxicity and oxidative stress induced by 'naked' Fe_3O_4 naoparticles in human hepatocyte. *Chem. Res. Chinese Universities* 28(1), 114–118 (2012).

48 Gazeau F, Wilhelm C. Magnetic labeling, imaging and manipulation of endothelial progenitor cells using iron oxide nanoparticles. *Future Med. Chem.* 2, 397–408 (2010).

49 Thorek DL, Tsourkas A. Size, charge and concentration dependent uptake of iron oxide particles by nonphagocytic cells. *Biomaterials* 29(26), 3583–3590 (2008).

50 Divakaran SA, Sreekanth KM, Rao KV, Nair CKK. D-aminoacid oxidase–Fe_2O_3 nanoparticle complex mediated antitumor activity in swiss albino mice. *J. Cancer Ther.* 2, 666–674 (2011).

Research Article

Heparin and Carboxymethylchitosan Metal Nanoparticles: An Evaluation of Their Cytotoxicity

Adriana Bava,[1] Francesca Cappellini,[1] Elisa Pedretti,[1] Federica Rossi,[1] Enrico Caruso,[2] Elena Vismara,[3,4] Maurizio Chiriva-Internati,[5] Giovanni Bernardini,[1,4] and Rosalba Gornati[1,4]

[1] *Dipartimento di Biotecnologie e Scienze della Vita, Università dell'Insubria, 21100 Varese, Italy*

[2] *Dipartimento di Scienze Teoriche ed Applicate, Università dell'Insubria, 21100 Varese, Italy*

[3] *Dipartimento di Chimica, Materiali e Ingegneria Chimica "G. Natta," Politecnico di Milano, 20131 Milano, Italy*

[4] *Interuniversity Center "The Protein Factory," Politecnico di Milano, ICRM-CNR Milano and Università dell'Insubria, 20131 Milano, Italy*

[5] *Division of Oncology and Hematology, Texas Tech University Health Sciences Center, Lubbock, TX 79409, USA*

Correspondence should be addressed to Rosalba Gornati; rosalba.gornati@uninsubria.it

In the search for noninvasive diagnostic techniques and new therapies, "nanosystems", which are capable of binding and targeting bioactive molecules, are becoming increasingly important. In this context, biocompatible coatings are gaining interest, not only for their biological effects but also because they are considered capable to mask nanoparticle toxicity. In this work, we have compared the toxicity of nanoparticles coated with heparin and carboxymethylchitosan in the SKOV-3 cell line. Our results indicate that heparin and carboxymethylchitosan coatings do not guarantee the decrease of nanoparticle intrinsic toxicity which is often envisaged. Nonetheless, these coatings provide the opportunity for further functionalization with a variety of biomolecules for their use in theranostics.

1. Introduction

Nanomedicine, the application of nanotechnology in healthcare, offers numerous and promising possibilities to significantly improve medical diagnosis and therapy. New sensitive diagnostic devices, in fact, will permit very early personal risk assessment, and the abatement of costs for the disease treatment is a must for healthcare. Due to its high potential, nanomedicine holds the promise to greatly improve the efficacy of pharmaceutical therapy, reduce side effects, and make drug administration more convenient [1].

In this context, nanoparticles (NPs), particularly magnetic nanoparticles (MNPs), coated with biodegradable polymers, are attracting widespread attention for targeted therapy and imaging. These coatings can stabilize the NP systems also in hydrophilic fluids, minimize opsonization by the mononuclear phagocytic system, and prolong blood circulation [2–7]. Furthermore, this surface layer can be functionalized with a variety of biological moieties for tumor-specific targeting [8–10].

Among the biological molecules used for NP coating, chitosan, particularly carboxymethylchitosan (CMCS), and heparin appear very interesting also because they are considered capable to mask NP toxicity [11, 12]. We should not, in fact, oversee the toxicity of cobalt and nickel oxide NPs [13–16] nor their potential effect on the environment [17]. Even though heparin is predominantly used as anticoagulant, its ability to interact with proteins makes it very attractive. NPs coated with heparin (NP@heparin) are extensively studied because of their several biomedical applications ranging from tissue engineering to biosensors passing for its use in cancer therapy [3]. As well as heparin, also chitosan NPs have demonstrated anticancer activity *in vitro* as well as *in vivo* even though the mechanisms remain to be elucidated [18].

In this paper, we have reported cytotoxicity and uptake of some transition metal oxide NPs (Co_3O_4, Fe_3O_4, and
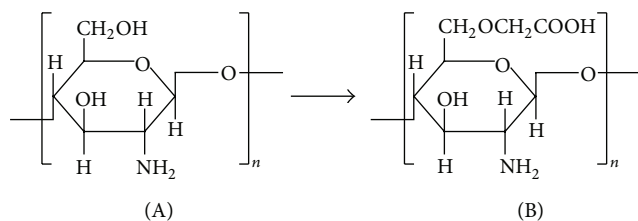
Figure 1: Chemical structure of chitosan (A) and carboxymethyl-chitosan (B).

NiO) coated with heparin and of Fe_3O_4 NPs coated with CMCS (Fe_3O_4@CMCS) in SKOV-3 cell. Transition metal NPs are especially used to enhance surface electrochemical reactivity to further improve the performance of lithium-ion batteries [19] as well as in catalysis [20, 21]. Nevertheless, the therapeutic use of transition metal conjugates was already known in the sixteenth century because of their different oxidation states and ability to interact with negatively charged molecules forming chelation complexes [22].

The results here reported indicate that heparin and CMCS alone did not show any cytotoxicity effect at the concentration used in the experiments. Unfortunately, they did not seem to be able to drastically reduce NP toxicity.

2. Materials and Methods

2.1. Chemicals. Iron oxide (Fe_3O_4), cobalt oxide (Co_3O_4) and nickel oxide (NiO) NPs (<50 nm particle size), chitosan powder (75% degree of acetylation), monochloroacetic acid, 1-ethyl-3-(3-dimethylaminopropyl)carbodiimide hydrochloride (EDC·HCl), and N-hydroxysuccinimide (NHS) were purchased from Sigma-Aldrich, Milan, Italy. Heparin, in the form of sodium salt, was kindly provided by LDO Company, Trino Vercellese, Italy. CellTiter-Glo Luminescent Cell Viability Assay was purchased from Promega, Milan, Italy. Isopropanol was purchased from J.T.Baker, Milan, Italy. All other reagents, analytical or cell culture grade, were purchased from Sigma-Aldrich, Milan, Italy. The Milli-Q ultrapure water was used.

2.2. Nanoparticles Characterization. The particle size distribution was studied by transmission electron microscopy (TEM) using a 90 keV JEOL-1010 electron microscope (Tokyo, Japan). TEM samples were prepared by placing 10 μL of a dilute suspension of Fe_3O_4 nanoparticles in ethanol on a carbon-coated copper grid and allowing the solvent to evaporate at room temperature. The average particle size (D_{TEM}) and distribution were evaluated by measuring the largest internal dimension of 100 particles.

2.3. Synthesis of Carboxymethylchitosan (CMCS). CMCS was prepared as reported by Zhu et al. [23]. The chemical structures of chitosan and CMCS are reported in Figure 1.

2.4. Coating of Metal Nanoparticles

2.4.1. NP@heparin. A suspension of NPs (Co_3O_4 or Fe_3O_4 or NiO) in distilled water (100 mg/5 mL) obtained by ultrasonication for 5 min (Sonica 5300MH-Soltec) was transferred

into a solution of heparin, (1.045 g/25 mL, pH 7 adjusted with 0.01 N NaOH). The mixture was stirred overnight (130 rpm, 25°C, Julabo SW22). Co_3O_4@heparin and NiO@heparin were separated by centrifugation (1 h, 6300 ×g, Hettich Zentrifugen-Rotina 35 F), while Fe_3O_4@heparin was separated by a neodymium magnet (NdFeB Nickel plated, magnetization N45). NP@heparin were collected in diethyl ether, recovered after solvent elimination and dried at 50°C for 1 h.

2.4.2. Fe_3O_4@CMCS Electrostatic Bound. A suspension of 100 mg of Fe_3O_4 NPs in 5 mL water was prepared by ultrasonic bath for 10 min. Separately, 100 mg of CMCS was dissolved in 20 mL of water using a magnetic stirrer until complete dissolution, then added to the Fe_3O_4 NPs dispersion and mixed by ultrasonic bath at 0°C for 1 h. After reaction, the Fe_3O_4@CMCS was separated from unbound CMCS by a neodymium magnet, washed several times with water, and centrifuged at 15000 ×g, 20 min. The pellet was resuspended in ethyl alcohol then, after anhydrification, Fe_3O_4@CMCS was dried overnight at 50°C.

2.4.3. Fe_3O_4@CMCS-Covalent Bound. The covalent immobilization of CMCS on Fe_3O_4 NPs was conducted following Liang and Zhang method [24] with some modifications. Briefly, 75 mg of Fe_3O_4 NPs were added to 4 mL of sodium phosphate buffer (200 mM, pH 5) containing 25 mg of EDC·HCl and 20 mg of NHS; the mixture was left in an ultrasonic bath for 30 min. The Fe_3O_4 NPs activated were separated from excess of reagents by magnetic decantation, then resuspended in 3 mL of 200 mM sodium phosphate buffer (pH 7) by sonication for 10 min. 1 mL of CMCS solution (25 mg/mL in 200 mM sodium phosphate buffer, pH 7) was added to the suspension of the NPs and the reaction mixture was sonicated for 3 h. Finally, the Fe_3O_4@CMCS was recovered by magnet, washed with water, and dried overnight at 50°C.

2.4.4. Determination of Unbound Fe. 5 mg of Fe_3O_4 NPs, or Fe_3O_4@heparin, or Fe_3O_4@CMCS electrostatically bound or Fe_3O_4@CMCS covalently bound were resuspended in 5 mL of H_2O, sonicated for 20 min, and left at 37°C for 72 h. Afterwards, NP systems were separated from the supernatant by a neodymium magnet, centrifuged twice at 15000 ×g for 15 min at 4°C, then ultracentrifuged at 300000 ×g for 2 h at 4°C. After centrifugation, supernatants were filtered using a 0.22 μm pore size membrane. The amount of Fe (II), eventually released in solution, was determined by complexometric analysis with the o-phenanthroline [25]. The Fe (II), in the presence of o-phenanthroline, form the stable red-orange complex $[(C_{12}H_{18}N_2)_3Fe]^{2+}$. The intensity of the color does not vary in the range of pH between 3 and 9. The maximum absorption wavelength occurs at 510 nm. The possible Fe (III) is reduced to Fe (II) by treatment with hydroxylamine hydrochloride.

2.5. FT-IR Spectra Analysis. Characterization of the samples was performed using the solid phase Fourier transform infrared spectroscopy (FT-IR). Spectra were obtained using a

Nicolet, Avatar 360. Samples were mixed with infrared grade KBr in a proportion of 2 : 100 (w/w).

2.6. Cell Culture.

SKOV-3 cell line was maintained as adherent cells in RPMI 1640 medium, at 37°C in a humidified 5% CO_2 atmosphere. Medium was supplemented with 10% fetal bovine serum and 2 mM L-glutamine. Cells were passaged as needed using 0.5% trypsin EDTA.

2.7. Cell Viability.

Cell viability was determined measuring ATP content by the CellTiter-Glo Assay according to the manufacturer's instructions. In details, 200 μL of cell suspension (containing 2×10^4, 1×10^4, 5×10^3, 25×10^2 cells depending of the exposure time) were seeded into 96-well assay plates and cultivated for 24 h at 37°C in 5% CO_2 to equilibrate and become attached prior to the treatment. Then, cells were exposed to 100 μL of increasing concentrations of heparin, NP@heparin, CMCS, Fe_3O_4@CMCS electrostatic, and Fe_3O_4@CMCS covalent for 0.5, 1, 2, 24, 48, and 72 h. After the treatment, plates were equilibrated for 30 min at room temperature and then 100 μL of CellTiter-Glo reagent was added to each well. Plates were shaken for 2 min and left at room temperature for 10 min prior recording luminescent signals using the Infinite F200 plate reader (Tecan Group, Switzerland). Cell viability, expressed as ATP content and normalized against control values, was recorded. All the experiments were performed in triplicate.

2.8. Cellular Uptake.

10^4 cells were seeded on a coverslip (12 mm Ø) into 12-well assay plate and cultivated for 24 h at 37°C in 5% CO_2 to equilibrate and become attached before treatment. Cells were then incubated for 4 or 24 h with 25, 50, and 100 μg/mL Fe_3O_4@heparin, Fe_3O_4@CMCS electrostatic, and Fe_3O_4@CMCS covalent and visualized by Prussian blue staining for iron detection. For this microscopic technique, the cells were fixed in ice-cold ethanol for 5 min, stained with an equal volume of 2% hydrochloric acid and 2% potassium ferrocyanide trihydrate for 15 min, and counterstained with 0.5% neutral red for 3 min. The preparations were then washed with distilled water and dried by increasing concentrations of ethanol, than mounted in DePeX (Serva, Germany). Observations were performed by a Zeiss Axiophot microscope under bright light illumination and photographs were acquired by a Zeiss AxioCam ERc5s camera.

Furthermore, for TEM studies, 10^6 cells, seeded in a 10 cm Petri dish, are exposed to 40 μg/mL of NP@heparin, Fe_3O_4@CMCS electrostatic, and Fe_3O_4@CMCS covalent, for 30 min or 3 h. Then cells were harvested, fixed in 2% glutaraldehyde in 0.1 M sodium cacodylate buffer (pH 7.2) for 10 min on ice and for 30 min at room temperature, washed in the same buffer, and postfixed in dark for 1 h with 1% osmium tetroxide in 0.1 M sodium-cacodylate buffer (pH 7.2) at room temperature. After dehydration standard steps with a series ethyl alcohol, samples were embedded in an Epon-Araldite 812 1 : 1 mixture. Thin sections (90 nm), obtained with a ReichertUltracut S Ultratome (Leica, Nussloch, Germany), were stained with uranyl acetate and lead citrate according to the standard methods and observed with a Jeol 1010 electron microscope (Jeol, Tokyo, Japan) operated at 90 keV.
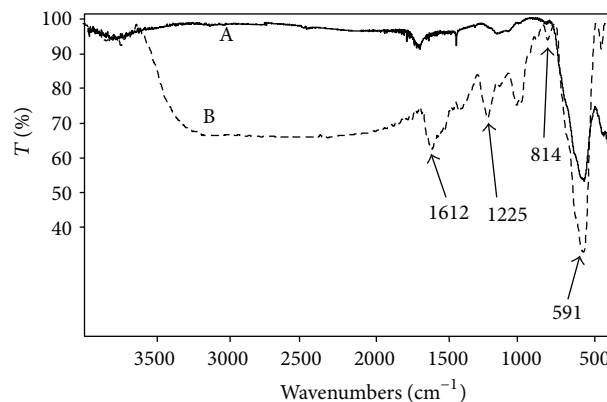

FIGURE 2: FT-IR spectra of Fe_3O_4NPs (A) and Fe_3O_4@heparin (B). The peaks at 814 cm^{-1}, between 1000 and 1400 cm^{-1} and those at 1225, and 1612 cm^{-1} are indicative of the heparin coating.

2.9. Statistical Analysis.

Cell viability values were expressed as mean ± standard error (SE). Analysis of variance (two-way ANOVA), for balanced mixed-effect experiments (uncoated NPs, coated NPs, and exposure times), was performed using KaleidaGraph 4.0 (Synergy Software). Statistical significant differences were fixed at $P \leq 0.05$ (*), $P \leq 0.01$ (**), and $P \leq 0.005$ (***).

3. Results

3.1. Nanoparticles Characterization.

To confirm the characteristics reported on the product label by Sigma-Aldrich, we have measured Fe_3O_4NPs diameter. D_{TEM} was 25.08 nm ± SD 4.09. The amount of Fe released from Fe_3O_4NPs, or Fe_3O_4@heparin, or Fe_3O_4@CMCS-electrostatic bound or Fe_3O_4@CMCS-covalent bound, in our experimental conditions, was under the limit of detection of the method (0.02 ppm).

3.2. FT-IR Spectra Analysis.

In Figure 2, we have reported, as example, the FT-IR spectra of Fe_3O_4NPs (A) and Fe_3O_4@heparin (B). Spectrum (B) shows, at 591 cm^{-1}, the characteristic peak of Fe–O stretch, while, between 1000 and 1400 cm^{-1}, peaks associated to C–O and C–C bonds due to the presence of heparin are present. Other peaks at 814, 1225, and 1612 cm^{-1} can be assigned to the stretching of –C–O–S, –S=O, and –COO$^-$ of the sulphates and carboxylate groups. Lambda shifts toward lower values compared to heparin alone are probably ascribable to the interaction with iron oxide.

FT-IR spectra of chitosan (A) and CMCS (B) are shown in Figure 3. Spectrum A shows the basic characteristic peaks of chitosan: 3550 cm^{-1} (O–H stretch), 2930 cm^{-1} (C–H stretch), 1648 cm^{-1} (NH bending), 1405 cm^{-1} (O–H bending), and 1080 cm^{-1} (C–O stretch). In addition to the peaks at 3550, 2930, 1405, and 1080 cm^{-1}, CMCS spectrum (B) reports an expanded and intense peak at 1612 cm^{-1} probably due to the overlapping of the signals of NH bending (1648 cm^{-1}) and COO$^-$ (1598 cm^{-1}) [23].
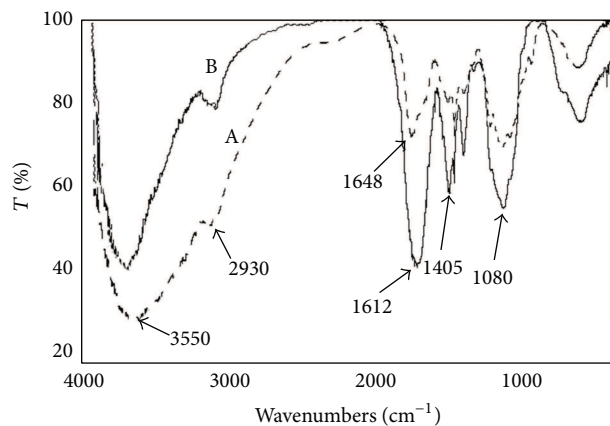
FIGURE 3: FT-IR spectra chitosan (A) and CMCS (B). Chemical modification of chitosan is confirmed by the presence of the intense peak at $1612 \, cm^{-1}$, attributed to the overlapping of the signals of NH bending and $–COO^−$.
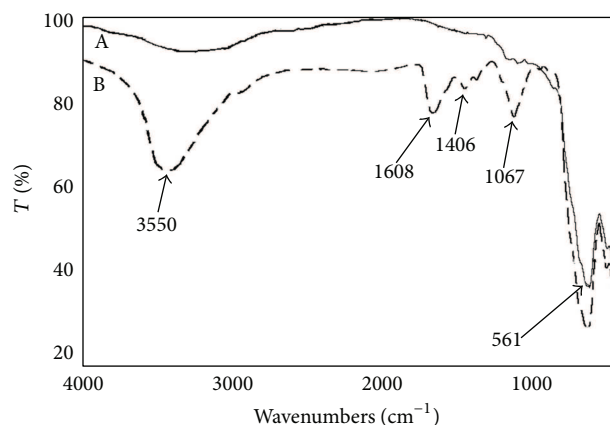

FIGURE 4: FT-IR spectra Fe_3O_4NPs (A) and $Fe_3O_4@CMCS$ (B). The peaks at 1067, 1406, 1608, and $3550 \, cm^{-1}$ indicate the presence of CMCS on the Fe_3O_4NPs surface.

Fe_3O_4NPs (A) and $Fe_3O_4@CMCS$ (B) spectra are shown in Figure 4. In spectrum A, the peak at $561 \, cm^{-1}$ is that characteristic of Fe–O stretch. Spectrum B, beside to the peak at $561 \, cm^{-1}$, reports the absorbance of CMCS molecule, in particular $1067 \, cm^{-1}$ (C–O stretch), $1406 \, cm^{-1}$ (O–H bend), $1608 \, cm^{-1}$ (overlapping of the peaks of NH_2, COOH, and $COO^−$), and $3550 \, cm^{-1}$ (O–H stretch). No significant differences were observed between spectra of $Fe_3O_4@CMCS$ electrostatically and covalently bound.

3.3. Cell Viability after NP@heparin Treatment. As reported in Figure 5(a), heparin alone was not toxic in the examined concentration range. A dose- and time-dependent reduction in cell viability was observed for all the examined NP systems, although Fe_3O_4NPs appear less toxic than Co_3O_4 NPs which is less toxic than NiO NPs, see Figures 6(a), 7(a), and 8(a).

Regarding the comparison between uncoated and coated NPs, our data indicate that the coating did not decrease the NPs toxicity. As demonstrated in Figure 6, Co_3O_4NPs were

less toxic than Co_3O_4@heparin for all the examined concentrations and time of treatment. The differences were less indicative for Fe_3O_4NPs and NiO NPs (Figures 7 and 8). For further details, see Supplementary Material Tables 1, 2, and 3 available online at http://dx.doi.org/10.1155/2013/314091.

3.4. Cell Viability after $Fe_3O_4@CMCS$ Treatment. The ATP content of SKOV-3 treated with Fe_3O_4NPs, $Fe_3O_4@CMCS$-electrostatic, and $Fe_3O_4@CMCS$ covalent are displayed in Figure 9. The percentage of CMCS bound to NPs was less than 4% of the total weight; therefore, it was reasonable to compare the amount of coated and uncoated Fe_3O_4NPs neglecting the weight of CMCS bound. As previously reported (Figure 5(b)), CMCS itself did not show cytotoxicity at the tested concentrations. On the contrary, $Fe_3O_4@CMCS$ covalent, and electrostatic, caused a dose-dependent reduction of ATP (Figures 9(a), 9(b) and 9(c)) more pronounced compared to the bare Fe_3O_4NPs. For further details see Supplementary Material Table 4.

3.5. Cellular Uptake. Figures 10(a)–10(d) show the uptake of coated Fe_3O_4NPs by using the classical Prussian blue method. The cytoplasm is full of NPs around the nucleus but never inside. $Fe_3O_4@heparin$ (Figure 10(d)) are more internalized compared to $Fe_3O_4@CMCS$ covalent (Figure 10(b)) and electrostatic (Figure 10(c)). Apparently, no differences are observed between the two chitosan systems. Coated Fe_3O_4NPs are readily incorporated into the cells already after 4 h; therefore, it is not possible to assert a time and dose dependence. In addition, for all the NP systems, it is observed that internalized NP did not interfere with mitosis process (Figures 10(b)–10(d)).

TEM images (Figure 11) confirmed that NP@heparin are readily internalized; in fact, already after 30 min of incubation NPs appeared inside the cells. Once entered most of the NPs remained in the cytoplasm, free or inside vesicles (Figures 11(a)–11(c)). As already highlighted by optical microscope, besides being rapid, internalization of the nanoparticles was aspecific. In these pictures, NP@heparin are identified as high electron density objects since NPs maintained the morphology observed in cell-free environment (Figure 11(d)). Worth to note is that, also after 3 h of exposure, no NP@heparin was observed in the nuclei even though the massive internalization of NPs can modify nucleus shape (Figure 12).

From our observations, the internalization did not seem to be influenced by the coating. Our hypothesis is confirmed by TEM picture (Figure 13) that did not show appreciable differences in cellular localization between $Fe_3O_4@CMCS$ electrostatically or covalently bound and NP@heparin (Figures 11 and 12).

4. Discussion

In recent years, the use of NPs, particularly MNPs, has expanded into biomedical research. Due to their unique properties such as small size, large surface area, and high reactivity, they are particularly suitable for diagnosis and therapy [1, 26–29]. Often, NPs have to be covered with molecules to get a core@shell system capable to bind bioactive
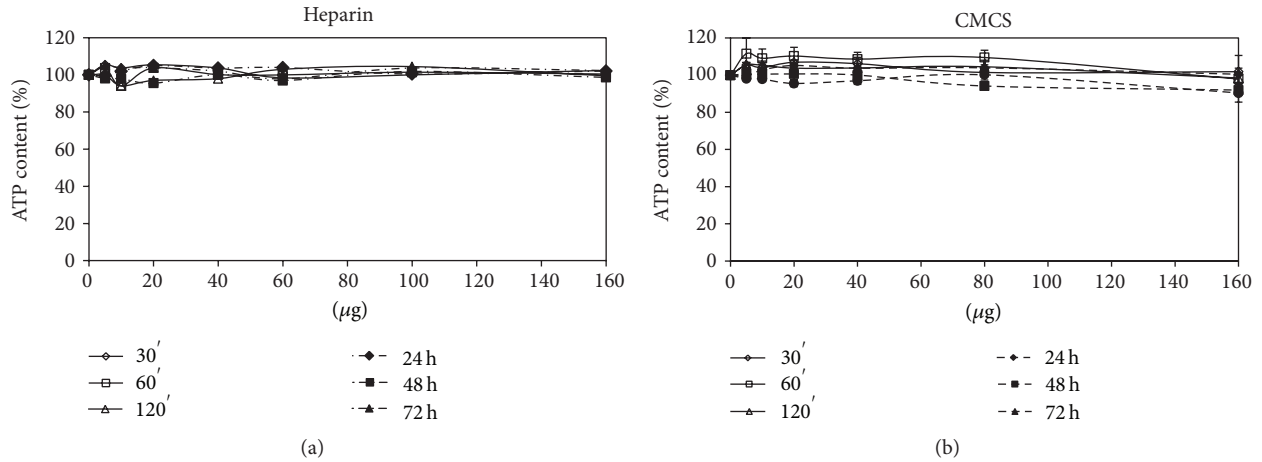
FIGURE 5: Percentage of ATP content, normalized to control, in SKOV-3 exposed to heparin (a) and carboxymethylchitosan (b) for different times.
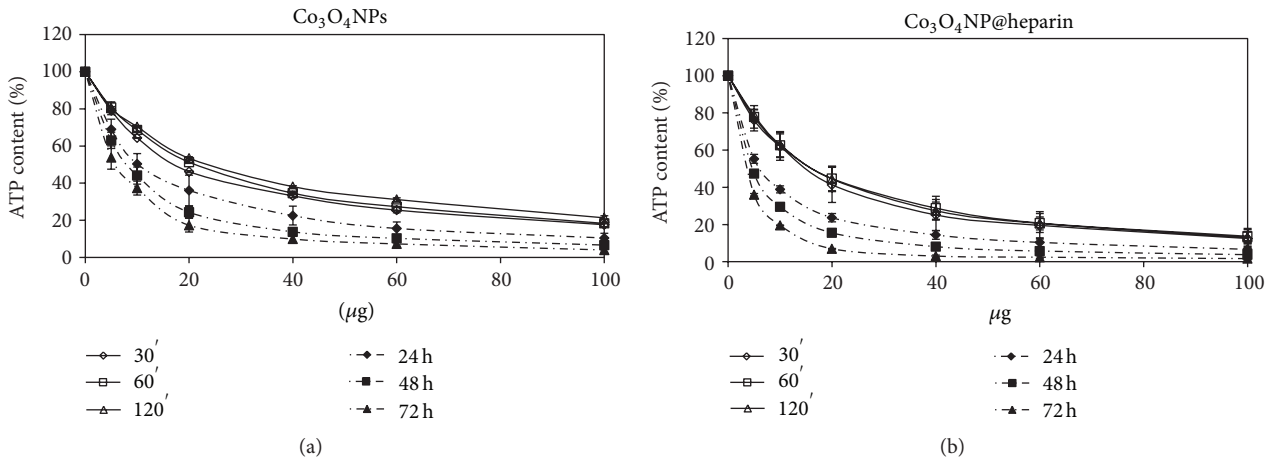

FIGURE 6: Percentage of ATP content, normalized to control, in SKOV-3 exposed to Co_3O_4NPs (a) and Co_3O_4@heparin (b) for different times.
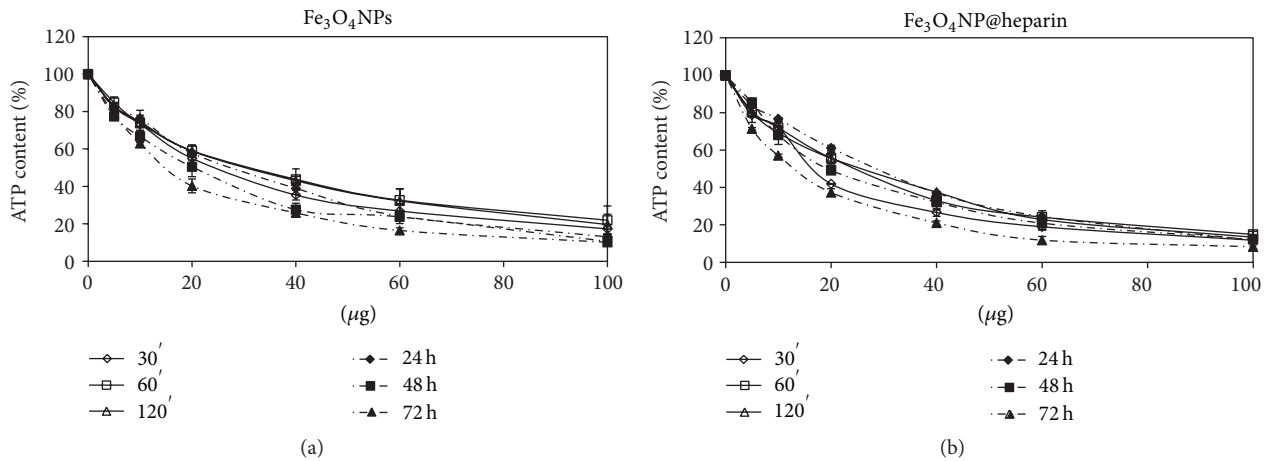

FIGURE 7: Percentage of ATP content, normalized to control, in SKOV-3 exposed to Fe_3O_4NPs (a) and Fe_3O_4@heparin (b) for different times.
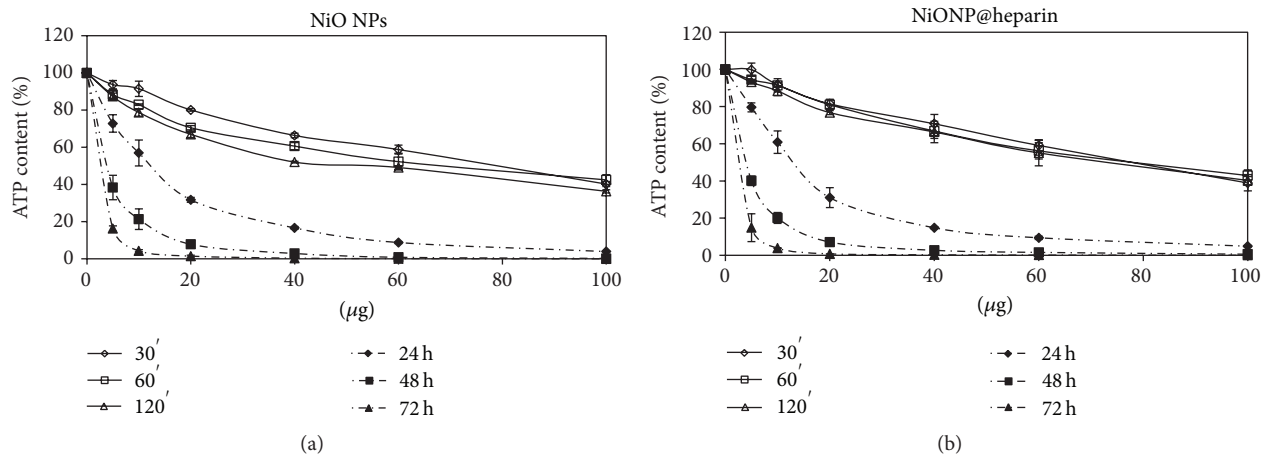
FIGURE 8: Percentage of ATP content, normalized to control, in SKOV-3 exposed to NiO NPs (a) and NiO@heparin (b) for different times.
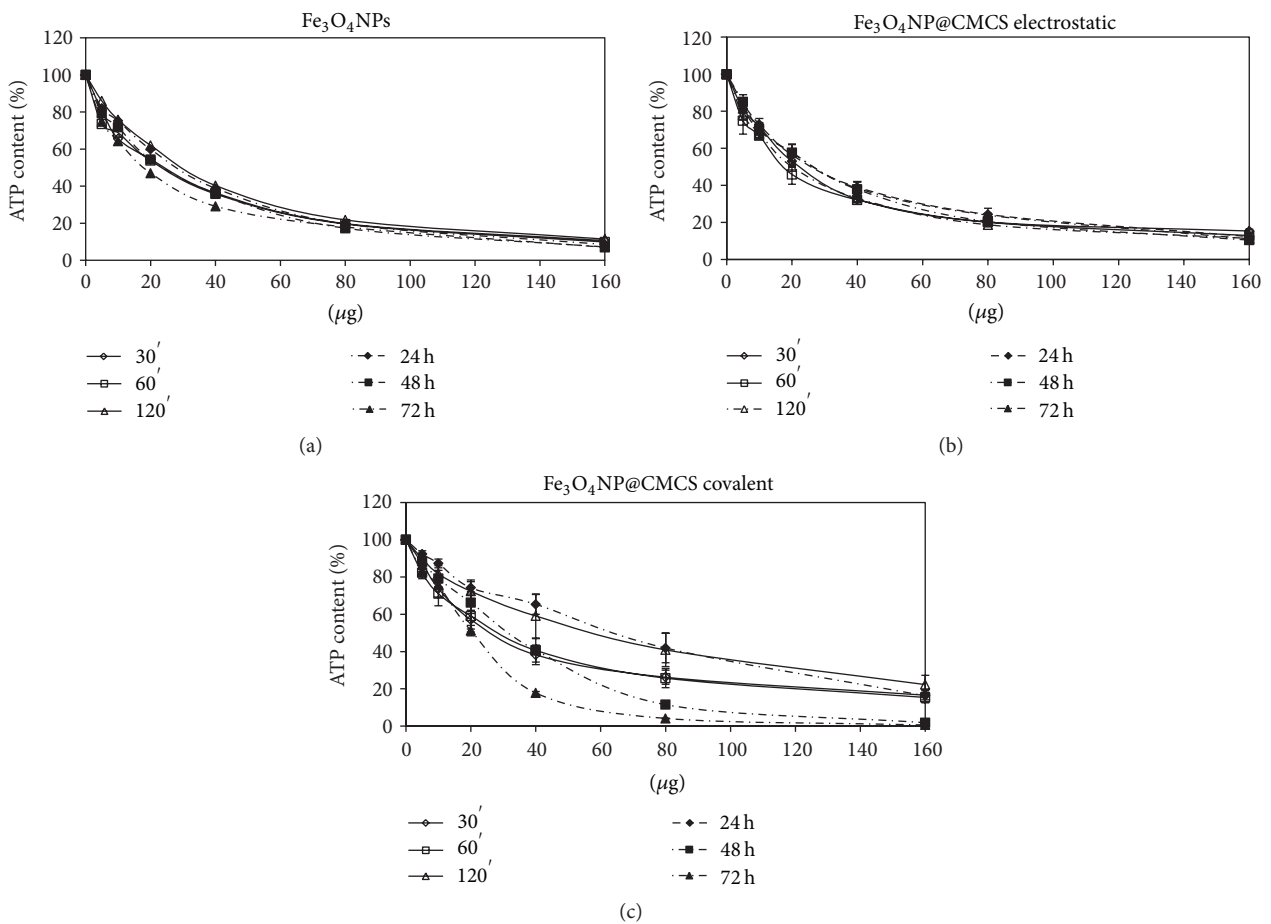

FIGURE 9: Percentage of ATP content, normalized to control, in SKOV-3 exposed to Fe_3O_4NPs (a), Fe_3O_4@CMCS electrostatic (b), and Fe_3O_4@CMCS covalent (c) for different times.
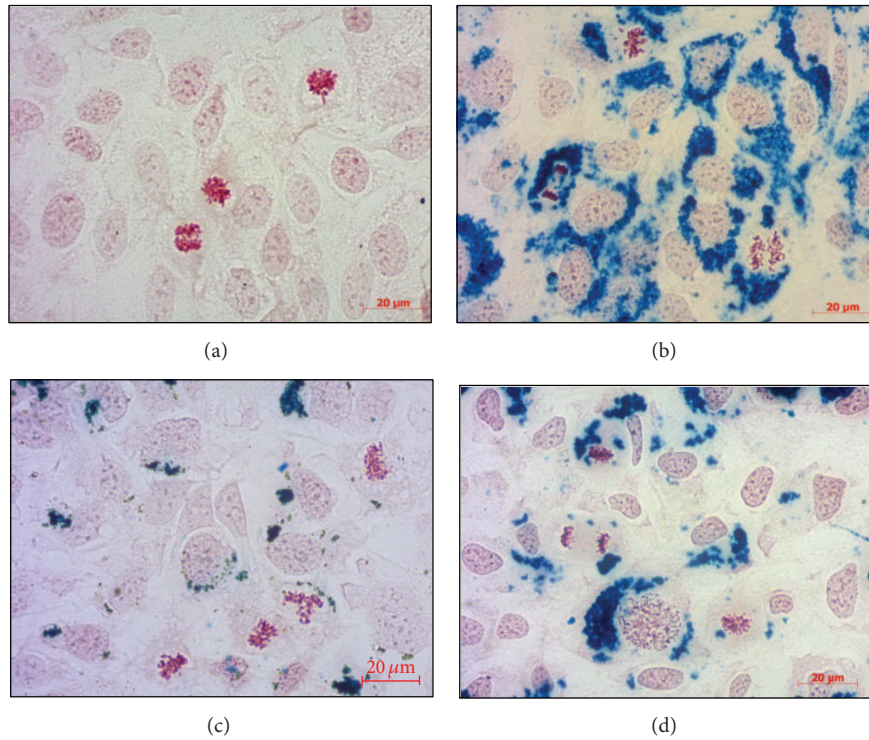
(a)

(b)

(c)

(d)

FIGURE 10: Uptake of SKOV-3 cells after 24 h of incubation with 25 mg/mL of anionic NPs. (a) Control cells; (b) Fe_3O_4@CMCS covalent; (c) Fe_3O_4@CMCS electrostatic; (d) Fe_3O_4@heparin. As shown in (b, c, and d) internalized NPs did not interfere with mitosis process. Magnification: 40x.
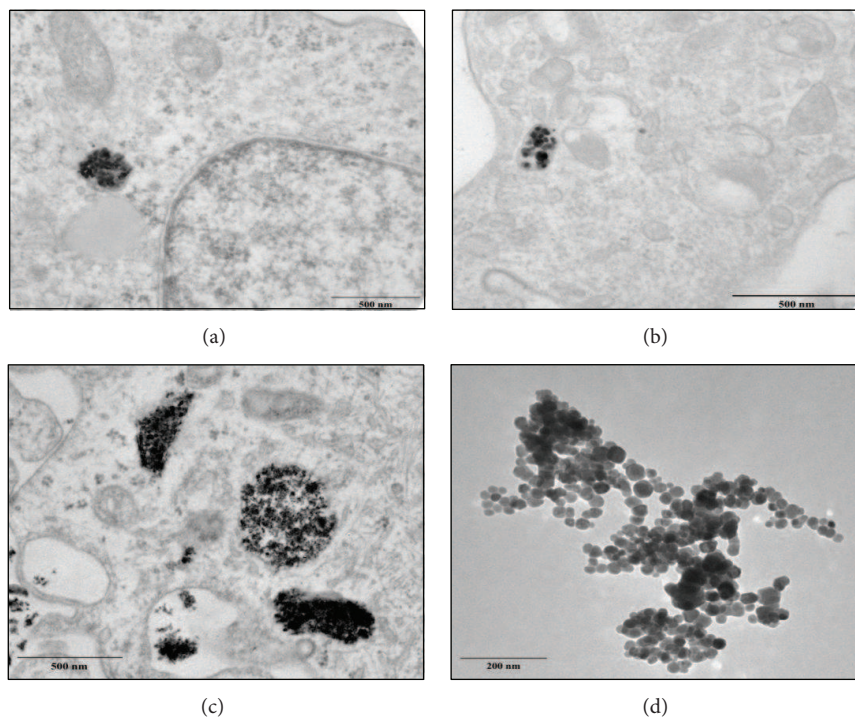

(a)

(b)

(c)

(d)

FIGURE 11: TEM pictures of SKOV-3 cells exposed to Co_3O_4@heparin (a), Fe_3O_4@heparin (b), and NiO@heparin (c) for 30 min. (d) A picture of Fe_3O_4@heparin deposited on a formvar carbon coated grid.
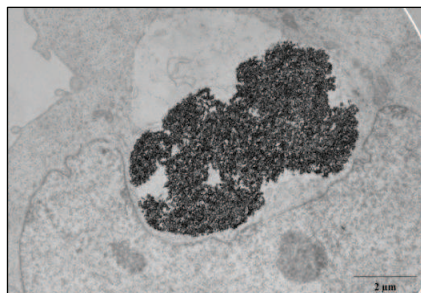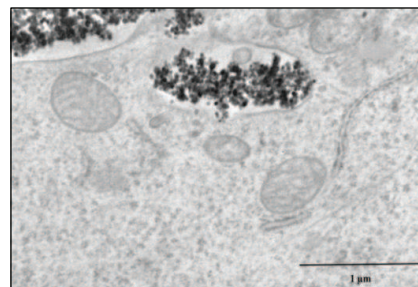
FIGURE 12: TEM picture showing a large agglomerate of Co_3O_4@heparin which modifies the shape of a SKOV-3 nucleus. Cells were fixed after 30 min of exposure.

(a)

(b)

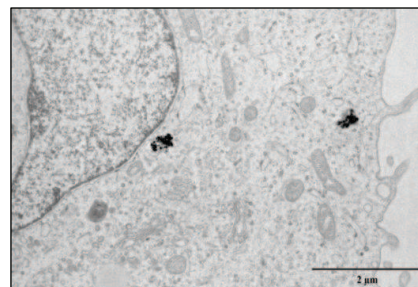FIGURE 13: TEM pictures of SKOV-3 cells exposed for 30 min to Fe_3O_4@CMCS electrostatic (a) and covalent (b).

molecules, stable in physiological fluids and possibly not toxic to the body. Among the innumerable coating materials, polymers such as heparin, dextran, carboxydextran, chitosan, and polyethylene glycol are considered more advantageous to satisfy the above-mentioned characteristics [30–33].

In particular, the literature reports several applications of NPs covered with heparin, ranging from use as imaging agent to apoptosis-induced agent in cancer cell, as well as components of nanodevices [34–36]. Unfortunately, this wide number of publications does not include toxicity studies of the synthesized systems. In particular, the literature lacks data on the comparison between the toxicity of core and core@shell. To try to fill this gap, in our laboratory, we have studied the characteristics and behavior of Co_3O_4, Fe_3O_4, and NiO NPs covered with heparin.

From our experiments resulted that the coating had significantly increased the colloid stability and hydrophilic property of metal NPs. In fact, the systems NP@heparin did not agglomerated thanks to the presence of negatively charged groups around the metallic core. The experiments on cytotoxicity, performed on SKOV-3 cells, have shown that heparin itself was not toxic within the range of the examined concentrations (see Figure 5(a)). Furthermore, as expected, Fe_3O_4@heparin was the less toxic system, while NiO@heparin was the most toxic one. Contrary to what one would expect, NP@heparin had not been found less toxic compared to the naked NPs for all the examined metals (see Figures 6, 7, and 8). Depletion of ATP content, observed in these experiments, could be due to the massive internalization of NP@heparin by the cells, phenomenon substantiated by Prussian blue staining for iron detection. Nevertheless, at the concentrations used in these experiments, internalized Fe_3O_4@heparin did not arrest mitosis process and nanoparticles were shared between the daughter cells. Further analysis by TEM have demonstrated that NP@heparin were already present inside the cell after 30 min of exposure (Figures 11(a), 11(b), and 11(c)). In this work, we have not investigated the mechanisms of internalization even though, as shown in Figures 11(a), 11(b), and 11(c) and as reported by the literature [37–39], endocytosis is certainly a possible way. Notwithstanding in our previous work we had observed the presence of NPs also in the mitochondria and in the nuclei [40], in these experiments NPs were confined only in cytoplasmic vesicles, even though, sometimes, the vesicle size was so enormous to modify nuclear shape and/or cause mechanical damages to the cell (see Figure 12). When the endocitotic vesicles had sizes that did not justify the mechanical damage, we could assume that cell toxicity could be due to the release of metal ions by the NP system; this hypothesis was supported by the data of cell viability in which Fe_3O_4 NPs resulted the least toxic metal.

Chitosan, but even better CMCS, preferred because the carboxymethylation increases the chitosan solubility in physiological fluids, is widely studied for theranostic applications [41, 42]. Despite the Prussian blue staining indicated that Fe_3O_4@chitosan uptake was less efficient compared to that of Fe_3O_4@heparin, TEM analysis showed that no differences were noticeable between the two NP systems. Furthermore, as previously reported for heparin, the presence of negative charges on NP surface enhances interactions with the cell membrane facilitating cellular uptake [6, 38]. Thanks to its biocompatibility and the presence of active functional groups (amino, carboxyl, and hydroxyl), CMCS is a valid instrument to design novel biocompatible materials with tailored chemical and biophysical properties [43–46]. Despite the wide use of CMCS little or nothing is known about its behavior when it is associated with metal NPs. This lack of data suggested us to evaluate the properties and the potential toxicity of the system Fe_3O_4@CMCS itself and compared to the naked Fe_3O_4NPs. For our studies, we have set up two different systems: Fe_3O_4@CMCS-electrostatic bound and Fe_3O_4@CMCS-covalent bound. The interest in coating Fe_3O_4NPs by covalent bond resided in an attempt to get a system characterized by a more stable shell in hydrophilic fluids.

Our studies on cell viability confirmed the biocompatibility of free CMCS at the tested conditions. When cells are exposed to Fe_3O_4@CMCS electrostatic, viability decreases with the same trend of Fe_3O_4NPs treatment (Figures 9(a) and 9(b)). The higher toxicity observed for Fe_3O_4@CMCS-covalent bond (Figure 9(c)) suggested that the method of preparation of the NPs could influence the cellular response.

Also in this case, uptake by SKOV-3 cells was relevant showing massive internalization already after 30 min with NPs stored in cytoplasmic vesicles (Figure 13) with no detectable difference between NP@heparin and Fe_3O_4@CMCS.

Our results have confirmed the data present in the literature about the biocompatibility of heparin and CMCS and their capability to get stable suspensions in hydrophilic fluids when conjugated to metal NPs, but not the ability to reduce the cytotoxicity of metal NPs coated with these polymers. Nevertheless, it is difficult to compare data derived from different experimental conditions such as different concentration ranges rather than diverse cell types which can give diverse responses to the same treatment [2, 47]. Moreover, the published data are often related to the whole system prepared and not to the single component, as we did, then the comparison is very difficult if not impossible.

In conclusion, the reactive groups, present on the surface of core@shell systems that we have synthesized, provide the opportunity for further functionalization so that a variety of biomolecules may be immobilized to enhance specific cell recognition for their use in targeting studies. Moreover, as regards Fe_3O_4NPs, even though the coating does not reduce their toxicity, the amount of NPs present in the systems is usually so low to render their toxicity negligible. Furthermore, due to their magnetic properties, Fe_3O_4NPs can be directed to the site of interest thanks to an external magnet. From this point of view, they could be promising tools as drug carrier for diagnosis and therapy.

Conflict of Interests

No conflict of interests is present. The authors have no financial involvement or interest with any organization or company about subjects or materials discussed in the paper.

Acknowledgments

References

[1] A. G. Cattaneo, R. Gornati, E. Sabbioni et al., "Nanotechnology and human health: risks and benefits," *Journal of Applied Toxicology*, vol. 30, no. 8, pp. 730–744, 2010.

[2] H. Eidi, O. Joubert, G. Attik et al., "Cytotoxicity assessment of heparin nanoparticles in NR8383 macrophages," *International Journal of Pharmaceutics*, vol. 396, no. 1-2, pp. 156–165, 2010.

[3] M. M. Kemp and R. J. Linhardt, "Heparin-based nanoparticles," *Wiley Interdisciplinary Reviews: Nanomedicine and Nanobiotechnology*, vol. 2, no. 1, pp. 77–87, 2010.

[4] V. K. Mourya, N. N. Inamdar, and A. Tiwari, "Carboxymethyl chitosan and its applications," *Advanced Materials Letters*, vol. 1, no. 1, pp. 11–33, 2010.

[5] R. Riva, H. Ragelle, A. des Rieux, N. Duhem, C. Jérôme, and V. Préat, "Chitosan and chitosan derivatives in drug delivery and tissue engineering," *Advances in Polymer Science*, vol. 244, pp. 19–44, 2011.

[6] A. Zhu, L. Yuan, and T. Liao, "Suspension of Fe_3O_4 nanoparticles stabilized by chitosan and o-carboxymethylchitosan," *International Journal of Pharmaceutics*, vol. 350, no. 1-2, pp. 361–368, 2008.

[7] H. Y. Hwang, I. S. Kim, I. C. Kwon, and Y. H. Kim, "Tumor targetability and antitumor effect of docetaxel-loaded hydrophobically modified glycol chitosan nanoparticles," *Journal of Controlled Release*, vol. 128, no. 1, pp. 23–31, 2008.

[8] R. Dinarvand, N. Sepehri, S. Manoochehri, H. Rouhani, and F. Atyabi, "Polylactide-co-glycolide nanoparticles for controlled delivery of anticancer agents," *International Journal of Nanomedicine*, vol. 6, pp. 877–895, 2011.

[9] C. E. Mora-Huertas, H. Fessi, and A. Elaissari, "Polymer-based nanocapsules for drug delivery," *International Journal of Pharmaceutics*, vol. 385, no. 1-2, pp. 113–142, 2010.

[10] A. Bava, R. Gornati, F. Cappellini, L. Caldinelli, L. Pollegioni, and G. Bernardini, "D-amino acid oxidase-nanoparticle system: a potential novel approach for cancer enzymatic therapy," *Nanomedicine*, 2013.

[11] A. Nel, T. Xia, L. Mädler, and N. Li, "Toxic potential of materials at the nanolevel," *Science*, vol. 311, no. 5761, pp. 622–627, 2006.

[12] S. Singh and H. S. Nalwa, "Nanotechnology and health safety - Toxicity and risk assessments of nanostructured materials on human health," *Journal of Nanoscience and Nanotechnology*, vol. 7, no. 9, pp. 3048–3070, 2007.

[13] E. Papis, R. Gornati, J. Ponti, M. Prati, E. Sabbioni, and G. Bernardini, "Gene expression in nanotoxicology: a search for biomarkers of exposure to cobalt particles and ions," *Nanotoxicology*, vol. 1, no. 3, pp. 198–203, 2007.

[14] E. Papis, R. Gornati, M. Prati, J. Ponti, E. Sabbioni, and G. Bernardini, "Gene expression in nanotoxicology research: analysis by differential display in BALB3T3 fibroblasts exposed to cobalt particles and ions," *Toxicology Letters*, vol. 170, no. 3, pp. 185–192, 2007.

[15] M. Di Gioacchino, N. Verna, L. Di Giampaolo et al., "Immunotoxicity and sensitizing capacity of metal compounds depend on speciation," *International Journal of Immunopathology and Pharmacology*, vol. 20, no. 2, pp. 15–22, 2007.

[16] A. Munoz and M. Costa, "Elucidating the mechanisms of nickel compound uptake: a review of particulate and nano-nickel endocytosis and toxicity," *Toxicology and Applied Pharmacology*, vol. 260, pp. 1–16, 2012.

[17] A. G. . Cattaneo, R. Gornati, M. Chiriva-Internati, and G. Bernardini, "Ecotoxicology of nanomaterials: the role of invertebrate testing," *Invertebrate Survival Journal*, vol. 6, pp. 78–97, 2009.

[18] Y. Xu, Z. Wen, and Z. Xu, "Chitosan nanoparticles inhibit the growth of human hepatocellular carcinoma xenografts through an antiangiogenic mechanism," *Anticancer Research*, vol. 29, no. 12, pp. 5103–5109, 2009.

[19] P. Poizot, S. Laruelle, S. Grugeon, L. Dupont, and J. M. Tarascon, "Nano-sized transition-metal oxides as negative-electrode materials for lithium-ion batteries," *Nature*, vol. 407, no. 6803, pp. 496–499, 2000.

[20] L. D. Pachón and G. Rothenberg, "Transition-metal nanoparticles: synthesis, stability and the leaching issue," *Applied Organometallic Chemistry*, vol. 22, no. 6, pp. 288–299, 2008.

[21] M. Moreno-Mañas and R. Pleixats, "Formation of carbon-carbon bonds under catalysis by transition-metal nanoparticles," *Accounts of Chemical Research*, vol. 36, no. 8, pp. 638–643, 2003.

[22] S. Rafique, M. Idrees, A. Nasim, H. Akbar, and A. Athar, "Transition metal complexes as potential therapeutic agents," *Biotechnology and Molecular Biology Reviews*, vol. 5, no. 2, pp. 38–45, 2010.

[23] A. Zhu, M. B. Chan-Park, S. Dai, and L. Li, "The aggregation behavior of O-carboxymethylchitosan in dilute aqueous solution," *Colloids and Surfaces B*, vol. 43, no. 3-4, pp. 143–149, 2005.

[24] Y. Y. Liang and L. M. Zhang, "Bioconjugation of papain on superparamagnetic nanoparticles decorated with carboxymethylated chitosan," *Biomacromolecules*, vol. 8, no. 5, pp. 1480–1486, 2007.

[25] D. R. Kester, I. W. Duedall, D. N. Connors, and R. M. Pytkowicz, "Preparation of artificial sea water," *Limnology and Oceanography*, vol. 12, no. 1, pp. 176–179, 1967.

[26] R. Bhattacharya and P. Mukherjee, "Biological properties of "naked" metal nanoparticles," *Advanced Drug Delivery Reviews*, vol. 60, no. 11, pp. 1289–1306, 2008.

[27] J. Conde, G. Doria, and P. Baptista, "Noble metal nanoparticles applications in cancer," *Journal of Drug Delivery*, vol. 2012, Article ID 751075, 12 pages, 2012.

[28] J. L. Martinez-Hurtado, "Metallic nanoparticle block copolymer vesicles with enhanced optical properties," *Nanomaterials*, vol. 1, pp. 20–30, 2011.

[29] P. Tartaj, M. Del Puerto Morales, S. Veintemillas-Verdaguer, T. González-Carreño, and C. J. Serna, "The preparation of magnetic nanoparticles for applications in biomedicine," *Journal of Physics D*, vol. 36, no. 13, pp. R182–R197, 2003.

[30] M. M. Kemp, A. Kumar, S. Mousa et al., "Synthesis of gold and silver nanoparticles stabilized with glycosaminoglycans having distinctive biological activities," *Biomacromolecules*, vol. 10, no. 3, pp. 589–595, 2009.

[31] H. Khurshid, S. H. Kim, M. J. Bonder et al., "Development of heparin-coated magnetic nanoparticles for targeted drug delivery applications," *Journal of Applied Physics*, vol. 105, no. 7, Article ID 07B308, 3 pages, 2009.

[32] C. Sun, J. S. H. Lee, and M. Zhang, "Magnetic nanoparticles in MR imaging and drug delivery," *Advanced Drug Delivery Reviews*, vol. 60, no. 11, pp. 1252–1265, 2008.

[33] O. Veiseh, J. W. Gunn, and M. Zhang, "Design and fabrication of magnetic nanoparticles for targeted drug delivery and imaging," *Advanced Drug Delivery Reviews*, vol. 62, no. 3, pp. 284–304, 2010.

[34] D. Y. Lee, "Highly effective T2 MR contrast agent based on heparinized superparamagnetic iron oxide nanoparticles," *Macromolecular Research*, vol. 19, no. 8, pp. 843–847, 2011.

[35] K. Lee, H. Lee, K. H. Bae, and T. G. Park, "Heparin immobilized gold nanoparticles for targeted detection and apoptotic death of metastatic cancer cells," *Biomaterials*, vol. 31, no. 25, pp. 6530–6536, 2010.

[36] K. A. Min, F. Yu, V. C. Yang, X. Zhang, and G. R. Rosania, "Transcellular transport of heparin-coated magnetic iron oxide nanoparticles (Hep-MION) under the influence of an applied magnetic field," *Pharmaceutics*, vol. 2, no. 2, pp. 119–135, 2010.

[37] A. Villanueva, M. Cãete, A. G. Roca et al., "The influence of surface functionalization on the enhanced internalization of magnetic nanoparticles in cancer cells," *Nanotechnology*, vol. 20, no. 11, Article ID 115103, 9 pages, 2009.

[38] E. Sabbioni, S. Fortaner, M. Farina et al., "Interaction with culture medium components, cellular uptake and intracellular distribution of cobalt nanoparticles, microparticles and ions in Balb/3T3 mouse fibroblasts," *Nanotoxicology*, 2012.

[39] C. Wilhelm and F. Gazeau, "Universal cell labelling with anionic magnetic nanoparticles," *Biomaterials*, vol. 29, no. 22, pp. 3161–3174, 2008.

[40] E. Papis, F. Rossi, M. Raspanti et al., "Engineered cobalt oxide nanoparticles readily enter cells," *Toxicology Letters*, vol. 189, no. 3, pp. 253–259, 2009.

[41] H. Arami, Z. Stephen, O. Veiseh, and M. Zhang, "Chitosan-coated iron oxide nanoparticles for molecular imaging and drug delivery," *Advances in Polymer Science*, vol. 243, pp. 63–184, 2011.

[42] X. G. Chen and H. J. Park, "Chemical characteristics of O-carboxymethyl chitosans related to the preparation conditions," *Carbohydrate Polymers*, vol. 53, no. 4, pp. 355–359, 2003.

[43] A. P. Zhu, N. Fang, M. B. Chan-Park, and V. Chan, "Interaction between O-carboxymethylchitosan and dipalmitoyl-sn-glycero-3- phosphocholine bilayer," *Biomaterials*, vol. 26, no. 34, pp. 6873–6879, 2005.

[44] P. Agrawal, G. J. Strijkers, and K. Nicolay, "Chitosan-based systems for molecular imaging," *Advanced Drug Delivery Reviews*, vol. 62, no. 1, pp. 42–58, 2010.

[45] D. Bhattacharya, M. Das, D. Mishra et al., "Folate receptor targeted, carboxymethyl chitosan functionalized iron oxide nanoparticles: a novel ultradispersed nanoconjugates for bi-modal imaging," *Nanoscale*, vol. 3, no. 4, pp. 1653–1662, 2011.

[46] T. T. Trang Mai, P. T. Ha, H. N. Pham et al., "Chitosan and O-carboxymethylchitosan modified Fe_3O_4 for hyperthermic treatment," *Advances in Natural Sciences: Nanoscience and Nanotechnology*, vol. 3, Article ID 015006, 5 pages, 2012.

[47] C. F. Jones and D. W. Grainger, "*In vitro* assessments of nanomaterial toxicity," *Advanced Drug Delivery Reviews*, vol. 61, no. 6, pp. 438–456, 2009.